The role of the EVC in development

Yu-Ning Liu

Thesis submitted in partial fulfilment of the requirements for the degree of Doctor of Philosophy

Newcastle University

Faculty of Medical Sciences

Institute of Human Genetics

September 2009

Abstract

Ellis-van Creveld syndrome (EvC, MIM 225500) is an autosomal recessive disease caused by the mutations in *EVC* or *EVC2* genes. Human patients with EvC syndrome showed clinical features as short limbs, short ribs, postaxial polydactyly and orofacial defects and about 60% of affected individuals showed atrial septum defects. *Evc*$^{-/-}$ mice showed short limbs and short ribs similar with those observed in human patients. However, the cardiac phenotype of *Evc*$^{-/-}$ mice had not been studied. In this study, histological analysis was performed in both C57Bl/6J X 129Sv mixed background and inbred C57Bl/6J 25 background mouse embryos. No obvious cardiac development defects were observed. Parallel to this, the *Evc* mRNA and Evc protein were also analyzed by *in situ* hybridization and using the *lacZ* reporter system. X-gal positive cells were observed at the dorsal to atrial wall and primary atrial septum in E11.5 and E12.5, respectively. No *Evc* mRNA was detected in developmental heart by *in situ* hybridization by probes located at c.926 to c.1717.

Previous study demonstrated that Evc and Evc2 protein are localized to the base of cilia. In this study, two different methods, deciliation and immuno-TEM, were applied to localize the Evc protein more precisely. The deciliation treatment sheared the cilia off at the distal end of transition zone and the immunofluorecent staining results indicated that the localization of the Evc protein was not beyond the distal end of transition zone. In the immuno-TEM experiment, although several factors were modified for proper staining, no informative results were obtained from this experiment. As the mutations of ciliary proteins might result in malformation of cilia, the ciliary structure of chondrocytes were also examined in this study. No structural

difference was observed in *Evc*$^{-/-}$ cells comparing to wildtype control.

The Evc2 protein was undetectable at the base of cilia in MEFs, chondrocytes and osteoblasts when Evc protein was absent. The existence of Evc2 protein was detected in total lysate *Evc*$^{-/-}$ cells by western blot, indicating rather than affecting the expression of Evc2 protein, Evc plays a role in Evc2 protein correct localization.

In human fibroblasts, EVC protein was localized to the base of cilia and the nucleus. The nuclear localization of Evc protein was never been observed in mouse cells by immunofluorescence staining. This inconsistence was examined through subcellular fractionation assay. The western blotting results demonstrated that the Evc protein exists in the nuclear fraction in the mouse MEFs. Several potential Evc associated proteins suggested by yeast two-hybrid study were also examined in subcellular fractionation assay. No distribution differences between wildtype and *Evc*$^{-/-}$ cells were observed.

Table of Contents

List of Figures

List of Tables

List of Abbreviations

7-DHC	7-dehydrocholesterol
A	activative form (i.e. CiA - activative form of Ci); adenine (i.e. G>A - guanine to adenine); ampere (i.e. mA - milliampere)
AMCA	amino-methyl-coumarin-acetate
Arl13b	ADP-ribosylation factor-like 13B
AV	atrioventricular
BBS	Bardet-Biedl syndrome
BCIP	5-Bromo-4-chloro-3-indolyl phosphate
BMP	Bone Morphogenetic Protein
botv	brother of tout velu
bp	base pair
BSA	bovine serum albumin
Ci	Cubitus interruptus
Cos2	Costal-2
Cys	cysteine
D2lic	dynein 2 light intermediate chain
DAPI	4-6-diamidino-2-phenylindole
DHCR7	7-dehydrocholesterol reductase
Dhh	Desert hedgehog
Disp	Dispatched
Dlp	Dally like protein
DMEM	Dulbecco's Modified Eagle Medium
DMSO	dimethyl sulfoxide
DNA	deoxyribonucleic acid
dNTP	deoxyribonucleotide triphosphate
DTT	dithiothreitol
E	embryonic stage
EDTA	ethylenediaminetetraacetic acid
EGTA	ethylene glycol tetraacetic acid
ENU	N-ethyl-N-nitrosourea
EvC	Ellis-van Creveld syndrome
FBS	fetal bovine serum
FITC	fluorescein isothiocyanate
Fu	Fused
G	guanine (i.e. G>A - guanine to adenine)
GDP	guanosine diphosphate
Gli	GLI-Kruppel family member Gli
Gly	glycine

GTP	guanosine triphosphate
HEPES	4-(2-hydroxyethyl)-1-piperazineethanesulfonic acid
Hh	Hedgehog
HhN	N-terminal of Hedgehog
HRP	horseradish peroxidase
HSPG	heparan sulfate proteoglycans
IFT	intraflagellar transport
IgG	immunoglobulin G
Ihh	Indian hedgehog
IMCD3	inner medullary collecting duct
kb	kilobase
kDa	kiloDalton
Kif	the kinesin superfamily protein
l	litter
LA	left atrium
LV	left ventricle
m	meter; milli (i.e. mm - millimeter)
M	molar
MEF	mouse embryonic fibroblast
NBT	nitro blue tetrazolium
NF1	neurofibromin 1
NFATc1	nuclear factor of activated T-cells, cytoplasmic, calcineurin-dependent 1
NP40	nonyl phenoxylpolyethoxylethanol
NPHP	nephronophthisis
Ofd1	oral-facial-digital syndrome type 1
OFT	outflow tract
P	postnatal day
PAS	primary atrial septum
PBS	phosphate buffered saline
PBST	PBS containing Tween-20
PCR	polymerase chain reaction
PDGFRα	platelet-derived growth factor receptor alpha
PFA	paraformaldehyde
pH	measure of the concentration of dissolved hydrogen ions
PKA	protein kinase A
Ptch1	Patched homolog 1
R	repressive form (i.e. CiR - repressive form of Ci)
RA	right atrium
rcf	relative centrifugal force
RNA	ribonucleic acid

RPGR	retinitis pigmentosa GTPase regulaor
RT-PCR	reverse transcription polymerase chain reaction
RV	right ventricle
SDS	sodium dodecyl sulfate
Shh	Sonic hedgehog
Shh-N	Sonic hedgehog N-terminal signaling domain
SLOS	Smith-Lemli-Opitz syndrome
Smo	Smoothened
Snx	Sorting nexin
sotv	sister of tout velu
SSC	saline-sodium citrate
Sufu	Suppressor of Fused
TAE	Tris-acetate-EDTA
TBS	Tris buffered saline
TBST	TBS containing Tween-20
TEM	transmission electron microscopy
TGF-β	transforming growth factor beta
THM1	tetratricopeptide repeat-containing hedgehog modulator-1
Tris	tris(hydroxymethyl)aminomethane
ttv	tout-velu
U	units
V	voltage
Vangl2	Van-gou like 2
VEGF	vascular endothelial growth factor
X-Gal	bromo-chloro-indolyl-galactopyranoside
β-gal	beta-galactosidase
μ	micron

Acknowledgement

Thanks to my supervisors, Prof. Judith Goodship and Dr. Deborah Henderson, for their expert guidance, help and supervision. I would like to acknowledge the entire Evc research group for their help and advice throughout. Thanks to Dr. Helen Blair, who gave me lots of suggestions about the bench works and was also patient to explain things not familiar to me.

I am very grateful to all the members of the Institute of Human Genetics. Special thanks to Dr. Mitsushiro Nakatomi, not only the suggestions of *in situ* works, the common habits we shared made my life more fun here. Thanks to EM unit staff who helped and advised me a lot during my TEM works.

I’m particularly grateful to my family who gave me all their support. Great thanks to Yen, her accompany and encouragement helped me through these tough years.

Chapter 1 Introduction

1.1 Ellis-van Creveld (EvC) syndrome

1.1.1 Clinical features of EvC syndrome

Ellis-van Creveld syndrome (EvC, MIM 225500) is an autosomal recessive disease first reported by Ellis and van Creveld in 1940. This syndrome causes progressive shortening of the proximodistal axis of the limbs, with zeugopod (radius-ulna/tibia-fibula) shortening more pronounced than the stylopod shortening (humerus/femur). Autopod shortening of the distal phalanges is more marked than that of the proximal phalanges. "Six-fingered dwarfism" is a useful function for defining EvC syndrome, and served as an alternative name in the 1960s. This term is no longer used because of the polydactyly reference to "freakish" labeling. To date, Ellis-van Creveld (abbreviated EvC) is the only satisfactory designation for this syndrome. The EvC syndrome is sometimes hard to differentiate from two other forms of skeletal dysplasia, asphyxiating thoracic dysplasia or Jeune syndrome and short-rib polydactyly syndrome type III, due to the overlap of their clinical features. Figures on the worldwide prevalence of EvC syndrome is unavailable (Ruiz-Perez and Goodship, 2009; Vinay et al., 2009). However, the live birth prevalence in the Old Order Amish community of Lancaster Country, Pennsylvania is 5 in 1000 (McKusick *et al.*, 1964).

EvC syndrome is a complex condition involving several developmental defects, most of which appear in the skeleton and skin. Patients display a wide spectrum of developmental defects, which might vary greatly between patients. Common characteristics of the EvC syndrome include short limbs, short ribs, postaxial polydactyly (Figure 1.1 A), fingernail dystrophy, multiple oral frenula, neonatal teeth, delayed tooth eruption (Figure 1.1 B) and cardiac defects (Biggerstaff and Mazaheri, 1968; Ellis and Van Creveld, 1940; McKusick et al., 1964; Taylor et al., 1984). The finger and toenails are small or have an unusual appearance, and the syndrome affects hair in some cases. Some EvC patients exhibit craniofacial abnormalities. Other patients show multiple labiogingival frenulae, premature eruption of teeth, including the presence of teeth at birth, small conical teeth, and missing primary or permanent teeth (Ruiz-Perez and Goodship, 2009; Vinay et al., 2009).

Approximately 60% of affected individuals suffer from cardiac defects (Figure 1.1 C). The most frequent cardiac abnormalities in human patients are defects in atrioventricular septation and a single atrium (Digilio *et al.*, 1999; Katsouras *et al.*, 2003). Previous research reports clinical features such as hypoplastic aorta, enlarged pulmonary artery, transposition of great vessels, and mitral cleft (da Silva et al., 1980; McKusick et al., 1964). In McKusick's study, approximately 50% of the EvC patients were stillbirth or died in infancy. This is most likely to be due to the heart defects or respiratory problems associated with a short thoracic region (McKusick *et al.*, 1964).

A

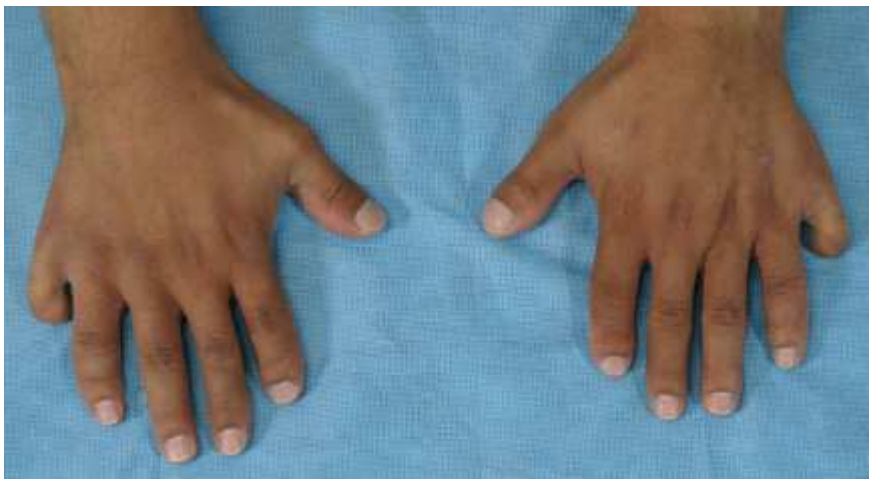

B

C

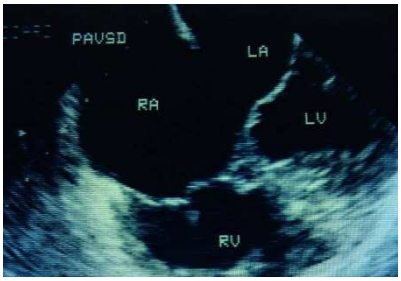

Figure 1.1 Some clinical features of patients with EvC syndrome
(A) Bilateral postaxial polydactly (adapted from Ulucan *et al.*, 2008) and (B) multiple frenulae and abnormal teeth (adapted from Alves-Pereira *et al.*, 2009) usually appear in patients with EvC syndrome. (C) Demonstrated defects in atrioventricular septation (adapted from Dr. Michael Wright) and a single atrium observed in EvC patients.

There is no clinical treatment for patients with EvC syndrome. However, some medical and surgical cares are available to improve the quality of EvC patients' life. For example, orthopedic procedures can correct polydactyly and bone deformities, especially knee valgus with depression of the lateral tibial plateau and dislocation of the patella. Surgery is also beneficial for patients with periperative morbidity. Some studies demonstrate that dental abnormalities, such as peg teeth or natal teeth, are more prone to dislodgement during use (Cahuana et al., 2004; Susami et al., 1999). However, the mortality rate due to heart failure remains significant. Chondrodysplasia of the legs can cause short stature in EvC

patients. Treatment with growth hormones is ineffective (Baujat and Le Merrer, 2007; Pirazzoli et al., 1989).

1.1.2 *EVC* and *EVC2* genes

In 1996, researchers mapped the EvC syndrome to the short arm of chromosome 4 between genetic markers D4S2957 and D4S827 in studies involving 9 interrelated Amish pedigrees and 3 unrelated families from Mexico, Ecuador, and Brazil (Polymeropoulos *et al.*, 1996). In 2000, researchers identified a novel gene, *EVC*, as responsible for EvC syndrome (Ruiz-Perez *et al.*, 2000). Mutations of the *EVC2* gene appeared in an EvC individual from a consanguineous Gypsy family in 2003 (Ruiz-Perez *et al.*, 2003). Takeda *et al.* previously mapped the *EVC2* gene to chromosome 4 under another name, *LIMBIN* (Takeda *et al.*, 2002). Galdzicka *et al.* reported other mutations in *EVC2* in an EvC patient (Galdzicka *et al.*, 2002).

Current knowledge of *EVC* and *EVC2* states that they are arranged in a head-to-head divergent configuration with transcription start sites separated by only 2,624bp in human and 1,647bp in mouse (Figure 1.2) (Ruiz-Perez *et al.*, 2003). Genes with this type of head-to-head configuration may be coregulated by a single promoter with bidirectional activity (Shimada *et al.*, 1989).

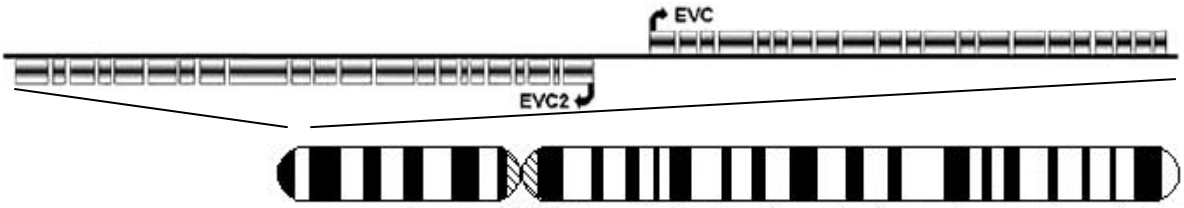

Figure 1.2 Human genetic structures of *EVC* and *EVC2* (adapted from Tompson *et al.*, 2007)
EVC and *EVC2* genes are located on chromosome 4p in a head-to-head configuration.

The longest *EVC* protein translated from gene contains 21 exons within a 117kb genomic region, and encodes a protein consisting of 992 amino acids. Previous research indicates three more *EVC* variants (http://www.ebi.ac.uk/astd/geneview.html). One of them contains 12 exons with the same 5'-end 11 exons and an alternative exon 12. The other two are short transcriptions, both of which contain two exons (http://www.ebi.ac.uk/astd/geneview.html). Low levels of *EVC* appear in developing bone, heart, kidney, and lung at Carnegie stages 19 and 21 in human embryonic tissue using in situ hybridization (Ruiz-Perez *et al.*, 2000). In bone, *EVC* mRNA appears in the developing vertebral bodies, ribs, and both upper and lower limbs (Ruiz-Perez *et al.*, 2000).

EVC2 consists of 23 exons, and produces transcripts with at least three alternate transcription start sites and three prime ends. Exons 16 and 18 are also subject to alternative splicing, and have tissue-specific transcripts (Galdzicka *et al.*, 2002). Northern blot analysis demonstrates a 4.8kb *EVC2* transcript in heart, placenta, lung, liver skeletal muscle, kidney, and pancreas. The 4.8kb transcript also appears in lymphoblasts and chondrocytes using reverse transcription polymerase chain reaction

RT-PCR (Galdzicka *et al.*, 2002). *EVC* and *EVC2* encode novel proteins with putative transmembrane domains and regions of coiled-coiled structure, but have no similarity with the motifs of other proteins to give clues to their functions (Ruiz-Perez *et al.*, 2000). The functions of EVC and EVC2 proteins remain unclear.

Previous studies report 29 mutations in *EVC* and 35 mutations in *EVC2* in patients with EvC syndrome. These mutations include missense/nonsense mutations, splicing error mutations, small deletions, small insertions, and gross deletions (Galdzicka et al., 2002; Ruiz-Perez et al., 2003; Ruiz-Perez et al., 2000; Tompson et al., 2007).

1.1.3 The other disease caused by the mutations of *EVC* gene

Weyers acrofacial dysostosis (MIM 193530) is an autosomal dominant disorder also known as Curry-Hall syndrome, as Curry and Hall described a large Spanish-Mexican family in 1979 (Curry & Hall, 1979, cited by (Ye *et al.*, 2006)). Weyers acrofacial dysostosis shares the same clinical features as EvC syndrome, including polydactyly, dysplastic nails, and shortness of stature, but in a mild form. The only exception to this rule, reported in 1997, involved the proband of a four-generation Weyers acrofacial dysostosis family who showed a relatively severe phenotype similar to that of EvC (Howard *et al.*, 1997). In 2000, Ruiz-Perez and colleagues reported an EvC patient whose father had Weyers acrofacial dysostosis, suggesting an overlap in the clinical features of these two diseases. Linkage and haplotype analysis indicates that the disease locus of Weyers acrofacial dysostosis resides in the genetic markers D4S3007 and D4S2366. This

region includes the *EVC* locus. This finding highlights the possibility that Weyers acrofacial dysostosis is allelic to Ellis-van Creveld syndrome (Ruiz-Perez *et al.*, 2000). Ye *et al*. confirmed this hypothesis by reporting an *EVC2* gene mutation (c.3793delC) in a Weyers acrofacial dysostosis family (Ye *et al.*, 2006).

1.1.4 *Evc* knockout mice

A previous study by our research group reports that $Evc^{-/-}$ mice were generated by replacing *Evc* exon 1 with a β-galactosidase gene in an in-frame status (Figure 1.3). Absence of *Evc* transcript in $Evc^{-/-}$ mice was confirmed by RT-PCR (Ruiz-Perez *et al.*, 2007).

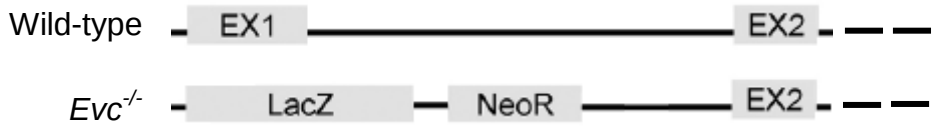

Figure 1.3 Exon1 replacement in $Evc^{-/-}$ mice (adapted from Ruiz-Perez *et al.*, 2007)
The exon 1 of *Evc* gene was in-frame replaced by *LacZ* gene, which can be used as reporter gene as Evc expression in $Evc^{+/-}$ and $Evc^{-/-}$ mice.

No discernable defects appeared in $Evc^{+/-}$ mice. Although no prenatal loss of *Evc* knockout offspring was detected, approximately half of the $Evc^{-/-}$ offspring were missing 2 days after birth (Ruiz-Perez *et al.*, 2007). The cause of neonatal death remains unclear. The surviving $Evc^{-/-}$ mutants were unable to feed on a normal diet, but were able to survive when supplied with soft, well-hydrated food. $Evc^{-/-}$ mice did not breed. Therefore, mice were maintained by crossing $Evc^{+/-}$ males to $Evc^{+/-}$ females.

Though the *Evc*$^{-/-}$ mice shared some EvC features of human patients, including short ribs, short limbs, and dental anomalies (Figure 1.4), they did not exhibit polydactyly. The teeth of *Evc*$^{-/-}$ mice revealed abnormalities of the incisors, including absence of the upper incisors and a single upper incisor. Compared with wild type dentition, a small first molar frequently appeared in *Evc*$^{-/-}$ mice (Ruiz-Perez *et al.*, 2007). Furthermore, β-gal staining of the *Evc*$^{-/-}$ mouse embryos and newborn demonstrated that Evc expressed in the mouth and tooth-forming area and in the developing skeleton. β-gal was also positive at the growth plates of distal and proximal tibia in newborn mice. On the other hand, the ossified centers of the long bones were-gal negative (Ruiz-Perez *et al.*, 2007).

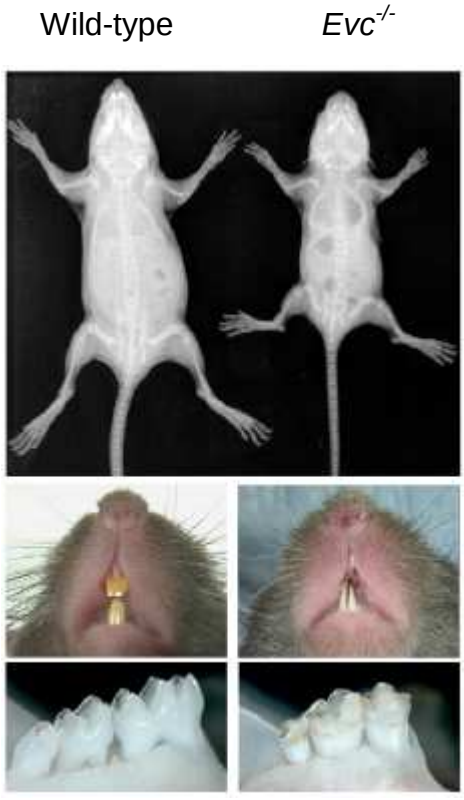

Figure 1.4 Phenotypes of *Evc*$^{-/-}$ mice (adapted from Ruiz-Perez *et al.*, 2007)
Developmental defects appeared *in Evc*$^{-/-}$ mice (right panel) compared to the wild-type littermate (left panel). The radiographs at P18 (upper row) show a small rib cage and shortness of long bone in *Evc*$^{-/-}$ mice (upper right). *Evc*$^{-/-}$ mice also showed the abnormalities in incisors (middle right) and molars (bottom right).

Shortening of the long bones and ribs is one of the major features of EvC syndrome. Although skeletal development involves many signaling molecules and pathways, Indian hedgehog (IHH) is one of the master regulators (Kronenberg, 2003). Previous studies demonstrate a drastic reduction of the expression of the Patched homolog 1 (*Ptch1*) and the GLI-Kruppel family member GLI1 (*Gli1*) in *Evc*$^{-/-}$ chondrocytes using RT-PCR. After exogenous stimulation of the Hedgehog (Hh) pathway with purmorphamine, RT-PCR analysis reveals that the RNA expression of *Ptch1* and *Gli1* level was greatly diminished in *Evc*$^{-/-}$ chondrocytes, whereas the wild type expressed both of these mRNA. Both the full-length GLI-Kruppel family member GLI3 (GLI3) and GLI3 repressor form in *Evc*$^{-/-}$ E10.5 embryos and E14.5 limb bud were normal in western blotting study. Since purmorphamine is an Hh agonist that targets Smoothened (SMO), these findings indicate that Evc might participate in the Ihh signaling pathway downstream of SMO (Ruiz-Perez *et al.*, 2007).

Approximately 60% of EvC patients show heart developmental defects, implying that EVC plays a role in heart development. Nevertheless, the heart development in *Evc*$^{-/-}$ mice at the beginning of this study and the expression of Evc in developmental heart remain unknown.

1.2 Cardiac development

1.2.1 Formation of primary heart tubes

Cardiac development begins as specification of the two bilateral precardiac mesodermal cells during embryonic gastrulation. Anterolateral precardiac mesodermal cells further differentiate to myocardial and endocardial

progenitors, which are generally referred to as the primary heart field. The two fields form the cardiac crescent as the embryo folds, and further fuse to form the primary heart tube (Tam *et al.*, 1997). The primary heart tube consists of outer myocardial cells, inner endocardial cells, and cardiac jelly between these two layers (Markwald *et al.*, 1977, cited by (Eisenberg and Markwald, 1995)). Heart development proceeds with the elongation of both ends of the primary heart tube. At the same time, the heart tube starts to loop toward the right (Figure 1.5) (Manner, 2004).

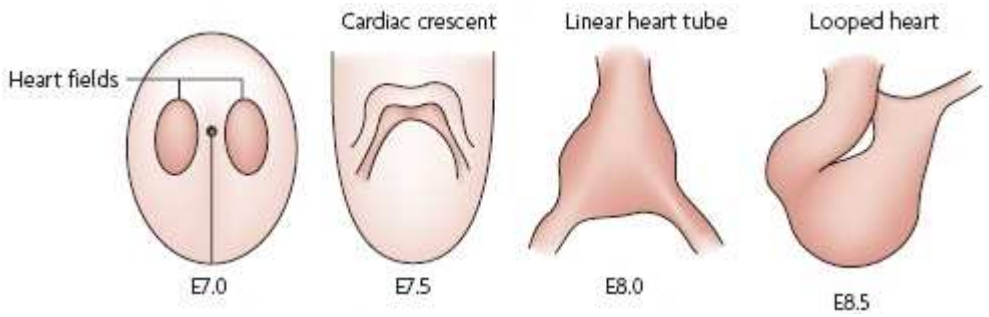

Figure 1.5 Schematic view of cardiac development I (adapted from High & Epstein, 2008)
Bilateral heart fields specified at E7.0. As the embryo folds, these two heart fields fuse at E7.5 and form a linear heart tube at E8.0. At E8.5, the middle part of heart tube starts to loop toward the right.

1.2.2 Heart looping and chamber formation

To allow looping, the middle part of heart tube disassociates from the body, leaving only the caudal and cranial ends of the heart tube connected to the body (Drake *et al.*, 2006). The future chamber region also expands, but remain connected in series for the moment. From the inflow pole to the outflow pole, these regions include the common atrium, left ventricle, and right ventricle.

1.2.3 Outflow tract (OFT) septation

As the heart tube loops to the right, cardiac neural crest cells, derived from the dorsal neural tube, migrate spirally into the OFT. These cells form the OFT cushions together with mesenchymal cells generated by endothelial cells through epithelial to mesenchymal transition (Kirby *et al.*, 1983). The cardiac neural crest cells collect in two prongs along the truncal OFT cushion and abruptly end upon reaching the conal portion of the OFT. The distal end of two prongs connect through a shelf of mesenchymal cells that protrudes into the dorsal wall of the aortic sac and is located between the origins of the fourth and sixth pairs of arch arteries (Waldo *et al.*, 1998). The elongation of the shelf at the expense of the prongs separates the truncal portion of the OFT into the ascending aorta and pulmonary trunk. The fusion of conal OFT cushions and the masculinization of this mesenchymal septum separates the aortic and pulmonary outlet components (Kruithof et al., 2003; van den Hoff et al., 1999). The formation of semi lunar valves through remodeling the OFT mesenchymal tissues and the rotation of the OFT wall also occurs during OFT septation. The OFT wall rotates counterclockwise through the hypoxia-driven programmed cell death of partial distal OFT myocardial wall. This aligns the aorta with the left ventricle and pulmonary trunk with the right ventricle (Bajolle et al., 2006; Sugishita et al., 2004).

1.2.4 Atrioventricular (AV) septation

While the heart tube loops towards the right, the cardiac jelly separating the myocardial and endocardial cells moves from its original place and

accumulates at the AV junction and OFT. The rich regions of the extracellular matrix containing cardiac jelly are called cushions. Two major cushions, the inferior AV cushion and the superior AV cushion, are involved in separating the atria from the ventricles (Figure 1.6). Two minor cushions, the left-lateral AV cushion and the right-lateral AV cushion, are involved in valve formation later in development (de Lange et al., 2004; Wessels et al., 1996). The inferior AV cushion and superior AV cushion fuse to form an AV mesenchymal septum in the midline of the AV canal, separating the atria from the ventricles.

1.2.5 Atrial septation

The primary atrial septum, a myocardial strand extending from the dorsal atrial wall, divides the common atrium. As the septum descends into the atrial cavity, a small mesenchymal tissue cap covers the leading edge of the primary atrial septum (Snarr *et al.*, 2007). This cap fuses with the superior AV cushion anteriorly and the dorsal mesenchymal protrusion posteriorly (Snarr et al., 2007; Wessels et al., 2000). The dorsal mesenchymal protrusion is a mesenchymal tissue derived from the secondary heart field located in the region anterior and medial to the primary heart field. The dorsal mesocardium associated with the dorsal mesenchymal protrusion wedges into the atrial cavity from the dorsal atrial wall (Wessels *et al.*, 2000). The fusion of the atrial septum, dorsal mesenchymal protrusion, and AV cushions separates the left and right atria.

1.2.6 Ventricular septation

The growth of the myocardial wall expands the ventricular chambers (Christoffels *et al.*, 2000). This expansion accompanies the extension of myocardium into the lumen of ventricular chambers. This process forms trabeculae and results in the sponge appearance in the ventricular chambers (Sedmera *et al.*, 1997). The ventricular septum grows from the myocardium at the greater curvature towards the atrioventricular mesenchymal septum separating the ventricular chambers (Figure 1.6). The membranous septum from the cushions fills the gap between the crest of the ventricular septum and atrioventricular septum (Solomon *et al.*, 1997).

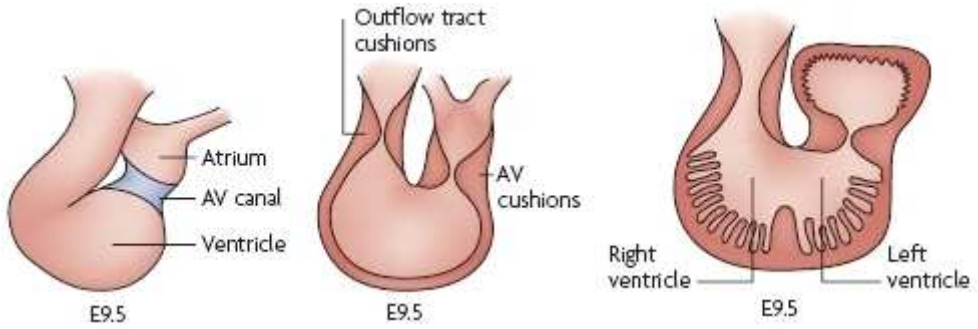

Figure 1.6 Schematic view of cardiac development II (adapted from High & Epstein, 2008)
Multiple developmental events occur at E9.5. Although still linearly connected, the future four chambers expand. The outflow tract cushions and AV cushions start to develop within the heart tube. The trabeculae structure also form from the extension of myocardium into the lumen of ventricular chambers.

1.2.7 Valve formation

The AV valves from cavitation of the AV cushion. The anterosuperior leaflet and posterior leaflet of the tricuspid valve develop from the right lateral

cushion, while the septal leaflet of the tricuspid valve develops from the inferior AV cushion. The mural leaflet of the mitral valve develops from the left lateral cushion, and the aortic leaflet of the mitral valve develops from the superior AV cushion. Sculpting of the myocardial wall releases the valve leaflet from the cushions (de Lange *et al.*, 2004). The distal ends of the leaflets attach to the papillary muscles via chordae tendineae.

1.3 Bone development

1.3.1 Bone structure

Bones are hard organs that form the skeletons of vertebrates. They are important for the movement, support, and protection of the organs, production of red and white blood cells, and storage of minerals (Kronenberg, 2003; Standring and Ellis, 2005). Adult humans have 206 bones, while infants have 270 (Standring and Ellis, 2005). The outer shell of long bones is a hard bone called cortical bone. This type of bone accounts for 80% of the total bone mass of an adult skeleton. This tissue gives bones their smooth, white, and solid appearance. The other 20% of bone mass is the interior trabecular bone tissue, an open cell porous network also called cancellous or spongy bone that consists of a network of rod- and plate-like elements (Standring and Ellis, 2005). Inner bone cavities contain marrow that produces blood cells (Standring and Ellis, 2005).

1.3.2 Bone formation

Bone formation, or osteogenesis, begins during the prenatal stage and continues through adulthood. It occurs either through direct ossification of

embryonic connective tissue, called intramembranous ossification (Syftestad *et al.*, 1985), or the replacement of hyaline cartilage, called intracartilaginous or endochondral ossification (Pelttari *et al.*, 2008). Bones formed by intramembranous ossificaion are called membrane bone (Syftestad et al., 1985), whereas bones formed by endochondral ossification are called cartilage bone (Pelttari et al., 2008).

1.3.2.1 Types of cells involved in bone development

References to bones or cartilage commonly call mesenchymal stem cells (MSC) osteochondrogenic cells because they can differentiate into chondrocytes or osteoblasts (Hall and Miyake, 2000; Pelttari et al., 2008). Chondrocytes, the only cells found in cartilage, produce and maintain a cartilaginous matrix that consists mainly of proteoglycans and collagen (Noonan *et al.*, 1998). Chondrocytes undergo terminal differentiation when they become hypertrophic during endochondral ossification (Kronenberg, 2003). The two types of cells that play important roles in bone formation are osteoblasts and osteoclasts. Osteoblasts, the specialized cells in bone tissue, deposit calcium into the bone matrix (Seeman, 2008). Osteoclasts dissolve calcium from bones and carry it into blood vessels (Hartmann, 2006).

1.3.2.2 Intramembranous ossification

Intramembranous ossification occurs primarily in the formation of flat bones of the skull (Pelttari et al., 2008). This process creates flat, membrane-like layers of early connective tissue, called mesenchyme tissue. In early development, blood vessel networks form between the

layers to provide a constant flow of nutrients (Pelttari et al., 2008). The mesenchymal cells then proliferate and further differentiate into osteogenic cells, which are the precursor of osteoblasts (Pelttari et al., 2008). Osteoblasts remove calcium from the blood and deposit it in the bone matrix (Reddi and Anderson, 1976), forming layers of spongy bone around the original cartilage (Caetano-Lopes *et al.*, 2007). In later stages of development, the space of the sponge bone fills with bone matrix and becomes compact bone. This process forms periosteum and compact bones (Pelttari et al., 2008).

1.3.2.3 Intracartilaginous (endochondral) bone formation

Endochondral ossification occurs in long bones, such as humerus and femur (Figure 1.7) (Syftestad et al., 1985). This process forms bone by replacing the cartilage model, or precursor, appearing earlier in embryonic development (Syftestad et al., 1985). The cartilage models first undergo rapid changes as the cartilage cells hypertrophy and the cartilage matrix becomes calcified. Following the disintegration of calcified matrix, a periosteum forms at the outside of the developing structure (Reddi and Anderson, 1976). Blood vessels and undifferentiated cells enter the center, disintegrating tissue and forming a primary ossification center (Blumer *et al.*, 2008). As a significant amount of spongy bone forms, osteoblasts fill portions of the porous spongy bone with calcium phosphate crystals to form a bone collar that holds the shaft together. This process forms the bone and continues toward both epiphyses, the ends of long bones. Interstitial and appositional growth increase the amount of cartilage outside the primary ossification center

(Hartmann, 2006; Kronenberg, 2003).

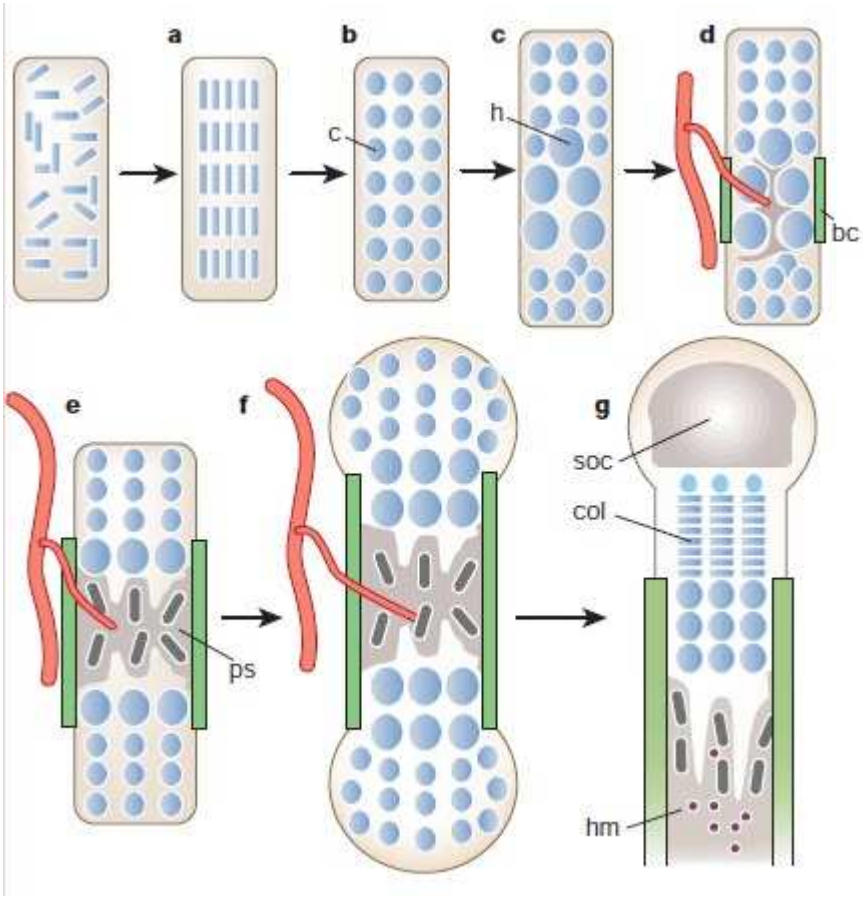

Figure 1.7 Intracartilaginous bone formation (adapted from Korneneburg HM, 2003)

(A) Mesenchymal stem cells (MSC) condense. (B) MSC differentiate to become chondrocytes (c). (C) Chondrocytes at the center of condensation stop proliferating and become hypertrophic chondrocytes (h). (D) Chondrocytes adjacent to hypertrophic chondrocytes become osteoblasts, forming a bone collar (bc). Hypertrophic chondrocytes direct the formation of mineralized matrix, attract blood vessels, and then undergo apoptosis. (E) Primary spongiosa (ps) form. (F) Chondrocytes continue to proliferate, leading to bone elongation. (G) A secondary ossification center (soc) forms. Below the secondary ossification center, a growth plate forms orderly columns of proliferating chondrocytes (col). Hematopoietic marrow (hm) expands in the marrow space.

At about the time of birth, a secondary ossification center appears in each epiphysis of long bones (Blumer et al., 2008). The growth of a secondary

ossification center is similar to that of a primary ossification center (Syftestad et al., 1985). The cartilage between the primary and secondary ossification centers is called the epiphyseal plate. This is where new cartilage forms, elongating the bone (Syftestad et al., 1985). Bone growth continues until the cartilage in the plate is completely replaced by bone (Kronenberg, 2003; Noonan et al., 1998).

1.4 Hedgehog signaling pathway

The hedgehog-signaling pathway is one of the most important key regulators of embryo development and conserved from flies to humans. This pathway is named from its intercellular signaling molecule in *Drosophila,* called Hedgehog (Hh). *Drosophila* larvae without this pathway have a hairy appearance (Nusslein-Volhard and Wieschaus, 1980). This pathway is vital to establishing the body plan and anterior-posterior body segmentation during the later stages of development.

1.4.1 Hedgehog signal in *Drosophila* – processing

After translation, the precursor Hh undergoes multiple processing steps for the generation and release of the active ligand from the producing cells. The signal sequence is firstly removed, and the C-terminal of this precursor Hh is then cleaved by an autocatalytic process between conserved Gly257 and Cys258, generating 19kDa N-terminal domains (HhN) (Lee *et al.*, 1994). After forming a thioester, the N-terminal Hedgehog signaling domain is modified by esterlinking cholesterol to its C-terminus (Porter *et al.*, 1996). This cholesterol modification associates HhN with the plasma membrane. Finally, the cholesterol-modified HhN molecule matures by adding a

palmitic acid moiety to the N-terminus through the acyltransferase activity of skinny hedgehog (Chamoun *et al.*, 2001). The active Hh signaling molecule thus has cholesterol modification at its C-terminus, and palmitate at its N-terminus (Figure 1.8).

1.4.2 Hedgehog signal in *Drosophila* – secretion and gradient formation

The mature Hh moves to the cell surface and secreted to form a concentration gradient that controls cell differentiation. The secretion of Hh from the producing cell requires the activity of dispathed (Disp), a 12 span transmembrane protein. Disp is a membrane belonging to the resistance-nodulation-division family of transport proteins. Accumulation of Hh in the producing cells and failure of long-range signaling appear in Disp mutant flies (Burke *et al.*, 1999).

The distance at which Hh acts is approximately 50 μm in *Drosophil* wing disc. Although the mechanism of Hh transportation remains unclear, this process involves heparan sulfate proteoglycan. In *Drosophila*, cells lacking the heparan sulfate synthesizing enzymes of the tout-velu (ttv)/ brother of tout velu (botv)/sister of tout velu (sotv) family hinder Hh transportation (Bellaiche et al., 1998; Han et al., 2004b; The et al., 1999). Dally and Dally-like protein (Dlp), two core proteins of heparan sulfate proteoglycan, are vital to the transportation of the Hh signal (Han et al., 2004a). Dally and Dlp also facilitate the binding of Hh to the cell surface (Han et al., 2004b; Lum et al., 2003).

When binding to the Hh receptor, Patched, Hh is internalized and targeted

with lysosome for degradation (Chen and Struhl, 1996). Patched is another Hh signaling targeting gene. With activating the signal pathway, receiving cells produce more Patched protein. This negative feedback limits the spread of Hh and facilitates the formation of Hh gradient from the secreting source.

1.4.3 Hedgehog signal in *Drosophila* – signal transduction

Two transmembrane proteins, iHog and boi, with their fibronectin repeats, facilitate the binding of Hedgehog to its receptor, Patched (Ptc) (Yao *et al.*, 2006). Ptc is a twelve-transmembrane protein that keeps the seven-transmembrane protein Smoothed (Smo) in an unphosphorylated state when Hedgehog is absent. Endocytosis removes unphosphorylated Smo from the membrane, and lysosomes subsequently degrade it (Jia *et al.*, 2004; Zhang *et al.*, 2004). The stimulation of Hedgehog results in hyperphosphorylation of Smo and subsequent conformation change in C terminus of Smo (Zhao *et al.*, 2007). The kinesin-like protein Cos2 that binds directly to the C terminus of Smo acts as a scaffolding protein that brings together various signal components, including the full-length form of transcription activator Ci (CiA), PKA, and kinase Fused (Fu) (Jia *et al.*, 2003; Lum *et al.*, 2003). PKA hyperphosphorylates CiA in the absence of Hh. This hyperphosphorylated CiA is then recognized by ubiquitin E3 ligase Slimb and catalyzed into transcription repressor form CiR (Price and Kalderon, 2002; Wang et al., 1999). When Smo accumulates and binds to Cos2 in response to Hh, it prevents the CiA to CiR conversion (Hooper, 2003; Jia *et al.*, 2003). Further investigation indicates that the Fu activity is required to fully activate the Hh signal by neutralizing the negative effects

of Suppressor of Fused (Sufu), which retains some CiA in the cytoplasm (Lefers et al., 2001; Ohlmeyer and Kalderon, 1998).

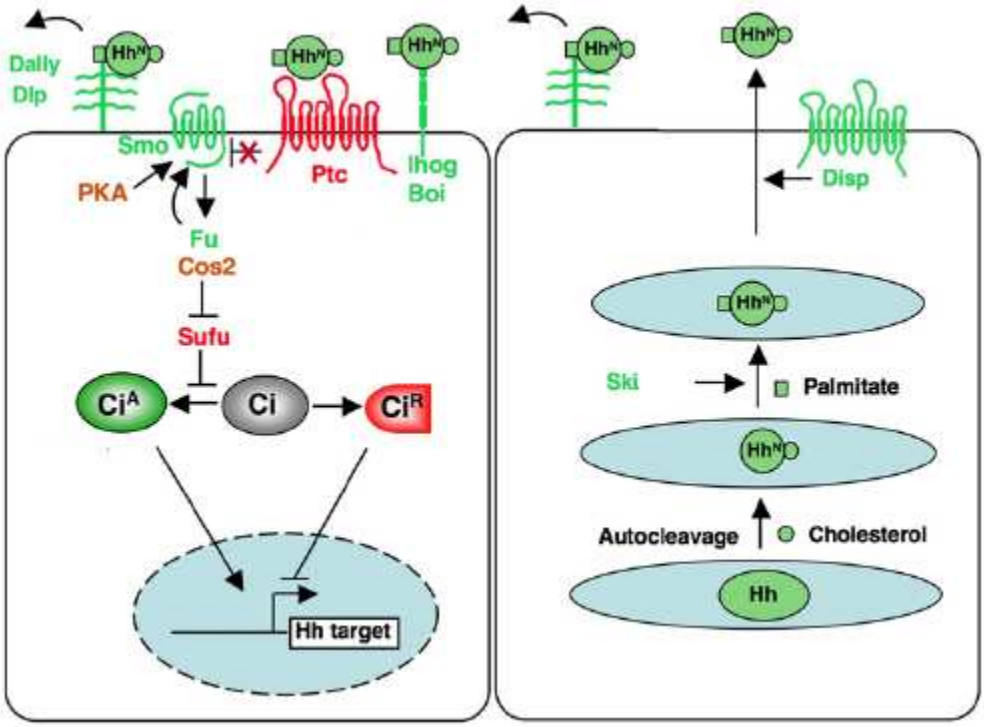

Figure 1.8 Hedgehog signal in *Drosophila* (adapted from Jiang & Hui, 2008)

In the producing cell (right), after autocleavage and cholesterol modification, Ski palmitate modifies Hh. The functional Hh is secreted by Disp and transported by Dally/Dlp. In the receiving cell, Ihog and Boi facilitate the binding to Ptc. The inhibition of Ptc releases Smo and stimulates Ci activation from Ci. The activated Ci eventually translocates to the nuclear and activates the Hh target genes.

1.4.4 Differences between *Drosophila* and vertebrate Hh signaling

The concept of hedgehog signaling transduction in vertebrates is similar to that found in *Drosophila*. One of the major differences is the pathway components. There are three different hedgehog homologues in vertebrates, including Desert hedgehog (Dhh), Indian hedgehog (Ihh), and Sonic hedgehog (Shh) (Echelard *et al.*, 1993). Dhh is mainly expressed in

the sertoli cells of the testis, the granulosa cells of the ovaries, and the Schwann cells in peripheral nerves. *Dhh* deficient mice show abnormalities in peripheral nerves, with thin perineurial sheaths surrounding the nerve fascicles. Male *Dhh*$^{-/-}$ mice fail to produce mature spermatozoa (Bitgood et al., 1996; Wijgerde et al., 2005; Yao et al., 2002). Ihh is expressed in primitive endoderm, gut, and prehypertrophic chondrocytes (Dyer et al., 2001; Vortkamp et al., 1996). In primitive endoderm, Ihh induces the formation of hematopoietic and endothelial cells in the adjacent epiblast. During gastrulation, Ihh is expressed in the posterior node and the visceral endoderm. Poor development of yolk-sac vasculature resulting from incomplete expression of Ihh causes a major loss of *Ihh*$^{-/-}$ embryos in early development. The role that Ihh plays in chondrocyte differentiation causes aberrant bone development in *Ihh*$^{-/-}$ mice (St-Jacques *et al.*, 1999). Shh is the most widely studied hedgehog molecule. Shh expresses at the node, notochord, and floor plate during early embryo development, and controls the patterning of left-right and dorso-ventral axes (Sampath et al., 1997; Schilling et al., 1999; Watanabe and Nakamura, 2000). Shh expression in the polarizing activity zone of the limb controls limb patterning (Chang *et al.*, 1994). Shh signal is also involved in the development of most epithelial tissue during organogenesis.

Besides the Hedgehog molecules, vertebrate express three Ci homologues, Gli1, Gli2 and Gli3 (Hui *et al.*, 1994). Gli1 functions only as a transcriptional activator (Hynes *et al.*, 1997). While Gli2 functions mainly as an activator, Gli3 functions primarily as a repressor (Ruiz i Altaba, 1998). The homologues of Cos2 and Fu that play important roles in the *Drosophila* Hh

signaling pathway also appear in vertebrates. However, there is no evidence of their involvement in vertebrate Hedgehog signaling (Chen *et al.*, 2005; Varjosalo *et al.*, 2006).

Another difference in the Hedgehog signaling pathway between *Drosophila* and vertebrates is the place at which signal transduction occurs. In *Drosophila*, Hh binding to Ptc triggers the translocation of Smo to the cell surface. In vertebrates, in the absence of Hedgehog molecule, Ptch1 localizes to the primary cilia. Once the signaling pathway is activated, Ptch1 translocates away from the cilia and Smo begins to accumulate in the cilia.

1.4.5 Shh signal in vertebrates

As with *Drosophila* Hh, Shh is processed into a 20 kDa N-terminal signaling domain (Shh-N) and a cholesterol molecule is added to the C-terminal of Shh-N. After secretion from the expressing cells, transportation of Shh is mediated the HSPG, which requires the heparan sulfate synthesizing enzymes of the EXT family (Bellaiche *et al.*, 1998). In the receiving cells, Shh binds to its receptor Patched-1 (Ptch1). Two transmembrane proteins, Cdo and Boc, facilitate this binding process (homologues of iHog and Boi, respectively) (Tenzen *et al.*, 2006). When Shh binds to Ptch1, it releases Smoothened (Smo) from inhibitory status and Smo further activates the Gli transcription factors by inhibiting the degradation of Gli2 and the proteolytic process to generate the repressive form of Gli3 (Figure 1.9).

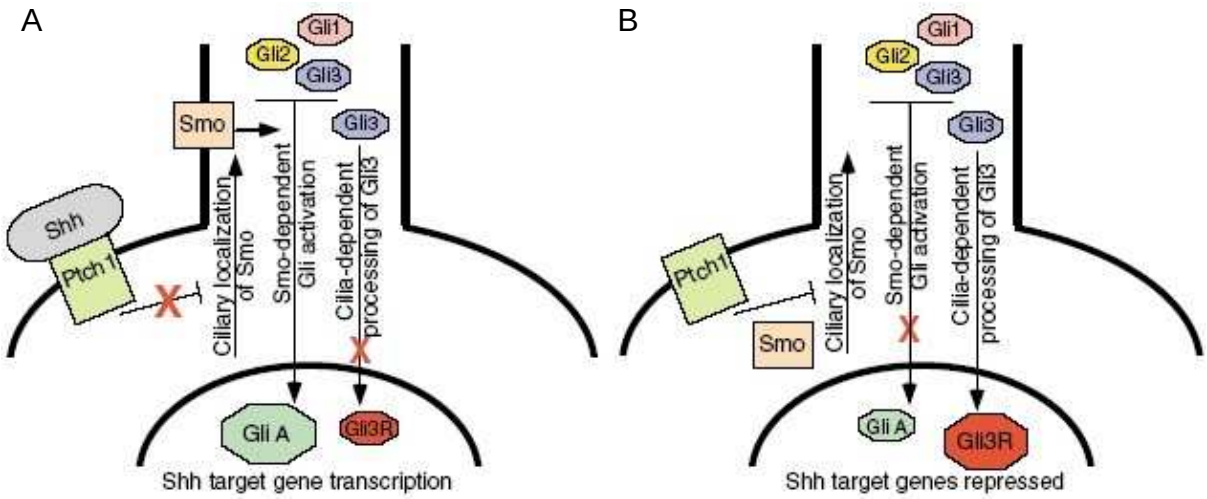

Figure 1.9 Sonic hedgehog signaling pathway (adapted from Bisgrove & Yost, 2006)

The inhibition of Smo stopes when Shh binds to Ptch1. Smo translocates to the cilium and controls the proteolytic processing of Gli3 to activator form (Gli3A). Shh target genes are transcribed after Gli translocates into the nucleus (A). Without Shh, the proteolytic process generates the repressor form of Gli3 (Gli3R) which represses the Shh target genes (B).

Previous research reports the conformation change of C terminal of Smo in the presence of Hh in mammalian cells (Zhao *et al.*, 2007). Unlike the Smo/Ci interaction in *Drosophila*, the interaction between Smo and Gli proteins in mammalian cells is unclear. Recent studies demonstrate that small molecules, such as cyclopamine, jervine, oxysterols and vitamin D3 derivatives, may modulte the activity of Smo (Bijlsma et al., 2006; Chen et al., 2002a; Chen et al., 2002b; Dwyer et al., 2007).

1.4.6 Hedgehog signal & cilium

Selecting phenotypes suggestive of disrupted Hh signaling in a forward genetic screen of N-ethyl-N-nitrosourea (ENU)-induced mutations revealed mutations in IFT complex B protein, IFT172, and IFT88 (Huangfu *et al.*, 2003). Studies on other IFT proteins (IFT52, Kif3a, Kif3b, Dyncb2 and D2lic)

provide further evidence of the involvement of cilium in Hh signaling (Haycraft et al., 2005; Huangfu and Anderson, 2005; Huangfu et al., 2003; Liu et al., 2005; Rana et al., 2004). The mutation of other genes encoding proteins involved in proper ciliogenesis, such as Ofd1 and Arl13b, can also disturb Hh signaling (Caspary et al., 2007; Ferrante et al., 2006). These findings suggest that primary cilia play an essential role in the Hh pathway.

Studies on the cellular localization of the components of Hh signal pathway provide further evidence of the importance of cilia. Immunofluorescence staining results demonstrate that Ptch1, Sufu, and three full length Gli proteins localize to the primary cilia (Haycraft *et al.*, 2005; Rohatgi *et al.*, 2007). Interestingly, Ptch1 leaves the cilia and Smo moves into the cilia in the presence of Hh. Corbit and colleagues suggested that the ciliary localization of Smo is essential for the activation of the Hh signaling pathway (Corbit *et al.*, 2005). However, recent studies on cyclopamine, the antagonist of Hh signaling pathway, show that treated MEFs decreased the ciliary accumulation of Smo. The authors suggested the ciliary localization of Smo is insufficient for the Hh response, and an additional step is necessary to active the Hh signaling pathway (Rohatgi *et al.*, 2009; Wilson *et al.*, 2009).

1.4.7 Shh signaling in heart development

The relationship between Shh signaling and cardiac development was first described in 1996 (Chiang *et al.*, 1996). *Shh* knockout mice showed a single OFT arising from the right ventricle, enlarged apex pointing toward right, and heart positioned at the left side of the thorax (normally centrally

positioned) (Tsukui *et al.*, 1999; Washington Smoak *et al.*, 2005). Other studies reported cardiac abnormalities when other components of the pathway (*Ptch1*, *Smo*, and *Sufu*) were mutated (Cooper et al., 2005; Goodrich et al., 1997; Zhang et al., 2001).

Table 1.1 Summary of cardiac phenotypes of mutant Hh signal components

	Cardiac phenotype	Reference
Shh	single outflow tract arising from the right ventricle enlarged apex pointing toward right positioned left in thorax cavity atrial septal defect	Chiang *et al.*, 1996 Tsukui *et al.*, 1999 Washington Smoak *et al.*, 2005
Ptch1	lethality between E9.0 and E10.5 the heart is not properly formed	Goodrich *et al.*, 1997
Smo	lethality around E9.5 linear heart tube	Zhang *et al.*, 2001
Sufu	lethality between E9.0 and E10.5 dilated descending aorta abnormal cardiac looping	Cooper *et al.*, 2005

The cardiac neural crest cells, a subgroup of neural crest cells, is essential for cardiovascular development (Kirby *et al.*, 1983). Neural crest cells undergo apoptosis in the absence of the Shh signal, indicating the necessity of the Shh the survival of neural crest cells in mice (Jeong *et al.*, 2004). Washington Smoak and colleagues demonstrated that though the neural crest cells were correctly specified and migrated into OFT, neural crest cells were mislocalized in OFT and underwent apoptosis in *Shh*$^{-/-}$ mouse (Washington Smoak *et al.*, 2005). The tissue specific gene ablation study of the Goddeeris group further clarified the role of the Shh signal in heart development. The secondary heart field contributes to OFT and right

ventricle development and both cardiac neural crest cells and secondary heart field are adjacent to pharyngeal endoderm in which Shh is expressed during embryonic morphogenesis. Thus, Goddeeris and colleagues posited that pharyngeal endoderm SHH expression is crucial for OFT septation because it affects cardiac neural crest cells and the secondary heart field (Goddeeris et al., 2007).

In a subsequent study, Goddeeris colleagues demonstrated that the secondary heart field derived cells distributed into the dorsal mesenchyme and dorsal myocardial wall of the atria at E10.5, the dorsal mesenchymal protrusion that wedges into the atria at E11.5, and much of the primary atrial septum at E12.5 to E16.5. When *Smo* was ablated in secondary heart field derived cells, the mutant mouse exhibited intracardiac septation defects similar to those in *Shh*$^{-/-}$ mice. These septation defects resulted from abnormal dorsal mesenchym differentiation and migration. These findings suggest an important role of the secondary heart field in atrial septum development (Goddeeris *et al.*, 2008). Hoffmann and colleagues identified the migration of Shh responsive cells from the secondary heart field into the atrial septum. Further study demonstrates that the Shh signal is not necessary for cell migration from secondary heart field into the atrial primordium, but is essential for the specification of cardiac progenitors in the secondary heart field (Hoffmann *et al.*, 2009). This data indicates that atrial septum development requires the proper Shh response in the secondary heart field. The disruption of Shh response in the secondary heart field could produce atrial septal defects.

1.5 Interaction of Wnt and Hedgehog signaling

1.5.1 Wnt signaling

The Wnt signaling pathway involves a large number of proteins whose interactions regulate embryogenesis (Dickinson and McMahon, 1992; Levay-Young and Navre, 1992; McMahon and Bradley, 1990), normal physiological processes in adult animals (Gavin et al., 1990; Iozzo et al., 1995; Sussman et al., 1994; Van Den Berg et al., 1998) and also cancer development (Dale et al., 1996; Hart et al., 1998; Iozzo et al., 1995). Although the presence and effects of the signaling depend on the Wnt ligands, cell types and organisms, some members in the pathway are remarkably similar between *Caenorhabditis elegans* and humans (Cadigan and Nusse, 1997; Gavin et al., 1990). The Wnt pathway includes two categories: the canonical Wnt pathway and the non-canonical Wnt signaling (Moon et al., 2002; Ziemer et al., 2001).

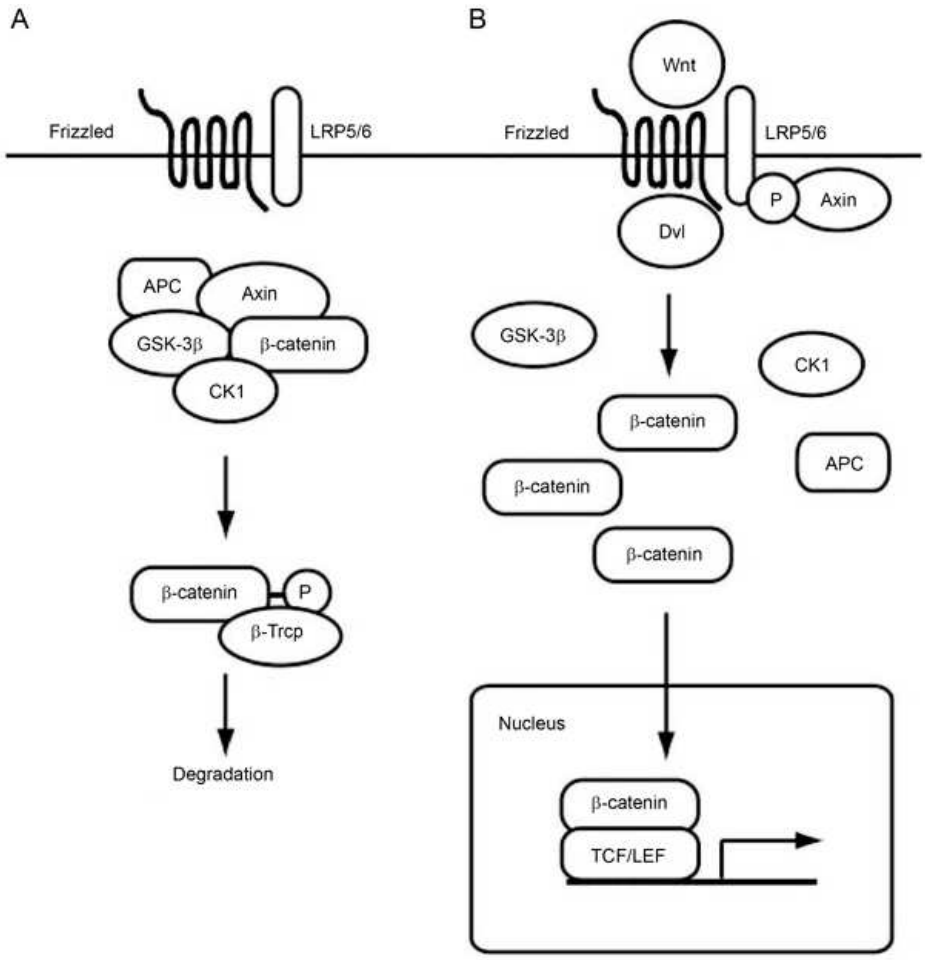

Figure 1.10 A schematic diagram of selected components of the canonical Wnt signaling (adapted from Nemeth et al., 2007).
(A) In the absence of the Wnt ligand, the Frizzled receptor, and LRP 5/6 co-receptor promotes the formation of a complex, including APC, Axin, GSK-3β and CK1, that induces the phosphorylation and subsequent degradation of β-catenin. In the absence of β-catenin, repressor proteins bind to the TCF/LEF transcription factors and prevent the translation of downstream genes. (B) In the presence of the Wnt ligand, co-receptors LRP5/6 are phosphorylated by membrane-bound casein kinase 1γ and GSK-3β. The phosphorylated LRP 5/6 recruit Axin to the cell membrane and disrupt the multi-protein complex. Without multi-protein complex, β-catenin accumulates and translocates to the nucleus, interacts with TCF/LEF, and induces the translation.

The canonical Wnt pathway begins when Wnt proteins bind to the cell surface receptors of the Frizzled family, activating the Disheveled family proteins. This consequently stabilizes cytoplasmic β-catenin, which enters

the nucleus and promotes specific gene expression (Boutros *et al.*, 2000; Habas *et al.*, 2001) (Figure 1.10). Without Wnt proteins, the axin/GSK-3/APC complex promotes the proteolytic degradation of the β-catenin and inhibits the transcription of downstream genes (Hsu et al., 1999; Kishida et al., 1998; Willert et al., 1999). Unlike canonical Wnt signaling, non-canonical Wnt pathway is β-catenin-independent (Moon et al., 2002; Ziemer et al., 2001).

1.5.2 Interactions of Shh and Wnt signaling

The Wnt and Shh signaling pathways are critical for the development and maturation of many mammalian tissues. However, the interaction between these pathways in mammalian systems remains unclear (Alvarez-Medina et al., 2008; Borycki et al., 2000; Lei et al., 2006). In patterning the neural tube, the Wnt likely works in an indirect inhibitory manner on sonic hedgehog. The Wnt signals from the dorsal neural tube function as mitogenic signals for neural tube cells (Cayuso and Marti, 2005; Dickinson et al., 1994; Megason and McMahon, 2002) and play a role in cell fate specification (Muroyama *et al.*, 2002). On the other hand, the activity of the Shh from the ventral neural tube is the major signaling pathway, and generates distinct classes of neurons in dorsal ventral neural tube (Jessell, 2000; Stamataki *et al.*, 2005). Several studies on mice and chickens demonstrate that Wnt activates and controls the expression of Gli3, one of the main inhibitors repressing the transcriptional activity of Shh/Gli in the dorsal region of the neural tube, and elicits dorsal cell fates (Alvarez-Medina et al., 2008; Borycki et al., 2000; Lei et al., 2006).

The Wnt and hedgehog signaling pathways in mice help establish boundaries between the oral and dental ectoderm to correctly determine the site of tooth formation (Sarkar et al., 2000). Ectopical expression of Wnt-7b in presumptive dental ectoderm in the mandibular arch explants leads to the down-regulation of the Shh expression in the ectoderm and the Ptc expression in the underlying ectomesenchyme, and subsequently arrests the tooth development. However, tooth development was complete rescue as implantation of beads soaked in Shh protein into Wnt-7b infected explants demonstrated the Wnt signaling specifically represses Shh signaling (Sarkar et al., 2000).

The expression of Shh expression is down-regulated in both Lef1 or Wnt10b knockout mice, where the Wnt/β-catenin signaling is eliminated (Iwatsuki et al., 2007). Organ culture demonstrates that activation of Wnt/β-catenin signaling up-regulates the expression of Shh (Iwatsuki et al., 2007). Furthermore, blocking Shh signaling in cultured tongue explants up regulated the Wnt/β-catenin signaling and subsequently enhanced papillae formation. This suggests that Wnt/β-catenin signaling plays a central role in the development of fungiform papillae and regulating Shh expression, while Shh inhibits the Wnt/β-catenin signaling (Iwatsuki et al., 2007).

Though Wnt and Shh are both important for tissue development, their interaction and regulation vary in different tissues (Borycki et al., 2000; Iwatsuki et al., 2007; Sarkar et al., 2000).

1.6 Cilium

1.6.1 Ciliary structure

Cilia, microtubule-based organelles, exist in almost all cells. The two major parts of cilia are the basal body and the axoneme. The basal body is structurally identical, but adds proteins to one of the centrioles, structures that are important components of mitotic spindle and facilitate the proper chromosome segregation in cell division. When cells become quiescent, centrioles move to the plasma membrane and the mother centriole forms the basal body as an anchor point of the later assembled axoneme. The axoneme consists of nine peripherally located doublet microtubules with (9+2; motile cilia) or without (9+0; primary cilia and nodal cilia) a central microtubule pair (Figure 1.11) (Satir, 2005). In motile cilia, the axoneme is a 9+2 arrangement characterized by the radial spokes and dynein arms that contribute to ciliary beating. The most well known cells containing motile cilia are the epithelium cells of the respiratory tract, which are responsible for moving mucus. Without a central doublet microtubule, primary cilia are generally immotile with one exception, the nodal cilia. Although without a central microtubule pair, nodal cilia have radial spokes and dynein arms and are motile to generate leftward flow in the embryonic node cells during development (Nonaka *et al.*, 1998). When the KIF3B protein, an intraciliary transport motor, was disrupted in mouse, nodal cilia were absent and the establishment of left-right asymmetry was disrupted. Though primary cilia were considered a nonfunctional organelle for years, recent studies reveal the correlations between primary cilia and human disease.

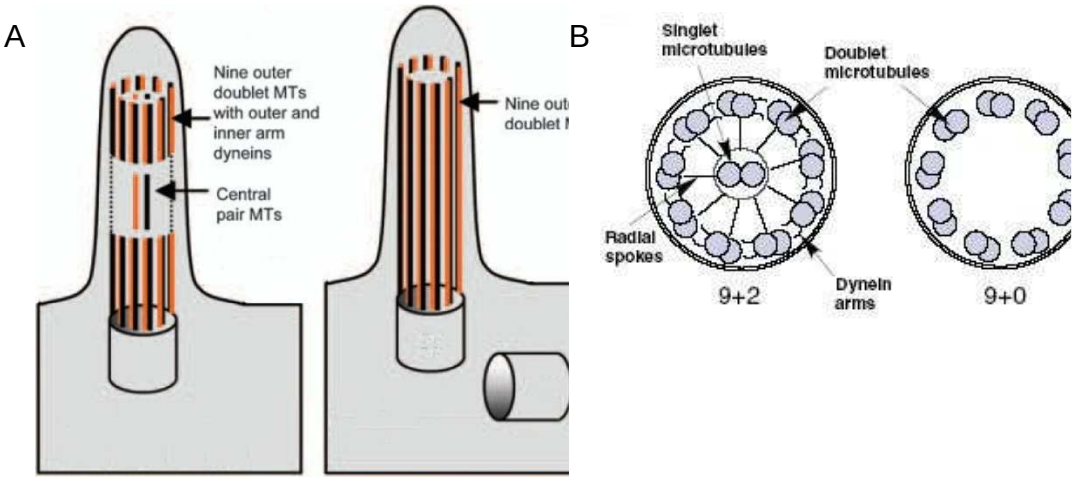

Figure 1.11 Schematic view of cilium

(A) The 9+2 cilum (left) was composed of nine outer doublet microtubules while the 9+0 cilium (right) lacks the central pair microtubules (adapted from Christensen *et al.*, 2007). (B) Transverse view of the 9+2 and 9+0 cilum shows that the dynein arms and radial spokes associate with 9+2 cilium and these structures could not be observed in 9+0 cilium (adapted from Bisgrove & Yost, 2006).

1.6.2 Intraflagellar transport

Elongation of the axoneme from the basal body, ciliogenesis, is completed by adding new subunits to the distal tip of the axoneme. As the cilia do not synthesize proteins, ciliogenesis depends on a system called intraflagellar transport (IFT) to complete the material transport. Kozminski et al. first described the IFT system in green alga (Kozminski *et al.*, 1993). At least 15 polypeptides participate in IFT complexes. The proteins in IFT complexes have been grouped into two subsets: complex A containing four or five polypeptides and complex B containing at least twelve polypeptides (Cole *et al.*, 1998; Piperno *et al.*, 1998). Because the microtubules in cilia are oriented with the plus end at the tip of the organelle, two different motors are required to complete the movement in the IFT system. The anterograde transport (from basal body to cilia tip) of the IFT particles is driven by the

heterotrimeric motor Kinesin-2 and the retrograde transport (from cilia tip to basal body) depends on the dynein motor (Figure 1.12).

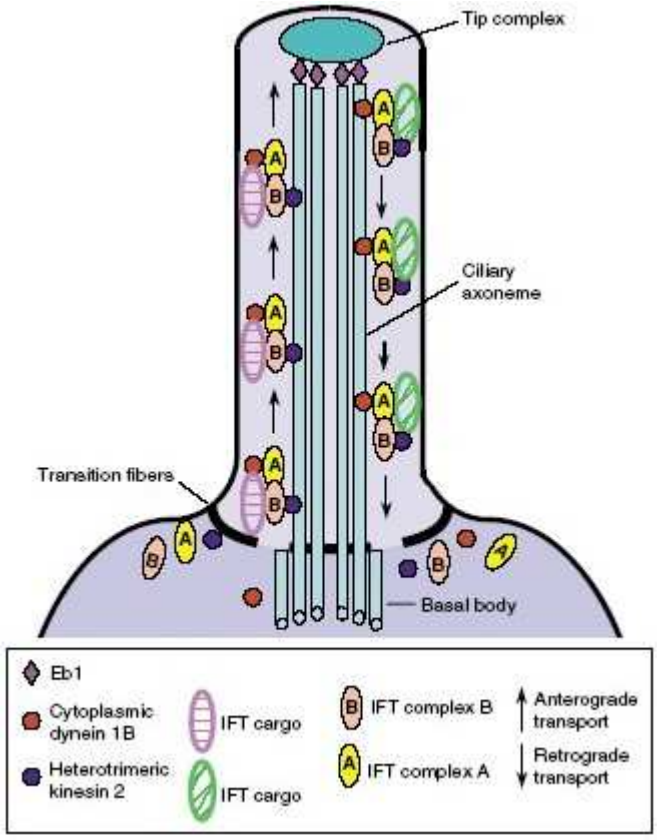

Figure 1.12 Intraflagellar transport (adapted from Bisgrove & Yost, 2006) Kinesin and dynein are responsible for anterograde and retrograde transport along the axoneme respectively.

A study in 2001 found that IFT52 was located on the transitional fibers, which are Y-shaped fibers connecting the microtubule outer doublets to the ciliary membrane just distal to the basal body. The transition zone, which is demarcated by the transition fibers, is thought not only to be a docking region for IFT particles but may also function as a filter controlling the molecular transport between cilia and cytoplasm. This speculation is based on evidence that the retinitis pigmentosa GTPase regulator (RPGR), a GTP exchange factor, appeared at the transition zone of cilia (Hong *et al.*, 2001; Hong *et al.*, 2003).

1.6.3 Function of cilium

First described decades ago, primary cilia were initially considered a vestigial organelle with unknown physiological function. In 1985, by analyzing primary cilia in chondrocyte, Poole and colleagues suggested that primary cilia have enormous potential to function as a chemical and physical sensory device (Poole *et al.*, 1985). Using chick embryo sternal cartilage as a tissue model, researchers discovered that primary cilia interacted with and were deflected by the extracellular matrix in 2001 (Poole *et al.*, 2001). The mechanosensor function of primary cilia was also reported when studying the human autosomal-recessive polycystic kidney disease. Abnormal short or absent of primary cilia appeared in mice with a mutation in the polycystic kidney disease gene, Tg737 (Pazour *et al.*, 2000). Other studies demonstrate that the bending of primary cilia caused the increase of intracellular Ca^{2+} in MDCK cells and such response was abolished when primary cilia were removed (Praetorius and Spring, 2001; Praetorius and Spring, 2003). The biochemosensory function of primary cilia was revealed in the study of the receptor tyrosine kinase platelet-derived growth factor receptor alpha (PDGFRα). Schneider *et al.* demonstrated that PDGFRαα, the homodimer of PDGFRα, targeted to the primary cilia and responded to the specific ligand in growth-arrested NIH3T3 cells and primary cultured mouse embryonic fibroblasts. This response did not appear in fibroblasts from Tg737 mutated mice with disrupted formation of primary cilia (Schneider *et al.*, 2005).

1.6.4 Mutations of genes encoding ciliary proteins

Bardet-Biedl syndrome (BBS, MIM 209900) is a rare genetic disease with clinical features including obesity, renal malformations, polydactyly, congenital heart defects and diabetes (Katsanis *et al.*, 2001). Twelve genes (*BBS1~ BBS12*) have been identified as mutated in this syndrome. Among these twelve, the BBS7 and BBS8 proteins are located at the base of the cilia. Blacque and coworkers found that the mutations of *bbs7* and *bbs8* genes in *C. elegans* cause structural and functional defects in the cilia. They suggested that BBS7 and BBS8 play important, selective roles in the normal localization/motility of IFT particle components (Blacque *et al.*, 2004).

Oro-facial-digital type 1 syndrome (MIM 311200) is a human developmental disorder characterized by craniofacial and digital abnormalities. Polydactyly in the limbs of *Ofd1*$^{\Delta 4\text{-}5/+}$ newborn females indicates that oral-facial-digital type 1 (OFD1) protein might be involved in the Shh signaling pathway (Ferrante *et al.*, 2006). OFD1 is associated with IFT machinery (motors and IFT particles), and is essential for the formation of primary cilia (Ferrante *et al.*, 2006).

Nephronophthisis (NPHP) encompasses a polygenic group of autosomal recessive cystic kidney diseases in children and young adults. Previous studies link mutations in six NPHP genes (NPHP1 - NPHP6) to NPHP (Hildebrandt et al., 1997; Mollet et al., 2002; Olbrich et al., 2003; Otto et al., 2002; Otto et al., 2003; Otto et al., 2005; Sayer et al., 2006). Moreover, NPHP proteins contain multiple protein-protein interaction domains and

appear to function as a complex in the primary cilia/basal body/centrosome apparatus (Olbrich *et al.*, 2003; Otto *et al.*, 2003; Otto *et al.*, 2005). Although *C. elegans* with mutated *nph-4* show no structural defects in cilia, their abnormal cilia-mediated sensory functions indicate that these proteins play a role in ciliary signaling (Winkelbauer *et al.*, 2005; Wolf *et al.*, 2005).

1.7 Summary of previous studies on Evc

Previous research on this topic demonstrates that mouse EVC is expressed at bone growth plates using β-gal as the reporter of Evc protein. The heart development defects appearing in 60% of the EvC patients demonstrate the importance of EVC protein in heart development. However, this study does not investigate whether *Evc*$^{-/-}$ mouse develops the heart defects appearing in EvC patients or the expression of Evc in developmental heart. The investigation of Evc in developmental heart reveals the pathomechanism of Evc in heart defects.

Subcellular studies demonstrate that Evc is expressed around the basal body of the cilia, which are important structures in Hh signaling. The relationships between Evc, the cilia, and the Hh signal remain unclear. Previous studies demonstrate that mutant ciliary proteins may cause abnormalities in the ciliary structure that lead to Hh signaling defects. Since the Ihh signal was perturbed in *Evc*$^{-/-}$ mice and Evc protein was localized to the region around the basal body, this study examines the cilia structure in the absence of the Evc protein. Although results strongly suggest the involvement of Evc in the Hh signaling pathway, the exact function of the Evc protein remains unknown.

Yeast two-hybrid analysis shows some plausible Evc interacting proteins,

including Evc2, Snx 5, and Snx 6 (Dr. S Tompson, personal communication). Although co-immunoprecipitation and co-localization studies confirm the interaction between Evc and Evc2 proteins, this study does not analyze the importance of the interaction of these two proteins. Confirming the interaction of Evc with Snx5 and Snx6 is a major priority for future research.

1.8 Aims

The main purposes of this study as follows.

- To analyze heart development in *Evc*$^{-/-}$ mice (Chapter 3).
- To characterize *Evc* expression in developmental heart in mice (Chapter 3).
- To determine the precise localization of Evc protein in cells (Chapter 4).
- To document the ciliary structure of *Evc*$^{-/-}$ cells (Chapter 4).
- To document the subcellular distribution of the potential Evc interacting proteins in *Evc*$^{-/-}$ cells (Chapter 4).

Chapter 2 Materials and methods

2.1 Mice

Evc$^{-/-}$ mice were generated by an inframe fusion of the β-galactosidase (β-gal) gene (*lacZ*) to the first amino acid of Evc and ablated gene function by deleting the remaining downstream *Evc* exon 1 sequence as previously described (Ruiz-Perez *et al.*, 2007). Mice carried the C57Bl/6J X 129Sv mixed genetic background. *Vangl2*$^{+/-}$ mice were kindly provided by Dr. Deborah Henderson. Noon of the day the vaginal plug appeared was considered as E0.5 when estimating the embryonic stage.

All mouse strain maintenance and experimental procedures were performed at the Functional Genetics Unit (FGU) of the Institute of Human Genetics, Newcastle University, UK in compliance with the regulations of the Animal Procedures Committee, Home Office, UK, and relevant local regulations.

2.2 Antibodies

Table 2.1 and 2.2 list the primary and secondary antibodies used in this study.

Table 2.1: Primary antibodies used in this study

Specificity	Host	Source	Clone	Immuno-fluorescence stain	Western blot
α-tubulin	Mouse	Sigma	B-5-1-2	-	1:10,000
γ-tubulin	Mouse	Sigma	GTU-88	1:400	1:400
Acetyl-tubulin	Mouse	Sigma	6-11B-1	1:1,000	-
Actin	Rabbit	Sigma	Polyclonal	-	1:2,000
c-Jun	Rabbit	Cell Signaling	60A8	-	1:1,000
EVC (Human)[#]	Sheep	Self produced (S42B)	Polyclonal	-	-
Evc (Mouse)[*]	Sheep	Self produced (S43B)	Polyclonal	1:400	1:400
Evc2 (Mouse)	Goat	Santa Cruz	Polyclonal	1:200	1:200
Snx5	Rabbit	Santa Cruz	Polyclonal	-	1:1,000
Snx6	Goat	Santa Cruz	Polyclonal	-	1:1,000
SuFu (Human)	Goat	Santa Cruz	Polyclonal	1:50	-

[#]Epitope: aa235-Stop (Genebank: NP_714928) (Ruiz-Perez *et al.*, 2007)

[*]Epitope: aa459-999 (Genebank: NP_067267) (Ruiz-Perez *et al.*, 2007)

Table 2.2: Secondary antibodies used in this study

Specificity	Host	Source	Conjugation	IF	Western blot
Goat IgG	Donkey	Molecular Probe	FITC	1:200	-
Goat IgG	Donkey	Santa Cruz	HRP		1:2,000
Mouse IgG	Rabbit	Jackson ImmunoRearch Laboratories	AMCA	1:400	-
Mouse IgG	Goat	Sigma	FITC	1:200	-
Mouse IgG	Goat	Pierce	HRP	-	1:4,000
Mouse IgG	Horse	Vector Laboratories	Texas Red	1:200	-
Rabbit IgG	Goat	Jackson ImmunoRearch Laboratories	HRP	-	1:20,000
Sheep IgG	Donkey	Molecular Probes	AlexaFluor 594	1:400	-
Sheep IgG	Donkey	DAKO	HRP	-	1:1,000

2.3 Genomic DNA extraction

Ear punch biopsies (2 mm diameter hole punch) were taken from 21-30 day old mice. Wiping the ear punch with 100% ethanol prevented cross contamination between animals. For DNA extraction, ear clippings from mice, tails from mouse embryos and MEFs were heated in 100µl of 25mM NaOH and 0.2mM EDTA at 95^{o}C for 20 minutes. The solution was then neutralized with 100µl of 40mM Tris-HCl (pH5.0). After vortexing, samples were used directly or stored at -20 ^{o}C for further processing.

2.4 Genotyping

2.3.1 *Evc* genotyping

For *Evc* genotyping, both *LacZ* and *Evc* exon 1 PCR products were amplified simultaneously. Amplification (10µl) was performed in the presence of genomic DNA, 1X PCR buffer (with $MgSO_4$) (Promega), 20µM dNTP (Roche), 0.25µM of each primer and 0.5U Taq DNA Polymerase (Promega) in a tube overlayed with mineral oil. Normal PCR cycles were 1 cycle of 94 ^{o}C, 4 minutes; 30 cycles of 94 ^{o}C, 30 seconds; 60 ^{o}C, 1 minute; 72 ^{o}C, 1 minute and 1 cycle of 72 ^{o}C, 10 minutes in a thermal cycler (Thermo).

Ten microliters of PCR product were mixed with 2µl of 6X loading dye (New England BioLabs Inc.) and subjected to electrophoresis on 2% agarose gel, containing 0.5µg/ml ethidium bromide in 1X TAE buffer at 100V for 50 minutes. A quick-Load 100bp DNA ladder (New England BioLabs Inc.) was used as the molecular weight marker. The gels were then scanned by a

Gene Genius Bio-Imaging System (Syngene, Synoptics Ltd) with GeneSnap version 7.04 software.

Evc exon 1 was amplified by primer set 5'-CGGCGGGATGCGGCGGGTCAC-3'and 5'-GCGCGACAGCCAAGCCACAAG-3', which produced a 170bp fragment in DNA isolated from the wild type and $Evc^{+/-}$ mice. The 475bp *lacZ* gene fragment was amplified by primer set 5'-GCGACTTCCAGTTCAACATC-3' and 5'-GATGAGTTTGGACAAACCAC-3' from DNA samples extracted from $Evc^{+/-}$ and $Evc^{-/-}$ mice.

2.3.2 *Vangl2* genotyping

Vangl2 genotyping was based on direct sequencing. Primers were designed with Primer3 (Rozen and Skaletsky, 2000) and synthesized by MWG-Biotech (Ebersberg, Germany). The *Vangl2* exon8 containing the G>A transition mutation at position 1391 was amplified by primer set 5'-GAATGAGCATAGAAACACCCTAGC-3' and 5'-AAACAAGAGCAAGAGGAAGTAGGA-3'. Amplification (20µl) was performed in the presence of genomic DNA, 1X PCR buffer (with $MgSO_4$) (Promega), 200µM dNTP (Roche), 1µM of each primer and 2.5U Taq DNA Polymerase (Promega) in a tube overlaid with mineral oil. Normal PCR cycles were 1 cycle of 94^{o}C, 4 minutes; 30 cycles of 94^{o}C, 1 minute; 55^{o}C, 1 minute; 72^{o}C, 1 minute and 1 cycle of 72^{o}C for 10 minutes in a thermal cycler (Thermo).

For purification, 1µl Exonuclease (NEB) and 1µl Shrimp Alkaline Phosphatase (USB) were added to 5µl of PCR product and the mixture was

incubated at 37^{o}C for 20 minutes then at 80^{o}C for 20 minutes. Sequencing reactions were performed with the same primer set using the Dye Terminator Cycle Sequencing Kit for MegaBACE DNA Analysis System (Amersham Biosciences). The sequencing reaction program was 1 cycle of 95^{o}C, 1 minute and 20 seconds; 30 cycles of 95^{o}C, 30 seconds; 55^{o}C, 15 seconds and 1 cycle of 60^{o}C, 1 minute in a thermal cycler (Thermo).

To precipitate the reaction product, 80µl of 80% isopropanol (BDH) was added to 20µl of the reaction product and incubated in the dark for 15 minutes. The mixture was centrifuged at 3000rcf for 30 minutes and the supernatant was discarded. An inverted spin at 700rcf for 30 seconds was performed to remove any remaining isopropanol. The sample palette was air dried and resuspended in a 10µl MegaBACE loading solution (Amersham Biosciences). MegaBACE, by IHG Sequencing Service, was used to analyze the sequencing products. Chromas Lite Version 2.01 (Technelysium) was used to analyze the sequencing data

2.5 Histological analysis

2.5.1 Preparation of samples

E13.5 and E14.5 embryos were dissected in PBS. The embryos were then fixed in 4% paraformaldehyde (PFA, Sigma) in PBS at 4 ^{o}C for 20 minutes. A Shandon Pathcentre Tissue Processor (Thermo Electron Corporation) performed the embedding procedures. The embryos were dehydrated in 70% ethanol for 30 minutes, in 95% ethanol for 1 hour, in 100% ethanol for 105 minutes, and in 100% ethanol for 2 hours. Tissues were then cleared by incubation in 100% xylene for 105 minutes and two changes of 100%

xylene for 2 hours. Specimens were further washed in two changes of paraffin wax at 60 ^{o}C for 105 minutes and two changes of paraffin wax at 60 ^{o}C for 2 hours. Specimens were then embedded in cooling paraffin wax.

Samples were sectioned (7µm thickness) by the microtome. The sections were then placed on water-covered slides. After removing superfluous water, the samples were placed into a 37 ^{o}C incubator for two days to ensure that sections were entirely dried out and firmly fixed on the slides.

2.5.2 Hematoxylin and Eosin staining

Immersion in two changes of a histological clearing reagent (Histo-clear) for 5 minutes removed the paraffin wax from the sections. Sections were rehydrated in serial concentrations of ethanol (100%, 75%, and 50%) for 5 minutes. After rinsing with ddH_2O, the sections were stained in Harris haematoxylin solution (Raymond A Limb) for 20 seconds and then washed in running water for 45 seconds to allow the stain to develop. The samples were rinsed in ddH_2O followed by staining in 1% Eosin (Raymond A Limb) for 30 seconds. After rinsing in ddH_2O, the samples were immersed in serial concentrations of ethanol (50%, 75%, and 100%) for 3 seconds. After clearing in a histological clearing reagent, the slides were mounted in histomount solution (Vector Laboratories). An Axioplan 2 imaging/AxioCam HRc microscope (Zeiss) was used to observe the slides. Photographs were processed with AxioVision Release 4.5 (Zeiss).

The basic dye, hematoxylin, produced a blue-purple stain on the basophilic structures, such as the nucleus and the RNA-rich cytoplasmatic regions, whereas eosin produced a bright pink stain on eosinophilic structures,

composed of intracellular or extracellular protein.

2.5 X-Gal staining

2.5.1 Whole-mount X-Gal staining

E11.5 and E12.5 embryos were dissected in PBS (pH7.3) and fixed in freshly prepared X-gal fixation solution containing 1% formaldehyde (Sigma), 0.2% glutaraldehyde (Sigma), 5mM EGTA (pH7.3, Sigma), 2mM $MgCl_2$ and 0.02% NP40 in PBS at 4^{o}C for 1 hour. The samples were washed three times in 0.02% NP40 in PBS at room temperature for 30 minutes. X-gal reaction was performed in X-gal substrate solution containing 5mM $K_3Fe(CN)_6$ (Sigma), 5mM $K_4Fe(CN)_6$ (Sigma), 5mM EGTA (pH7.3), 2mM $MgCl_2$, 0.02% NP40, 0.01% Na Deoxy Cholate, and 1mg/ml X-Gal overnight at 37 ^{o}C.

2.5.2 Preparation of sections

After the X-gal reaction, the samples were manually embedded in paraffin wax to prevent damage to the tissues. Embedding procedures were similar to that of the Shandon Pathcentre Tissue Processor (Thermo Electron Corporation) (Section 2.5.1) with a slightly different solution and incubation period. The embryos were dehydrated in 50% ethanol for 1 hour (once), in 70% ethanol for 1 hour (twice), in 95% ethanol for 1 hour (once) and in 100% ethanol for 1 hour (twice). Tissues were then cleared by incubation in two changes of histological clearing reagent for 20 minutes and histological clearing reagent/wax (1:1) at 65 ^{o}C for 20 minutes. Specimens were further washed in three changes of paraffin wax at 65 ^{o}C for 40 minutes and then

embedded in cooling paraffin wax.

Sections (14μm thickness) were prepared by a microtome and firmly attached to the slides as previously described (Section 2.5.1). Samples were twice immersed in histological clearing reagent for 5 minutes to remove the wax and then immersed for 5 minutes in each serial concentration of ethanol (100%, 75%, and 50%) to rehydrate them. After rinsing with ddH_2O, the samples were stained in nuclear fast red solution for 2 minutes and rinsed in ddH_2O. Then, the samples were immersed in serial concentrations of ethanol (50%, 75%, and 100%) for 3 seconds and a histological clearing reagent for 3 minutes. Slides were mounted in histomount solution and observed with an Axioplan 2 imaging/AxioCam HRc microscope. Photographs were processed with AxioVision Release 4.5.

2.7 *In situ* hybridization

2.7.1 Probes preparation

The plasmids containing *Shh*, *Ptc*, and *Evc* cDNA were kindly provided by Dr. M. Nakatomi. The details of probes were listed in Table2.3. For linearization, 30μg of plasmid was incubated overnight in 200μl of a relevant restriction enzyme and restriction buffer (HindIII for *Shh*, BglII for *Ptc*, and NotI for *Evc*) at 37 ^{o}C. 200μl ddH_2O with vortex and 400μl phenol/chloroform/isoamyl alcohol (25:24:1) (Sigma) with vortex were then added. After centrifuging at 12000rcf at 4 ^{o}C for 5 minutes, 380μl of the resulting supernatant was transferred into a new tube and mixed with an equal volume of chloroform. This mixture was then centrifuged at 12000rcf

at 4 ^{o}C for 5 minutes, after which, 350µl of supernatant was transferred into a new tube and mixed with 35µl of vortexed 3M NaOAc. 1ml 100% ethanol was added and the solution gently mixed prior to incubating at -80 ^{o}C for 1 hour. After centrifuging at 13000rcf at 4 ^{o}C for 20 minutes, the pellet was washed with 1ml of 70% vortexed ethanol. This was then centrifuged at13000rcf at 4 ^{o}C for 3 minutes, the supernatant was discarded, and the pellet was air-dried. Next, the pellet was suspended in a 20µl TE buffer and the concentration was measured. A transcription reaction was performed at 37 ^{o}C for 3 hours in 20µl total volume containing 1µg DNA, 2µl 10X buffer (Roche), 2µl Dig Mix (Roche), 1µl RNase inhibitor (Promega) and 2µl relevant polymerase (Roche; T3 for *Shh*, T7 for *Ptc*, and Sp6 for *Evc*). The products were mixed with 80µl TE buffer, 10µl 4M LiCl, and 250µl 100% ethanol gently shaken and incubated at -20℃ overni ght. After centrifuging at 13000rcf at 4 ^{o}C for 20 minutes, the supernatant was discarded and the pellet was air dried and suspended with 100µl TE buffer.

Table 2.3 Detail of probes used in this study

Probe Targeting Gene	Size (bp)	Location of Probe
Evc	792 bp	926-1717 (NM_021292)
Shh	643 bp	20-762 (NM_009170)
Ptc	4.3 kb	Full length (NM_008957)

2.7.2 Hybridization

The sections were deparaffinized two times in xylene for 5 minutes, two times in 100% ethanol for 5 minutes, two times in 70% ethanol for 5 minutes, and two times in PBS (pH7.4) for 10 minutes. After deparaffinization, the sections were treated with 200µg/ml of ProteaseK for

10 minutes and 2mg/ml of glycine for 10 minutes. The sections were then washed in PBS (pH7.4) for 5 minutes and fixed in 4% PFA in PBS (pH7.4) for 20 minutes. After washing in PBS (pH 7.4) three times for 5 minutes, the sections were immersed in water that was continually stirred for 10 minutes. This water contained 1.325% (v/v) triethanolamine, 0.175% (v/v) HCl, and 0.25% (v/v) acetic anhydrate, which was injected into the water at the rate of 100µl/15sec. The sections were washed in PBS (pH 7.4) three times for 5 minutes and then incubated with a hybridization buffer containing 50% formamide, 10mM Tris-HCl pH 7.6, 100µg/ml yeast tRNA, 1X Denhardt's solution, 5% Dextran sulphate, 600mM NaCl, 0.25% SDS, and 1mM EDTA pH 8.0 for 1hour. Probes were mixed with the hybridization buffer and denatured at 80^{o}C for 10 minutes. After applying the probes, the sections were covered with paraffin to avoid drying during incubation. The incubation chamber was kept humid by placing inside the chamber a 30ml solution containing 50% formamide, and 2X SSC. The whole chamber was covered by cling film. The sections were incubated overnight with probes at 70 ^{o}C. After incubation, the paraffin was removed with 5X SSC pH7.0 at 70 ^{o}C . The sections were washed in 2X SSC pH7.0 at 70 ^{o}C for 1 hour, all the while being gently shaken. After washing for 5 minutes with TBS containing 10mM Tris-HCl pH7.6 and 150mM NaCl, the sections were incubated with a blocking solution containing 100mg of blocking reagent/10ml TBS for 1 hour. The sections were then incubated overnight with the anti-Dig antibody (1µl/5ml TBS) at 4 ^{o}C. Next, the sections were washed in TBS three times for 5 minutes and, then, washed for 5 minutes in NTM solution containing 100mM Tris-HCl pH9.6, 100mM NaCl, and 5mM $MgCl_2$. A reacting solution containing 9% polyvinylalcohol, 90mM NaCl, 100mM

Tris-HCl pH9.6, 5mM $MgCl_2$, and 0.5% (v/v) NBT/BCIP solution was applied to the sections to start color development. To stop the reaction, the sections were rinsed with TBS, immersed in PBS for 5 minutes, and covered by cover glass with a mounting medium.

2.8 Cell culture

All cells were grown in a humidified atmosphere with 5% CO_2 at 37 ^{o}C.

2.8.1 Murine inner medullary collecting duct cells (mIMCD-3)

mIMCD-3 cells originally obtained from ATCC (Cat: CRL-2123^{TM}) were kindly provided by Dr. L. Eley. mIMCD-3 were grown in DMEM/F-12 (v/v = 1:1) supplemented with 10% fetal bovine serum (FBS) and 10% non-essential amino acids. In the case of purmorphamine treatment, cells were grown in a medium with 2μM of purmorphamine for 72 hours.

2.8.2 Mouse embryonic fibroblasts (MEFs)

Mouse embryonic fibroblasts were kindly generated from *Evc*$^{-/-}$ and wild type mice by Dr. H. Blair. MEFs were grown in DMEM supplemented with 10% FBS, 10% non-essential amino acids, and 5% penicillin/streptomycin. To induce cilia formation, cells were cultured in a serum free medium for 16-20 hours following the experiment.

2.8.3 Primary culture of osteoblasts and chondrocytes

The tibial cartilage and calvarial bone were dissected from mouse embryos at E18.5 and placed into a PBS containing 2% penicillin/streptomycin and 1% ampateracin. Then the tissues were treated with a 0.1% hyaluronidase

solution for 5 minutes, a 0.25% trypsin solution for 10min and a 0.3% collagenase solution for 4 hours. All solutions were prepared freshly and the treatments were performed with gentle rotation at 37 ^{o}C. The solution with the cells was centrifuged at 5,000rcf for 5 minutes. After discarding the supernatant, the pellets were resuspended in a medium containing 25mM HEPES, 10% FCS, 1% L-glutamine, 2% penicillin/streptomycin, 1% fungizone, and 1% non-essential amino acids and then plated on an 8-well chamber slide (Nunc) or Culture Inserts (Nunc). For cilia generation, cells were cultured in a serum free medium for 16-20 hours.

2.9 Deciliation

After washing with PBS, the cells were treated with 15.7mM Tris-HCl (pH7.5), 79.1mM NaCl, 1.56mM EDTA, 0.1% Triton X-100, 30mM $CaCl_2$, 1X protease inhibitor (Roche) and 0.5mM phenylmethanesulphonylfluoride (Roche) for 5 minutes at room temperature to remove the cilia (Fliegauf et al., 2006). After collecting the solution, the cells were then washed with PBS and were ready for the Immunofluorescence staining. The collected solution was centrifuged at 16,000rcf for 10 minutes at 4 ^{o}C. The supernatant was discarded and the pellets were resuspended in 3µl PBS and spotted onto a charged slide (Menzel-Gläser). After drying at 37 ^{o}C, the slide was finally ready for Immunofluorescence staining.

2.10 Immunofluorescence staining

A serum free growth medium induced cilia formation in cells cultured on a slide flask. Cells before and after deciliation treatment as well as the deciliated cilia

were collected and fixed in 4% PFA in PBS for 20 minutes at 4^{o}C and then washed three times for 5 minutes in PBS. The samples were treated with 0.1% Triton X-100 in PBS for 10 minutes at room temperature then washed twice for 5 minutes with PBS. After treating with PBST (0.1% Tween 20 in PBS) for 5 minutes at room temperature, the samples were incubated in 10% normal horse serum (Vector Laboratories) in PBST for 1 hour at room temperature. The samples were then incubated with the primary antibody (Table 2.1) and diluted in PBST containing 10% normal horse serum for 2 hours at room temperature. After washing three times for 10 minutes in PBST, the samples were exposed to the secondary antibody (Table 2.2) for 45 minutes at room temperature. The samples were then washed three times for 10 minutes in PBST and then mounted with a mounting medium containing 4'-6-diamidino-2-phenylindole (DAPI) (Vector Laboratories). When the AMCA conjugated secondary antibody was applied in staining, samples were mounted with a mounting medium without DAPI (Vector Laboratories). The samples were observed with an Axioplan 2 imaging/AxioCam HRm microscope (Zeiss). Photographs were processed with AxioVision Release 4.5.

2.11 Transmission electron microscope

2.11.1 Ciliary structure examination

Cells cultured in Culture Inserts (Nunc) were fixed with freshly prepared 2% PFA in PBS for 1 hour at 4 ^{o}C. After washing with PBS, the membrane with the cells on it was cut into strips and rinsed in a 0.1M phosphate buffer three times for 15min. The samples were treated with 70% ethanol for 1

hour, 50% ethanol in LRwhite resin for 1 hour and in LRwhite resin alone for 1 hour (twice), after which, samples were embedded overnight in LRwhite resin at 50 ^{o}C. Ultra thin sections (~80nm) on nickel grids were prepared by the EM unit service of the University of Newcastle upon Tyne.

2.11.2 Immuno-TEM

Standard staining procedures are described below. The sections were incubated in 80mM ammonium chloride in PBS for 10 minutes followed by two incubations in 0.5% BSA/Glycine in PBS for 5 minutes. After incubation with 10% rat serum/0.5% BSA in PBS for 30 minutes, sections were washed in 0.5% BSA in PBS three times for 5 minutes each time. Sections were then incubated overnight with the primary antibody (Table 2.1) or the antibody-free control at 4 ^{o}C. After washing in 0.5% BSA in PBS three times for 5 minutes each time, the sections were incubated at room temperature for 1 hour or overnight at 4 ^{o}C with the gold conjugated secondary antibody (Table 2.2) in 0.5% BSA in PBS which was pre-incubated with normal horse serum (antibody/serum: 2/1) for 1 hour at room temperature. The sections were then washed six times in 0.5% BSA in PBS for 5 minutes and 4 times in distilled water for 5 minutes. After incubating in 2% aqueous uranyl acetate for 20 minutes, the sections were rinsed in distilled water by dipping them 5 times in water that was changed with each dip. They were then dried with filter paper and were ready for observation with a TEM.

In the case of pre-section staining, cells grown in culture inserts were treated and stained with the S43B antibody following the procedures for Immunofluorescence staining described in section 2.10. After incubation

with S43B, the samples were washed with PBST three times for 5 minutes and sent to the EM unit in Newcastle University for the embedding and sectioning procedure. Staining steps followed the standard staining procedures but omitted the primary antibody incubation.

In the case of post-section staining, cells grown in culture inserts were fixed in 4%PFA in PBS at 4 ^{o}C for 20 minutes, after draining the growth medium. They were then washed in PBS three times for 5 minutes each time. Next, the cells were penetrated with 0.1% Triton/PBS for 10 minutes then washed twice for 5 minutes in PBS and 5 minutes in PBST. After these treatments, the samples were sent to the EM unit in Newcastle University for the embedding and sectioning procedure. Staining steps followed standard staining procedures and three different dilution concentrations (1/100, 1/400 and 1/1,000) of primary antibody were applied to the sections.

In the case of the detergent-free staining, cells grown in culture inserts were fixed in freshly prepared 2%PFA in PBS at 4 ^{o}C and left overnight after draining the growth medium. After three, separate, 5-minute washings with a phosphated buffer, samples were sent to the EM unit in Newcastle University for the embedding and sectioning procedure. Staining steps followed standard staining procedures and three different dilution concentrations (1/100, 1/400 and 1/1,000) of the primary antibody were applied to the sections.

2.12 Subcellular fractionation

Subcellular fractionation was performed following previously published

methods (Becker *et al.*, 1995). Both wildtype and *Evc*$^{-/-}$ MEFs from two T75 flasks were harvested with trypsin after serum starvation for 20 hours. After washing with ice cold PBS and centrifuging at 1,000rcf for 5 minutes at 4 ^{o}C, pellets were resuspended in ice cold PBS and transferred into eppendorfs. Cells were centrifuged at 6,000rcf for 2 minutes at 4 ^{o}C and the pellets were resuspended in 50µl of lysis buffer A containing 10mM HEPES pH7.9, 10mM KCl, 0.1mM EDTA, 0.1mM EGTA, 2mM DTT (freshly added) and a Protease Inhibitor (Roche, freshly added, 1 tablet in 10ml lysis buffer A). The resuspended cells were placed on ice for 15 minutes and an additional 2 minutes after adding 33µl 10% NP40. After centrifuging at 12,000rcf for 30 seconds at 4 ^{o}C, the supernatants were collected as cytoplasmic fraction 1 (C1). To ensure that the fraction worked efficiently, the pellets were resuspended in 50µl of lysis buffer A and centrifuged at 12,000rcf for 30 seconds at 4 ^{o}C. This step was repeated five times to obtain the fractions C2-C7. The pellets after fraction C7 were resuspended in 30µl of lysis buffer B containing 20mM HEPES pH7.9, 0.4mM NaCl, 1mM EDTA, 1mM EGTA, 2mM DTT (freshly added) and Protease Inhibitor (Roche, freshly added, 1 tablet in 10ml lysis buffer B) and incubated on ice for 1 hour with a strong vortex at 10 minutes intervals. After centrifuging at 12,000rcf for 5 minutes at 4 ^{o}C, the supernatant was collected as the nuclear fraction (N).

2.13 Western blotting

2.13.1 Preparation of protein samples

The MEFs from two T75 flasks were scrubbed with ice-cold PBS and centrifuged at 1,000rcf for 5 minutes at 4 ^{o}C. The subsequent pellets were

washed by resuspension and by centrifuging twice with ice-cold PBS. A 2X loading buffer was used to resuspend the pellet thoroughly and the samples were stored at –80 ^{o}C. The samples were heated at 95 ^{o}C before loading.

The subcellular fractionation, fractions (C1 ~ C7 and N) stored at –80 ^{o}C, were thawed on ice and then mixed with equal volumes of the 2X loading buffer for total volume 10µl. The samples were heated at 95 ^{o}C before loading.

2.13.2 Eletrophoresis and transfer

Samples were loaded into 7.5% Tris-HCl Ready-Gel (Bio-Rad Laboratories) or 4-12% Bis-Tris NuPAGE® gel (Invitrogen Corporation). In Tris-HCl Ready-Gel, the running buffer contains 1.5g/l Tris-base, 7.2g/l glycine, and 0.5% SDS. In Bis-Tris NuPAGE® gel, the electrophoresis system followed the manufacturer's instructions and contained the MES SDS-Running Buffer (Invitrogen Corporation) and NuPAGE® Sample Reducing Agent (Invitrogen Corporation). In both systems, the 5µl Rainbow marker was used as the protein marker and the electrophoresis was performed at 200V for 1 hour.

Protein transfer was performed with the Western blot transfer system (Bio-Rad Laboratories). For one hour, the protein samples were transferred to the transfer membranes (Hybond-C extra, GE Healthcare Bio-Sciences) with a transfer buffer containing 25mM Tris-base, 0.2M glycine and 20% methanol at 350mA. After washing twice in Tris-buffered saline Tween-20

(TBST) containing 50mM Tris (pH7.5), 150mM NaCl and 0.05% Tween 20, the membrane was stored in TBST at 4 ^{o}C.

2.13.3 Antibody staining

After blocking in 5% skimmed milk in TBST at room temperature for 1 hour or overnight at 4 ^{o}C, the membrane was incubated with primary antibodies diluted in 5% skimmed milk in TBST for 1 hour. After washing three times for 10 minutes each time in TBST, the membrane was incubated in a HRP-conjugated secondary antibody diluted in 5% skimmed milk in TBST. The unbounded secondary antibody was removed by three, separate, 10-minute washes in TBST. The ECL Regent (GE Healthcare) was used as the substrate for the HRP enzyme producing chemiluminescence, which could be detected with X-ray film (Kodak) and developed using an automatic X-ray film processor (Xograph Healthcare Ltd.).

The commercial goat anti-Evc antibody, obtained from Santa Cruz, was verified by pre-incubation with a blocking peptide (Santa Cruz) the sequence of which was not available.

2.14 Statistical analysis

Fisher's exact test was used to analyze whether the abnormalities observed in *Evc*$^{-/-}$ were significantly difference from the wild type. Fisher's exact test is a statistical test widely used to analyze contingency tables where sample sizes are small (Fisher, 1922).

Chapter 3: The role of Evc in heart development

3.1 Introduction

3.1.1 Cardiovascular malformation in EvC syndrome

EvC syndrome is an autosomal recessive disease characterized by short ribs, short limbs, postaxial polydactyly, fingernail dystrophy, multiple oral frenula, neonatal teeth, delayed tooth eruption, and cardiac defects (Biggerstaff and Mazaheri, 1968; Ellis and Van Creveld, 1940; McKusick et al., 1964; Taylor et al., 1984). Approximately 60% of affected individuals suffer from cardiac defects, which are the major reasons for early death in EvC syndrome. The most frequent cardiac abnormalities in human patients are defects in atrioventricular septation and a single atrium (Digilio *et al.*, 1999; Katsouras *et al.*, 2003). Although research has detected low levels of *EVC* expression at Carnegie stages 19 and 21 in developing bone, heart, kidney, and lung in human embryos (Ruiz-Perez *et al.*, 2000), the functions of EVC in developing heart and the pathomechanism of cardiovascular malformation in the absence of EVC protein are poorly understood.

3.1.2 *Evc* knockout mice

Evc$^{-/-}$ mice were generated through replacing *Evc* exon 1 with a β-galactosidase gene in an in-frame status in our group. The RT-PCR study confirmed the absence of *Evc* transcripts in *Evc*$^{-/-}$ mice (Ruiz-Perez *et al.*, 2007). Similar to human patients, *Evc*$^{-/-}$ mice have short ribs, short limbs, and dental abnormalities. The above study did not observe polydactyly in *Evc* knockout mice (Ruiz-Perez *et al.*, 2007), and had not studied

histological changes of the heart in *Evc*$^{-/-}$ mice at the beginning of the study.

3.1.3 Aims

This chapter focuses on analyzing the heart development in *Evc*$^{-/-}$ mice and the expression of Evc in mouse heart development.

3.2 Histological analysis of *Evc*$^{-/-}$ heart

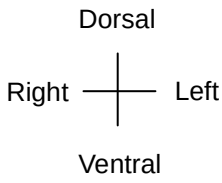

This section, if not specified, places the dorsal side of embryo sections toward the top of the page, while the right side of embryo sections are placed toward the left side of the page.
LA: left atrium; LV: left ventricle; PAS: primary atrial septum; RA: right atrium; RV: right ventricle

3.2.1 Genotype analysis

To understand the function of Evc in heart development, this study used *Evc*$^{-/-}$ mice. Genotyping the embryos from *Evc*$^{+/-}$ x *Evc*$^{+/-}$ parents (section 2.4) was undertaken on genomic DNA extracted from embryo tails or from MEFs (to check cell lines) amplified with primer sets specific to exon 1 of *Evc* and *LacZ* simultaneously (Ruiz-Perez *et al.*, 2007). The PCR products were separated by electrophoresis through 2% agarose. In the wild type mice, only *Evc* exon 1 was amplified, giving a single band of 180bp on gel. The samples from homozygous *Evc*$^{-/-}$ mice showed the single *LacZ* band of 450bp on gel whereas *Evc* exon 1 and lacZ fragments were amplified and 180bp and 450bp bands were observed in the agrose gel. The representative photos in figure 3.1 demonstrate that PCR is a rapid and

clear method to identify embryo genotypes.

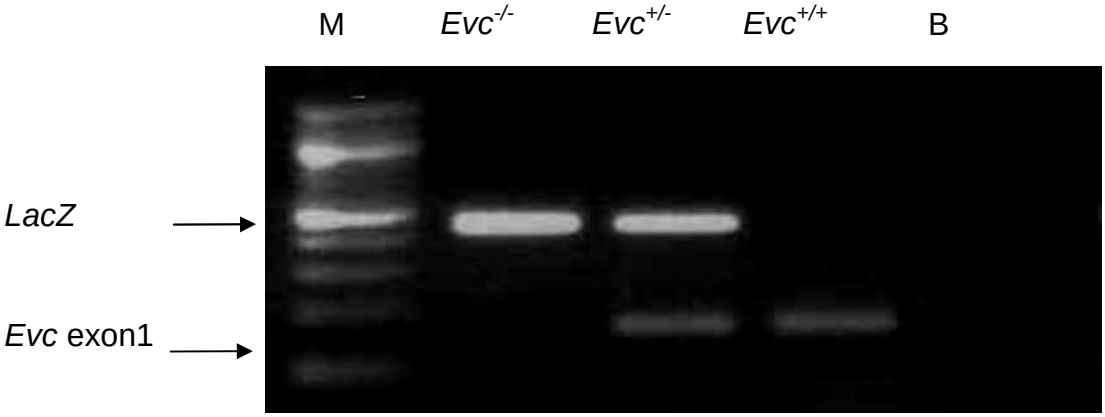

Figure 3.1 Electrophoresis analyses of PCR products for *Evc* genotyping.
Simultaneously amplified PCR products of *LacZ* and exon1 of *Evc* were analyzed by 2% agarose electrophoresis. M: 100bp DNA ladder (NEB); B: PCR blank

3.2.2 Characterization of heart development in *Evc*$^{-/-}$ mice

Histological analysis (section 2.5) of the thorax region of mice at different embryonic stages (E14.5, E15.5, and E18.5) and newborn mice were performed. The samples were sectioned and stained with H&E followed by histological analysis. Twenty-five offspring of *Evc*$^{+/-}$ × *Evc*$^{+/-}$ crosses were used in this study, 23 embryos at different developmental stages, and 2 newborn mice (Table 3.1).

Table 3.1 Numbers of mice offspring analyzed at each developmental stage

	Wild type	Heterozygous	Homozygous	Total
E14.5	2	4	8	14
E15.5	0	1	1	2
E18.5	3	0	4	7
Newborn	1	0	1	2
Total	6	5	14	25

Six litters were harvested and embedded in paraffin wax. The chest area was sectioned into 7μm thickness and H&E stained. To obtain the insight of Evc protein in heart development, sections from different areas of the heart were closely analyzed.

Among eight different litters collected (Table 3.2), no significant difference in cardiovascular variances was observed in *Evc*$^{-/-}$ mice (Table 3.3). Consisting with previous study in our group, the number of embryos observed in this study met to the estimation by Mendelian inheritance. In particular, no instance of common atrium or atrioventricular defects was observed. Several minor abnormalities were detected in the samples, including abnormalities of heart position, the ventricular septum muscle, the trabeculae, fusion of the ventricular septum with the atrioventricular cushion tissue, and atrioventricular valves, but these were also observed in wild the type and heterozygous controls. These observations are described below.

Table 3.2 Collected embryos and mice

Litter Number	Age	*Evc*$^{+/+}$	*Evc*$^{+/-}$	*Evc*$^{-/-}$	Total
1	E14.5	0	4	3	7
2	E14.5	2	5	4	11
3	E14.5	2	7	1	10
4	E15.5	3	7	1	11
5	E18.5	1	1	2	4
6	E18.5	2	4	2	8
7	E18.5	4	5	3	12
8	P0	2	5	1	8
Total		16	38	17	71

Table 3.3 Embryos and mice used for studying heart developmental defects

Mouse Number	Age	Genotype	Heart position	Apex of heart	Trabecula	Ventricular septum muscle	ventricular septum with atrioventricular	Atrioventricular valves
1	E14.5	*Evc*$^{+/-}$						
2	E14.5	*Evc*$^{+/-}$						
3	E14.5	*Evc*$^{-/-}$			X			X
4	E14.5	*Evc*$^{-/-}$	X	X		X		X
5	E14.5	*Evc*$^{-/-}$		X				X
6	E14.5	*Evc*$^{+/+}$				X		X
7	E14.5	*Evc*$^{+/-}$	X	X		X		X
8	E14.5	*Evc*$^{+/-}$	X	X	X			
9	E14.5	*Evc*$^{-/-}$			X			X
10	E14.5	*Evc*$^{-/-}$				X		X
11	E14.5	*Evc*$^{-/-}$	X	X	X			X
12	E14.5	*Evc*$^{+/+}$						
13	E14.5	*Evc*$^{-/-}$	X	X				
14	E14.5	*Evc*$^{-/-}$			X	X		X
15	E15.5	*Evc*$^{+/-}$					X	
16	E15.5	*Evc*$^{-/-}$						
17	E18.5	*Evc*$^{+/+}$						
18	E18.5	*Evc*$^{-/-}$	X	X				
19	E18.5	*Evc*$^{-/-}$	X	X		X		
20	E18.5	*Evc*$^{+/+}$	X	X	X	X		
21	E18.5	*Evc*$^{-/-}$	X	X		X		
22	E18.5	*Evc*$^{+/+}$	X	X	X	X		
23	E18.5	*Evc*$^{-/-}$	X	X				
24	P0	*Evc*$^{+/+}$	X	X		X		
25	P0	*Evc*$^{-/-}$		X	X	X		
			12	14	8	11	1	9

3.2.3 Heart and ventral apex positions

In mouse embryos, the heart is located in the middle of the chest cavity

with the apex inclined towards the left (You *et al.*, 2005). Among 12 of 25 samples analyzed, the heart was observed in the left half of the thorax (Figure 3.2). The right ventricle as the ventral apex typically accompanies an abnormal heart position. The 12 samples included 3 of 6 in the wild-type, 2 of 5 in the heterozygous type, and 7 of 14 in the homozygous embryos. No statistical significance was detected in the occurrence rate of heart deflection and apex of heart between the wild-type/heterozygous and homozygous samples (Fisher's exact test, p=1 and 0.43 respectively).

Figure 3.2 Abnormality in the position of heart and ventral apex
In normal mouse embryos, the heart is located in the middle of the chest. The figure shows deflection of heart position to the left side of the body in one of *Evc*$^{+/-}$ mice (E14.5). Bar: 500μm

3.2.4 The shape of the trabeculae

Trabeculae carnae located at the wall of the ventricle are normally pillar shaped (Figure 3.3, A and C). Clubbed trabeculae in the left ventricle were observed in 8 of 25 samples (Figure 3.3, B, and D). The eight samples included 2 of 6 in the wild-type, 1 of 5 in the heterozygous, and 5 of 14 in homozygous embryos and newborn. No statistical significant difference was observed in the occurrence rate of abnormality in the shape of trabeculae between wild-type/heterozygous and homozygous samples (Fisher's exact test, p= 1).

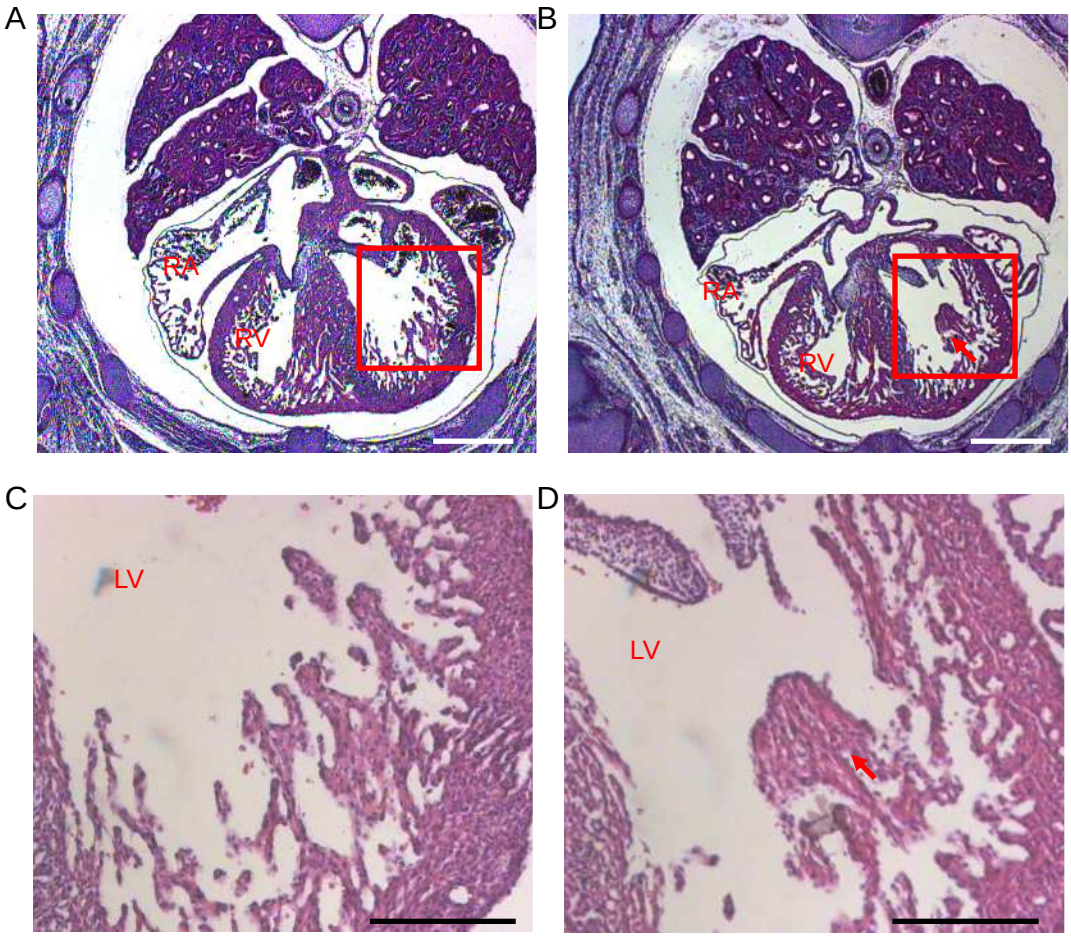

Figure 3.3 Representative figures on abnormality in the shape of trabeculae

In most mice, trabeculae are pillar shaped at the ventricle wall (A and C, *Evc*$^{+/-}$, E14.5). Clubbed and bud structural trabeculae, indicated by the red arrow, were observed in some mice (B and D, *Evc*$^{-/-}$, E14.5). C and D represent higher magnification of the red square region in A and B. Bar in A and B: 500μm; in C and D: 200μm.

3.2.5 Ventricular septum

The myocardial wall grows at the middle of the ventricle, forming the septum that eventually separates the left from the right ventricle. At E14.5, the ventricular septum should be well developed and fused with the AV cushion tissue (Figure 3.4, A and C). One E14.5 heterozygous embryo had

a space between the ventricular septum and the AV cushion, suggesting a ventricular septum defect in this embryo (Figure 3.4, B, and D). The analysis did not reach statistical difference even though variance was not observed in any of the 14 *Evc*$^{-/-}$ mice (Fisher's exact test, p=0.44).

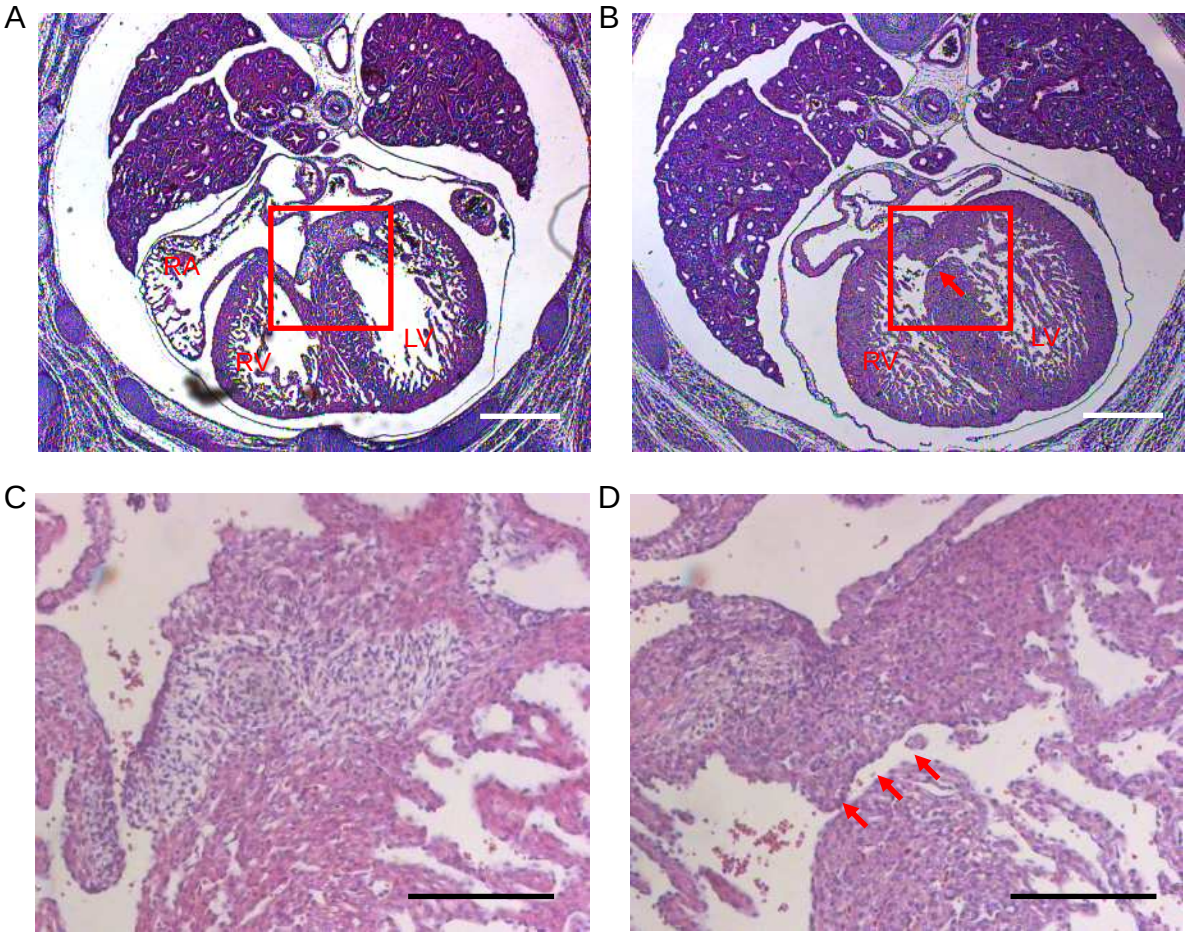

Figure 3.4 Representative figures on attenuation of ventricular septum

The ventricular septum is fused with the AV cushion tissue in the E14.5 embryo (A and C, *Evc*$^{+/-}$, E14.5). One of five heterozygous mice showed impaired development of the ventricular septum. The gap between the ventricular septum and the AV cushion tissue is indicated by red arrows (B and D, *Evc*$^{+/-}$, E15.5). C and D represent higher magnification of the red square region in A and B. Bar in A and B: 500μm; in C and D: 200μm

3.2.6 Structure of the ventricular septum

The interventricular septum is typically shown as a stout wall separating the ventricles of the heart (Figure 3.5, A and C). However, a thinner septum with spaces was observed in 11 out of 25 samples, including 4 of 6 in the wild-type, 1 of 5 in the heterozygous type, and 6 of 14 in homozygous embryos and newborn (Figure 3.5, B and D).

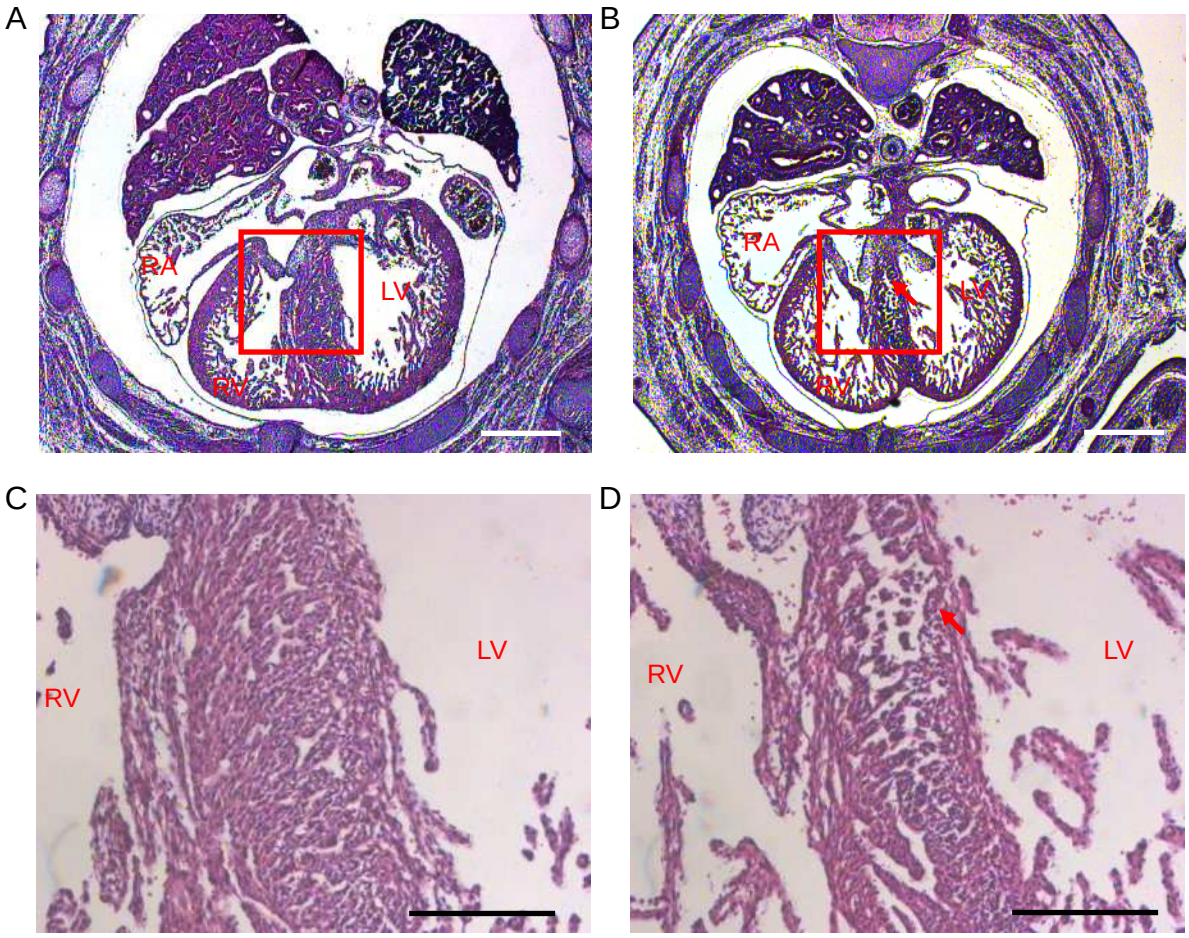

Figure 3.5 Loose structure of ventricular septum
The ventricular septum muscle is a solid structure as shown in A and C (*Evc*$^{+/-}$, E14.5). Eleven of 25 samples showed a loose structure of ventricular septum as indicated in red arrows in B and D (*Evc*$^{-/-}$, E14.5). C and D represent higher magnification focus on the red square region in A and B. Bar in A and B: 500μm; in C and D: 200μm.

No significant difference was observed between wild-type/heterozygous

and homozygous mice (Fisher's exact test, p=1).

3.2.7 AV valve structure

AV valves are located between the atria and the ventricles. The valves anchor to the ventricle wall by chordae tendineae and prevent backflow from the ventricles into the atria during systole. AV valves are differentiated from the extracellular matrix and mesenchymal cells and should be flat leaflet structures (Figure 3.6, A and C). An unusual structure with a dilated bubble at the end of the leaflet was observed (Figure 3.6, B, and D). One of 6 wild type, 1 of 5 heterozygous type, and 7 of 14 homozygous mice showed this phenotype. While the proportion of mice with this abnormality was higher in *Evc*$^{-/-}$ mice compared to the wild type and heterozygous littermates, this difference did not reach statistical significance (Fisher's exact test, p= 0.2).

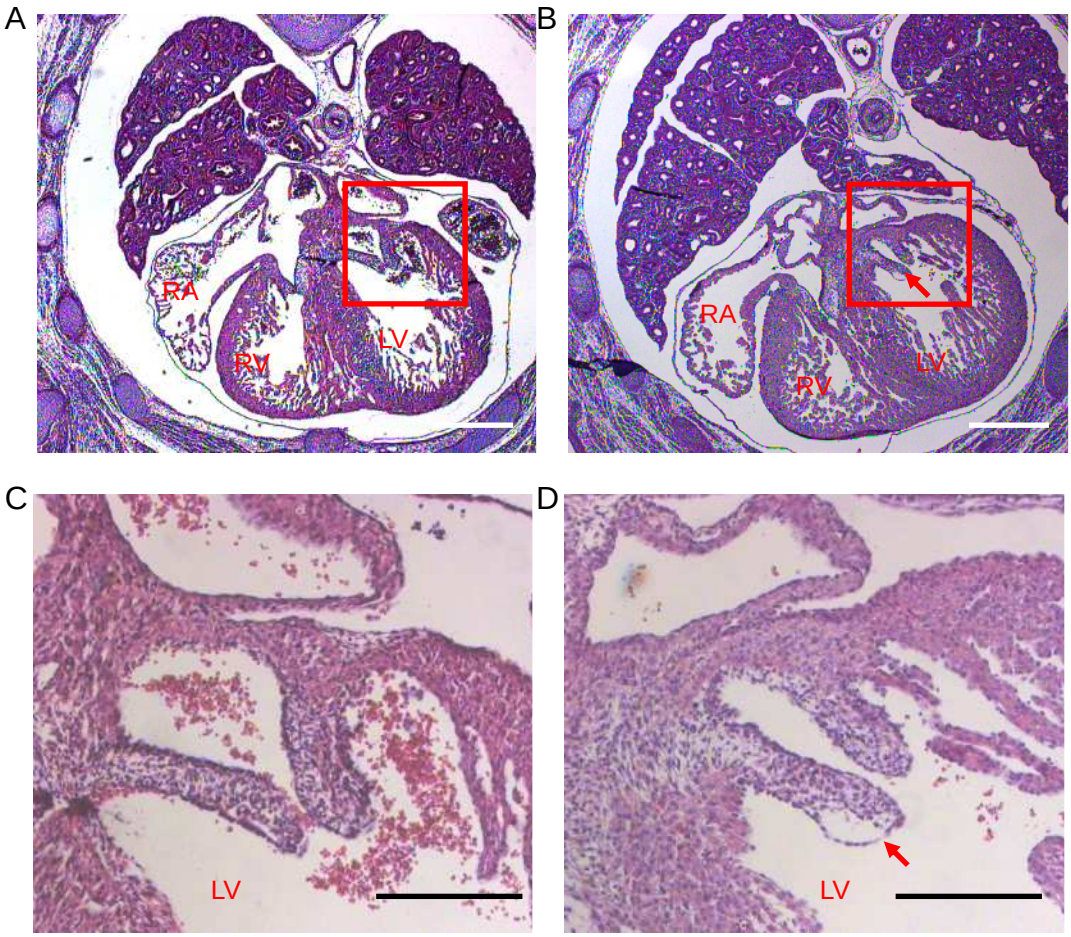

Figure 3.6 Unusual bubble structures at the end of AV valves
The valves and the homogenous structure are flat, as shown in A and C (*Evc*$^{+/-}$, E14.5). Red arrows indicate the bubble structure at the end of AV valves observed in this study (B and D, *Evc*$^{+/-}$, E14.5). C and D represent higher magnification focus on the red square region in A and B. Bar in A and B: 500μm; in C and D: 200μm

3.2.8 Summary

In conclusion, no statistical differences were observed in hearts between the wild type/heterozygous and homozygous samples among these uncommon phenotypes (Table 3.4 and Figure 3.7).

Table 3.4 Numbers of embryos of each genotype with heart abnormalities

Abnormality	*Evc*$^{+/+}$ (n=6)	*Evc*$^{+/-}$ (n=5)	*Evc*$^{-/-}$ (n=14)	p value
Heart position	3	2	7	1
Apex of heart	3	2	9	0.43
Trabecula	2	1	5	1
Fusion of ventricular septum with atrioventricular cushion tissue	0	1	0	0.44
Ventricular septum muscle	4	1	6	1
Atrioventricular valves	1	1	7	0.2

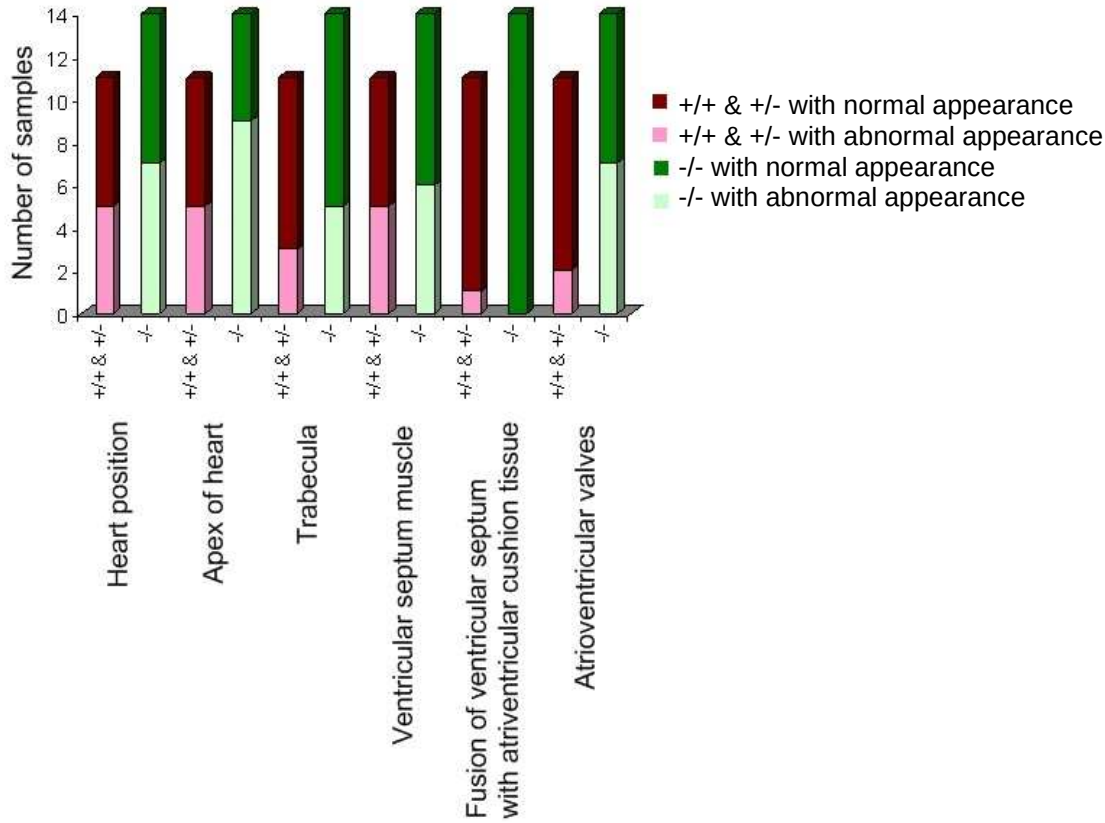

Figure 3.7 Occurrence rates of abnormalities in different mouse genotypes

Abnormalities of atrioventricular valves demonstrated a higher frequency in homozygous samples compared to those in wild type or heterozygous samples.

3.2.9 Cardiac development analysis in an inbred strain

As phenotypes are often more apparent in an inbred background than a mixed background, the *Evc*$^{-/-}$ mice with C57Bl/6J-129Sv genetic background were backcrossed with the inbred strain C57Bl/6J for nine generations. The mice carried 99.9% of the inbred C57BL/6J background. The thorax region of E14.5 inbred strain embryos was analyzed as previously described in three litters, twelve embryos in total. With the exception of the loose structure of the ventricular septum muscle, no other cardiac defects were observed in *Evc*$^{-/-}$ mice with inbred C57Bl/6J genetic background (Table 3.5; Figure 3.8).

Table 3.5 Numbers of embryos of each genotype from inbred strain C57Bl/6J mice with uncommon heart features

Abnormality	Wild type (3)	Heterozygous (4)	Homozygous (5)
Heart position	0	0	0
Apex of heart	0	0	0
Trabecula	0	0	0
Ventricular septum muscle	1	1	1
Fusion of ventricular septum with atrioventricular cushion tissue	0	0	0
Atrioventricular valves	0	0	0

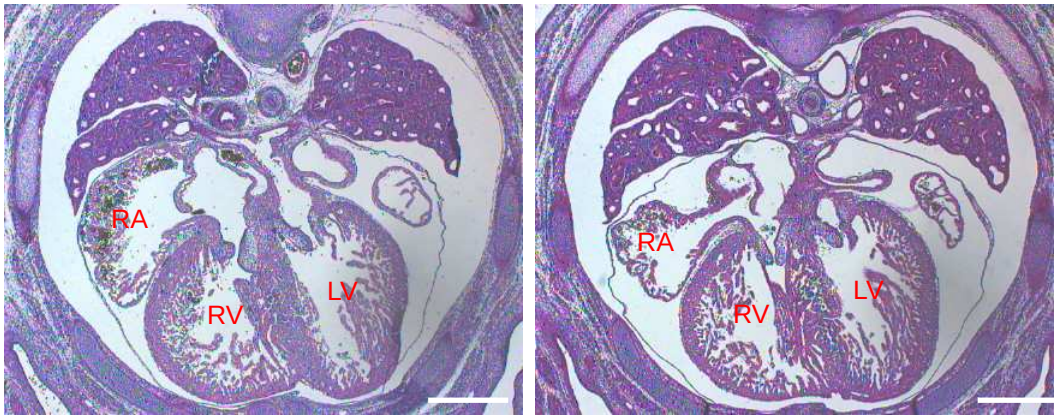

Figure 3.8 Loose structure of ventricular septum observed in inbred strain mice

In wild type (right panel), the solid muscular ventricular septum was observed in the left panel at E14.5. In one sample of each genotype from inbred strain mice (left panel, *Evc*$^{+/-}$), the loose structure of ventricular septum was observed. Bar: 500μm

The loose structure of the ventricular septum was found in the thorax region in one embryo of each genotype. No significant difference evidenced in the occurrence rate of this phenotype between the wild-type/heterozygous and homozygous samples.

3.2.10 *Vangl2* and *Evc* double knockout mouse study

This study observed no obvious heart developmental variance in *Evc*$^{-/-}$ mice. Among all (~1,500) *Evc* mouse stock, one of the *Evc*$^{+/-}$ mice revealed a curly tail phenotype while the loop tail is one of the abnormalities in *Vangl2*$^{+/-}$ mice (Phillips et al., 2008). The *Vangl2*, also known as *Strabismus*, *Lpp1* or *Ltap*, has been shown to encode a protein homologous to *Drosophila strabismus*/*van gogh* (vang)(Kibar et al., 2001). Mammalian Vangl2 and *Drosophila* Vang proteins contain four putative transmembrane domains and a PDZ-binding domain. In Drosophila, Vang is a key component of a frizzled/disheveled pathway, essential for regulating planar

cell polarity and, in some tissues, cell fate (Taylor et al., 1998; Wolff and Rubin, 1998). Although studies have not identified the activating ligand in *Drosophila*, the pathway is highly conserved in vertebrates where it appears to be activated by Wnt binding to the frizzled receptor (Taylor et al., 1998; Wolff and Rubin, 1998). The heterozygous *Vangl2* mouse shows the loop tail phenotype while the homozygous mouse shows the complete open neural tube in the hindbrain and spinal region.

Although the expression of EVC in the heart has not been verified, atrial septal defects were observed in 60% of *EVC* deficient patients. OFT defects were observed in *Vangl2* knockout mice. As the Shh pathway down-regulates in $Evc^{-/-}$ mice, Vangl2 is one of the members of Wnt signaling. Many different tissue developments have reported the crosstalk between Wnt and Shh signaling (Alvarez-Medina et al., 2008; Borycki et al., 2000; Iwatsuki et al., 2007; Lei et al., 2006; Sarkar et al., 2000). These researches suggest that the expression of Wnt signaling compensates for heart developmental defects in $Evc^{-/-}$ mice. To investigate the heart development in $Evc^{-/-}$ mice without Wnt signaling, this study planned to generate *Evc* and *Vangl*2 double knockout mice. To achieve this, $Evc^{+/-}$ female and $Vangl2^{+/-}$ male crosses were set up for the double heterozygous offspring to mate.

Since $Vangl2^{+/-}$ mice carry the G>A transition mutation in exon 8, all genomic DNA of the offspring were amplified by PCR and analyzed by direct sequencing (Figure 3.9).

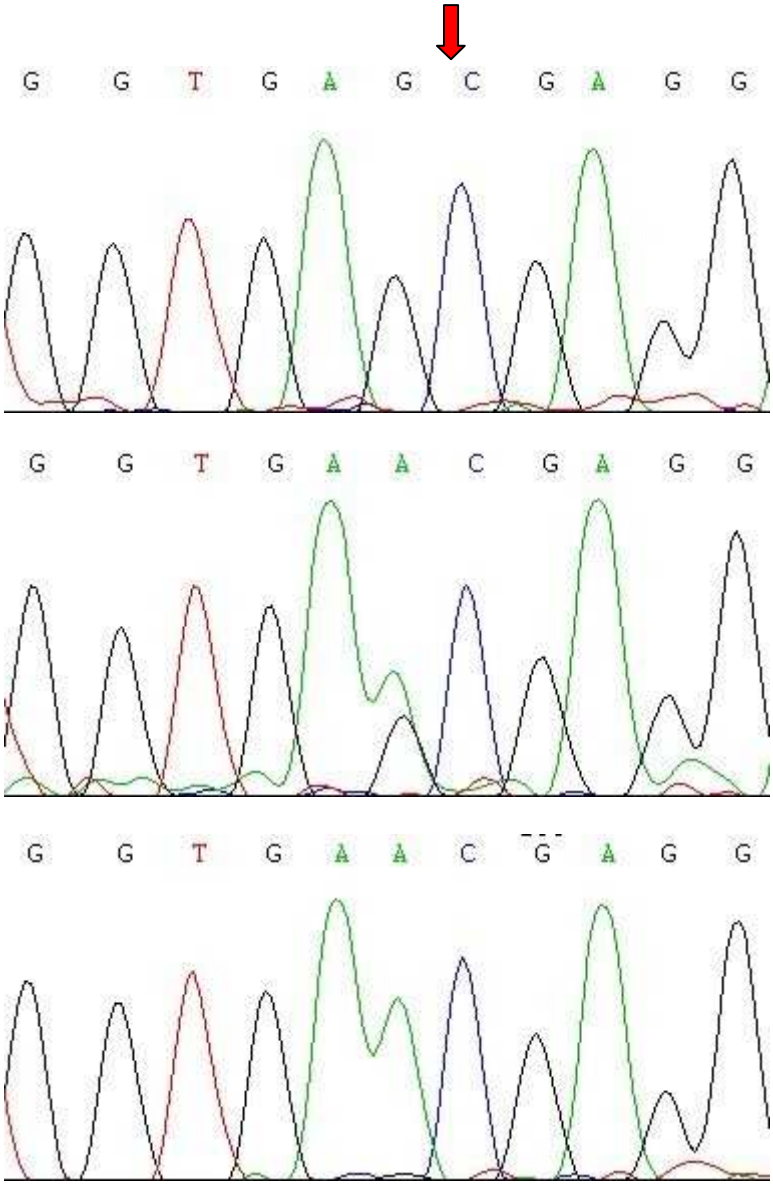

Figure 3.9 Sequencing analyses of different genotypes of the *Vangl2* gene

The transition mutation in exon 8 of the *Vangl2* gene (G>A, arrow) was analyzed with direct sequencing. Three genotypes, the wild type (A), the heterozygous type (B), and the homozygous type (C), could be distinguished with no ambiguities.

Six litters of the crosses of $Evc^{+/-}$ female and $Vangl2^{+/-}$ male were collected. Among 19 female offspring, only two females were $Evc^{+/-};Vangl2^{+/-}$. When these two $Evc^{+/-};Vangl2^{+/-}$ females were crossed with $Evc^{+/-};Vangl2^{+/-}$ males, no $Evc^{-/-}$; $Vangl2^{-/-}$ double knockout mice were obtained (Table 3.6).

Unfortunately, the study was not continued, due to time and cost restraints.

Table 3.6 Mouse embryos obtained from *Evc*$^{+/-}$;*Vangl2*$^{+/-}$ parents

	Evc		
Vangl2	+/+	+/-	-/-
+/+	1	1	1
+/-	3	1	1
-/-	0	1	0

3.3 Analysis of *Evc* gene expression

3.3.1 *LacZ* as in indicator of Evc protein expression

Since the anti-Evc antibody used in our group does not work on paraffin sections (Dr. H. Blair, personal communication), X-gal staining (section 2.6) was used as the exon1 of *Evc* gene to replace the *LacZ* in *Evc*$^{-/-}$ and *Evc*$^{+/-}$ mice as an indicator. X-gal staining positive cells detected in wild type samples represents endogenous β-galactosidase activity. The blue signal observed only in heterozygous or homozygous embryos after X-Gal staining, but not in the wild type, infers the expression of Evc protein.

As the atrial septum starts to develop from E10.5 to E13.5 in mice, E11.5 and E12.5 embryos were chosen for analyzing the expression pattern of Evc. One heterozygous and three homozygous embryos at E11.5 and one wild type, one heterozygous, and one homozygous embryo at E12.5 were collected and stained with X-gal. Blue stained cells observed only in heterozygous and homozygous embryos indicated the region where Evc might be expressed. The positive signals in wild-type samples indicated endogenous β-galactosidase activity. In the whole mount

heterozygous/homozygous embryos, the *LacZ* positive signal was mainly observed around the mouth region as previously shown (Ruiz-Perez *et al.*, 2007). However, it was difficult to analyze *LacZ* positive cells in the heart, which were in the deep region of the whole mount embryos.

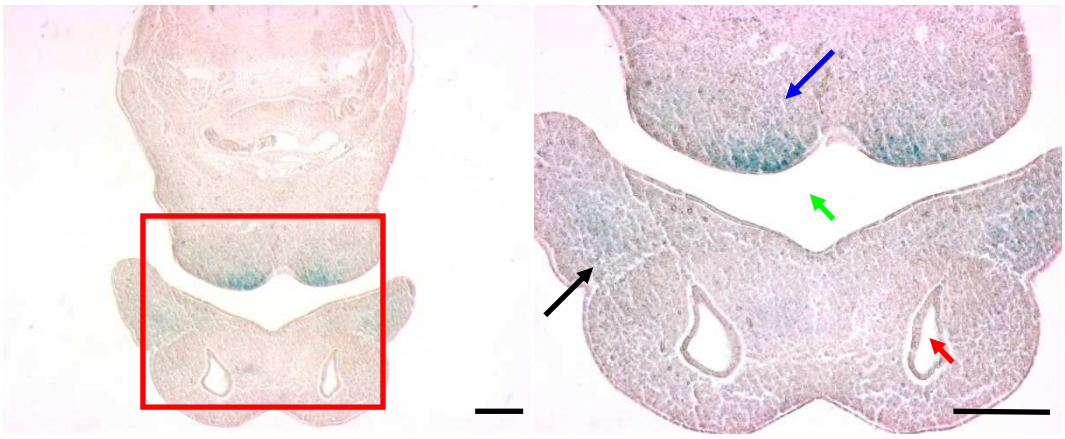

Figure 3.10 X-gal staining at the orofacial region in the *Evc*$^{+/-}$ embryo section

Whole mount embryos (E12.5) were stained with X-gal and sectioned. The X-gal positive cells were observed at the orofacial region in the *Evc*$^{+/-}$ embryo as previously described (Ruiz-Perez *et al.*, 2007). The right panel is the enlarged picture of the red squared region in the left panel. Black (maxillary process) and blue (mandibular process) arrows indicate positive X-gal staining signals. Green and red arrows indicate the stomodeum and primitive nasal cavity. Bar: 100 μm

To examine the heart, the X-Gal stained embryos were paraffin wax embedded and sectioned into 14μm thicknesses. In the E11.5 embryos, faint blue signals were observed at the dorsal side of the atrium wall in *Evc*$^{+/-}$ and *Evc*$^{-/-}$ samples (Figure 3.11).

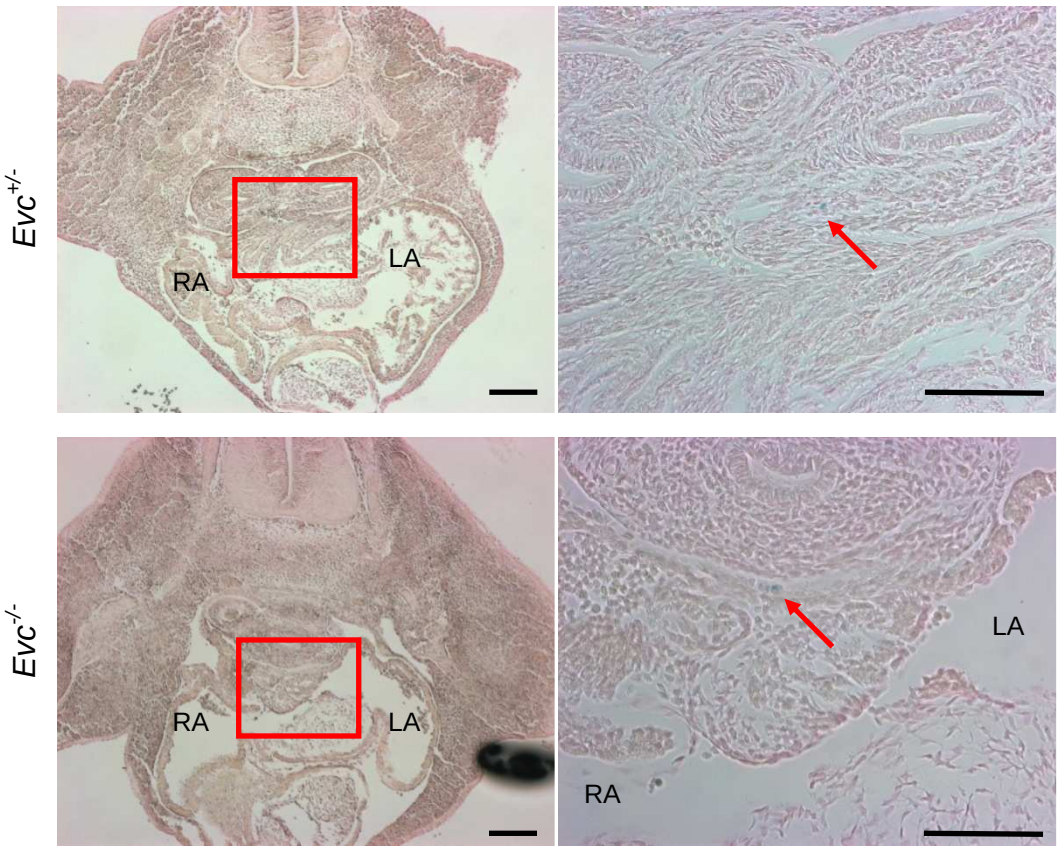

Figure 3.11 β-galactosidase activity in the heart region in E11.5 mouse embryos

The expression of Evc was detected by the reporter gene *lacZ*, which replaced the exon 1 of *Evc* gene in $Evc^{+/-}$ and $Evc^{-/-}$ embryos and can be detected by X-Gal stain. The blue signals were detected at the dorsal region to the atrial wall in $Evc^{+/-}$ and $Evc^{-/-}$ embryos (red arrows). The right panel is the enlarged picture of the red squared region in the left panel. Bar: 100 μm

In the E12.5 embryos, blue signals were observed at the atrial septum in $Evc^{+/-}$ and $Evc^{-/-}$ samples, but not in the wild-type samples (Figure 3.12).

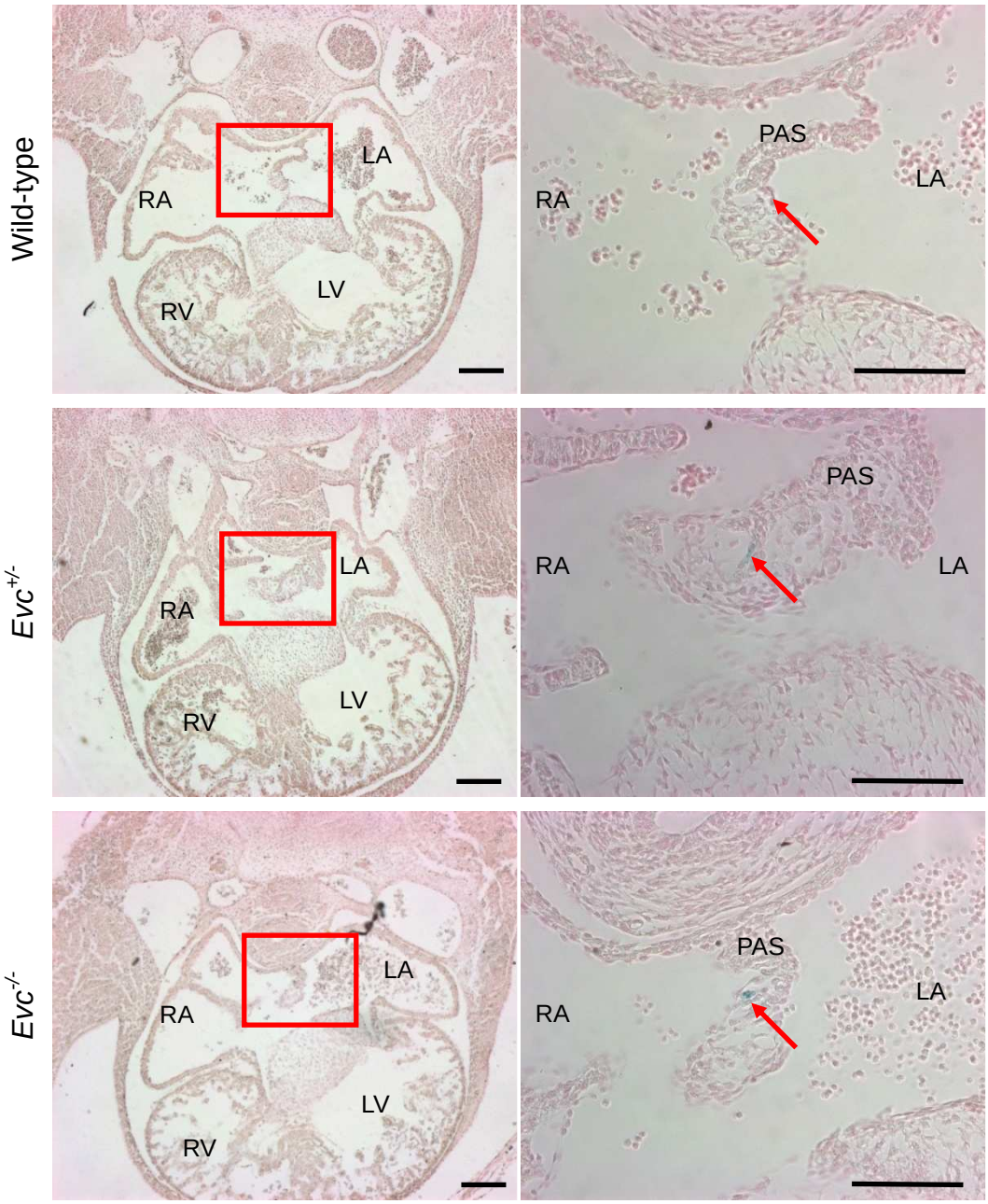

Figure 3.12 β-galactosidase activity as the reporter of Evc expression in the heart region in E12.5 mouse embryos

To eliminate the contamination of endogenous *lacZ* expression, the Evc expression region defined as the blue cells were only observed in *Evc*$^{+/-}$ and *Evc*$^{-/-}$ embryos, but not in the wild type embryos. In the region presented here, the tiny blue dots were detected in the primary atrial septum in *Evc*$^{+/-}$ and *Evc*$^{-/-}$ embryos (middle and lower panels, red arrows), whereas no blue signal was observed in the primary atrial septum in the wild type embryo (upper panel). Bar: 100 μm

In the lung bud (Figure 3.13) and gut (Figure 3.14) region, blue signals were observed in wild type embryos, indicating the false positive caused by endogenous β-galactosidase activity.

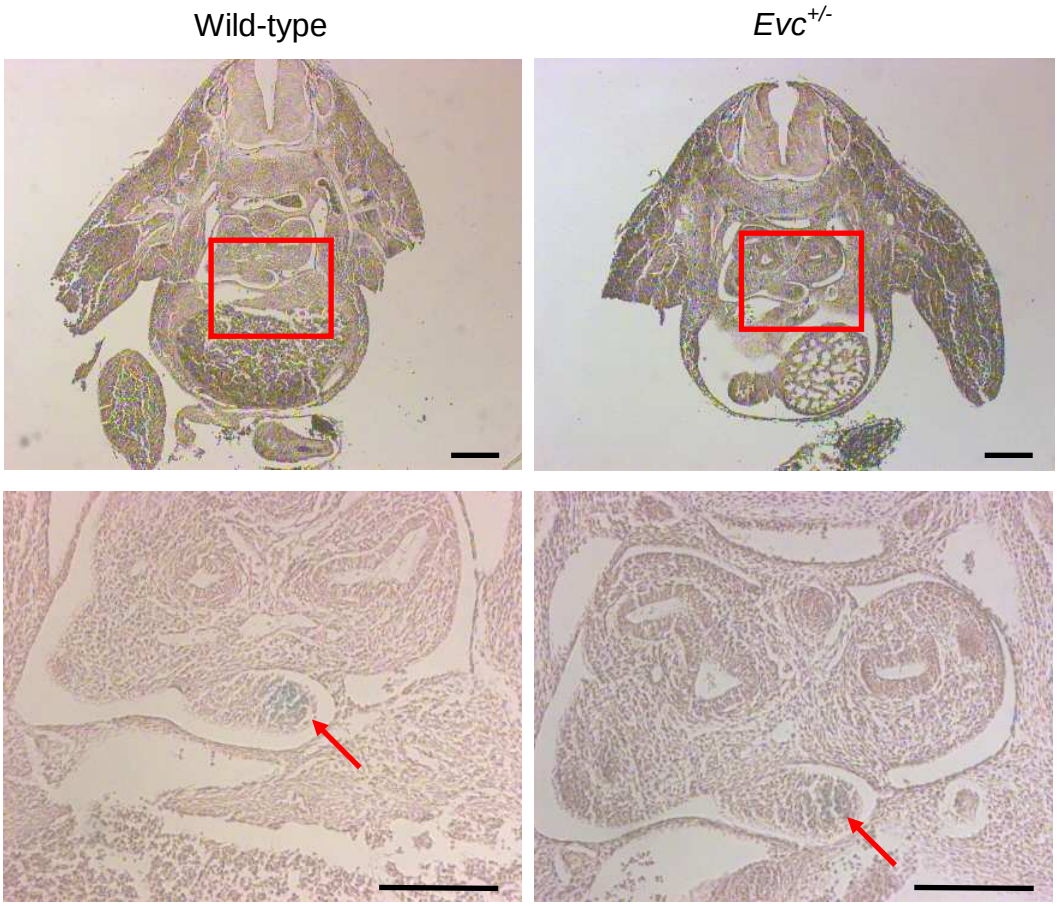

Figure 3.13 Endogenous β-galactosidase activity detected in wild-type and *Evc*$^{+/-}$ E12.5 embryos

In the right lung bud (accessory lung), β-galactosidase activity was detected in wild-type and *Evc*$^{+/-}$ E12.5 embryos (red arrows). Since no *lacZ* allele was driven by the *Evc* promoter in wild-type embryos, the blue *lacZ* stain detected in the accessory lung is attributed to endogenous β-galactosidase activity. Bar: 100 μm

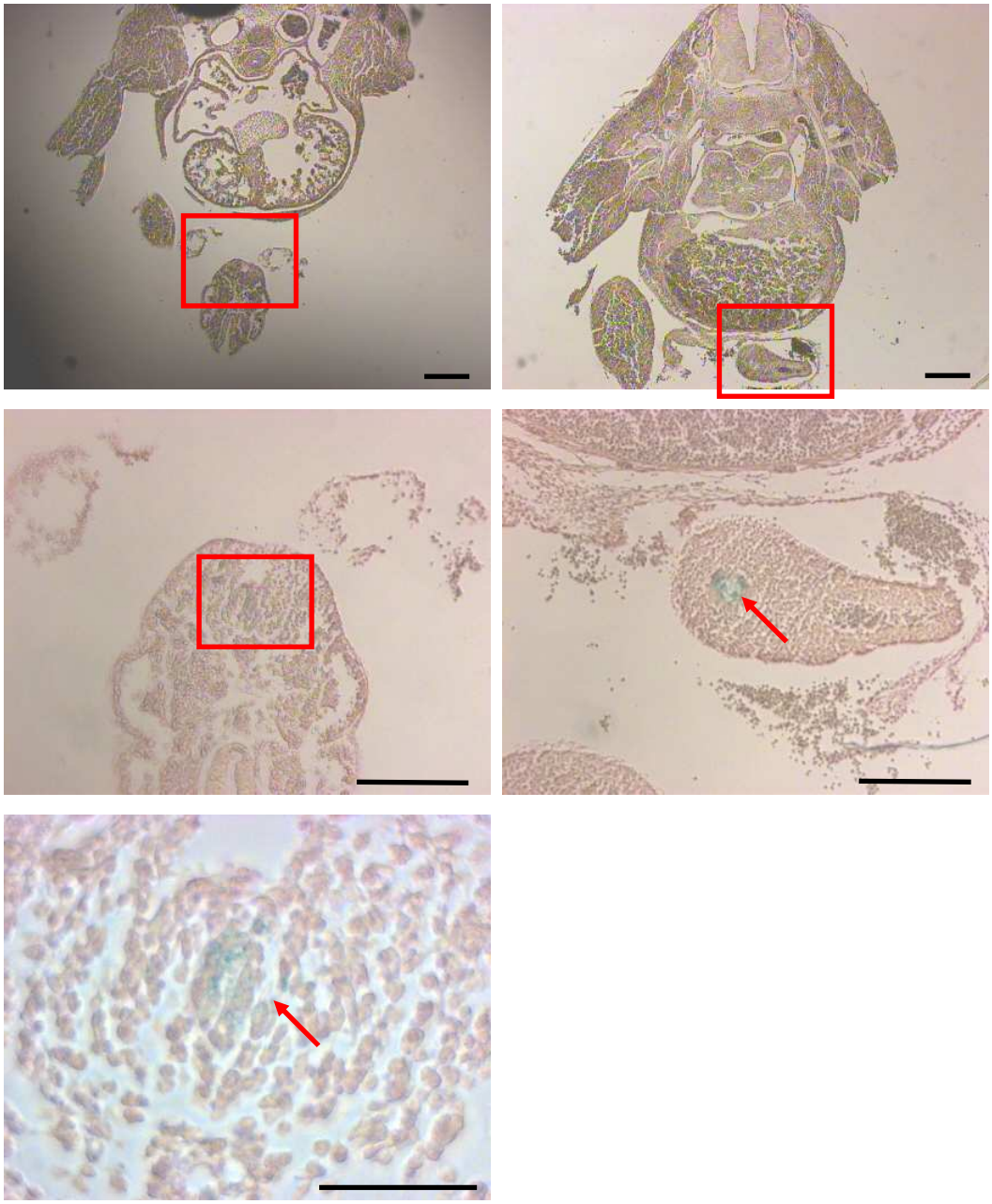

Figure 3.14 X-gal staining of endogenous β-galactosidase activity in the E12.5 wild-type embryo

Endogenous β-galactosidase activity was observed in the caudal extension of the hindgut diverticulum and the midgut loop within a physiological umbilical hernia. The left panel demonstrates β-galactosidase activity in the caudal extension of the hindgut diverticulum (red arrow). In the right panel, β-galactosidase activity was detected in the midgut loop within a physiological umbilical hernia (red arrow). Bar: 100 μm

3.3.2 Undetected *Evc* mRNA using *in situ* hybridization

Since *EVC* mRNA was detected in the human developmental heart by *in situ* hybridization (Ruiz-Perez *et al.*, 2000), this work analyzed *Evc* mRNA in the mouse heart by *in situ* hybridization (section 2.7). To examine *Evc* transcripts expressed in the heart region, *in situ* hybridization on *Evc* was performed. Shh and Ptc probes were used as positive controls in both genes expressed in the floor plate, notochord, and gut at E11.5 (Motoyama *et al.*, 1998). Although Shh was not detected in the heart at E11.5 (Goddeeris *et al.*, 2007), Ptc was observed at the dorsal mesenchymal protrusion (Goddeeris *et al.*, 2008).

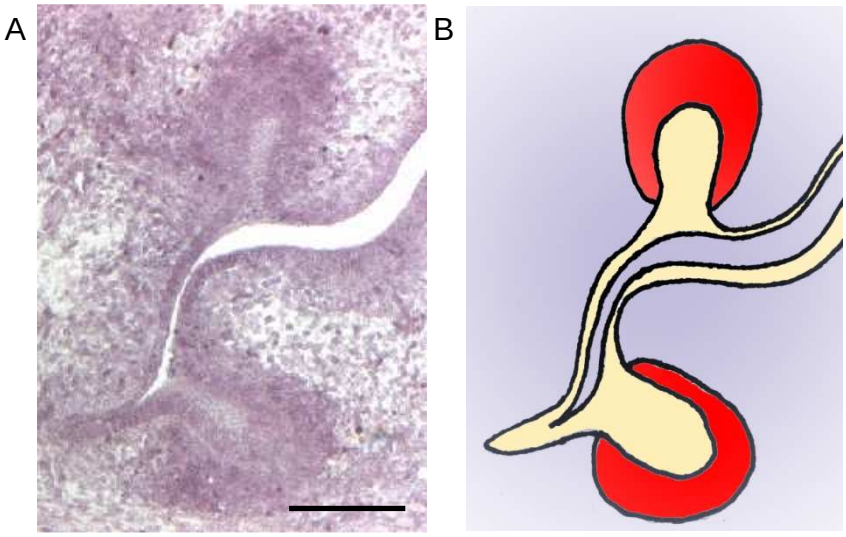

Figure 3.15 *Evc* mRNA detected at the tooth bud using *in situ* hybridization

The tooth bud sections from E13.5 embryo were used as a positive control in this study (n=6). Weak *Evc* positive signals were observed in the mesenchymal condensation region around the buds (A). The schematic view shows the epithelial cells in light orange and the mesenchymal condensation region in red (B). Bar: 100μm

E11.5 wild-type embryos were used in this study. Paraffin wax embedded

embryos were sectioned into 7µm thicknesses. Previous studies in our group demonstrated Evc protein expression in the teeth bud at E13.5 (Dr. M. Nakatomi, in press). E13.5 tooth sections were kindly provided by Dr. M. Nakatomi as positive controls (Figure 3.15).

Sections from E11.5 embryos were first chosen to detect the *Evc* mRNA in the heart region as the atrial septum begins to develop at this stage. Since abnormalities in the Shh signaling pathway have been observed in the tooth bud region in $Evc^{-/-}$ embryos (Dr. M. Nakatomi, in press), *Shh* and *Ptch1* probes were applied on the sister sections. In transverse sections of E11.5 embryos, *Shh* expression was observed in the floor plate notochord and along the digestive tract (Figure 3.16). *Ptch1* transcripts were observed near the *Shh* positive regions (Figure 3.17). However, no significant *Evc* signal was observed in sister sections (Figure 3.18).

A

B

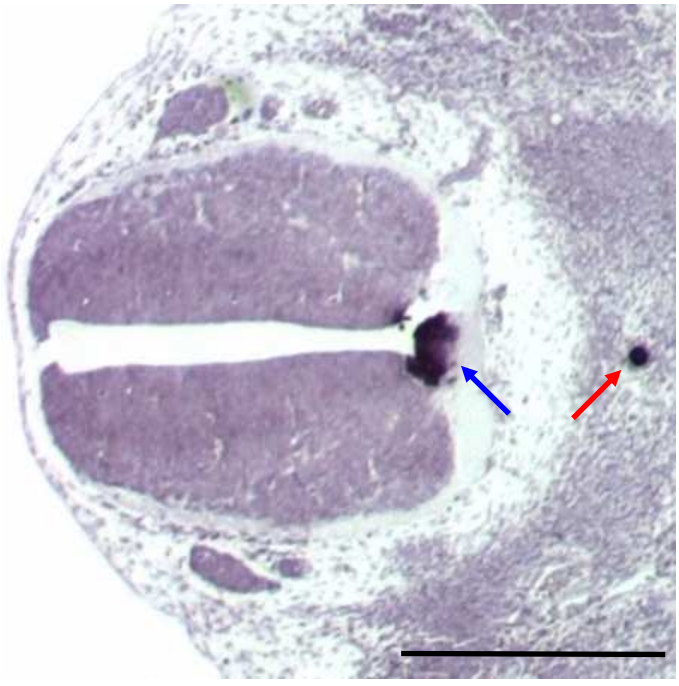

C

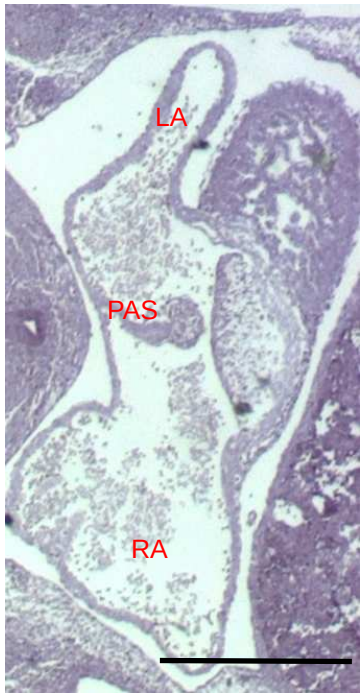

Figure 3.16 *Shh* mRNA detected in E11.5 mouse embryo section

Shh transcripts were analyzed in the transverse section of E11.5 mouse embryo by *in situ* hybridization (A) (n=4). Strong signals were observed at the floor plate (B, blue arrow) and the notorchord (B, green arrow). No signals were observed in the heart region (C). Bar: 500μm

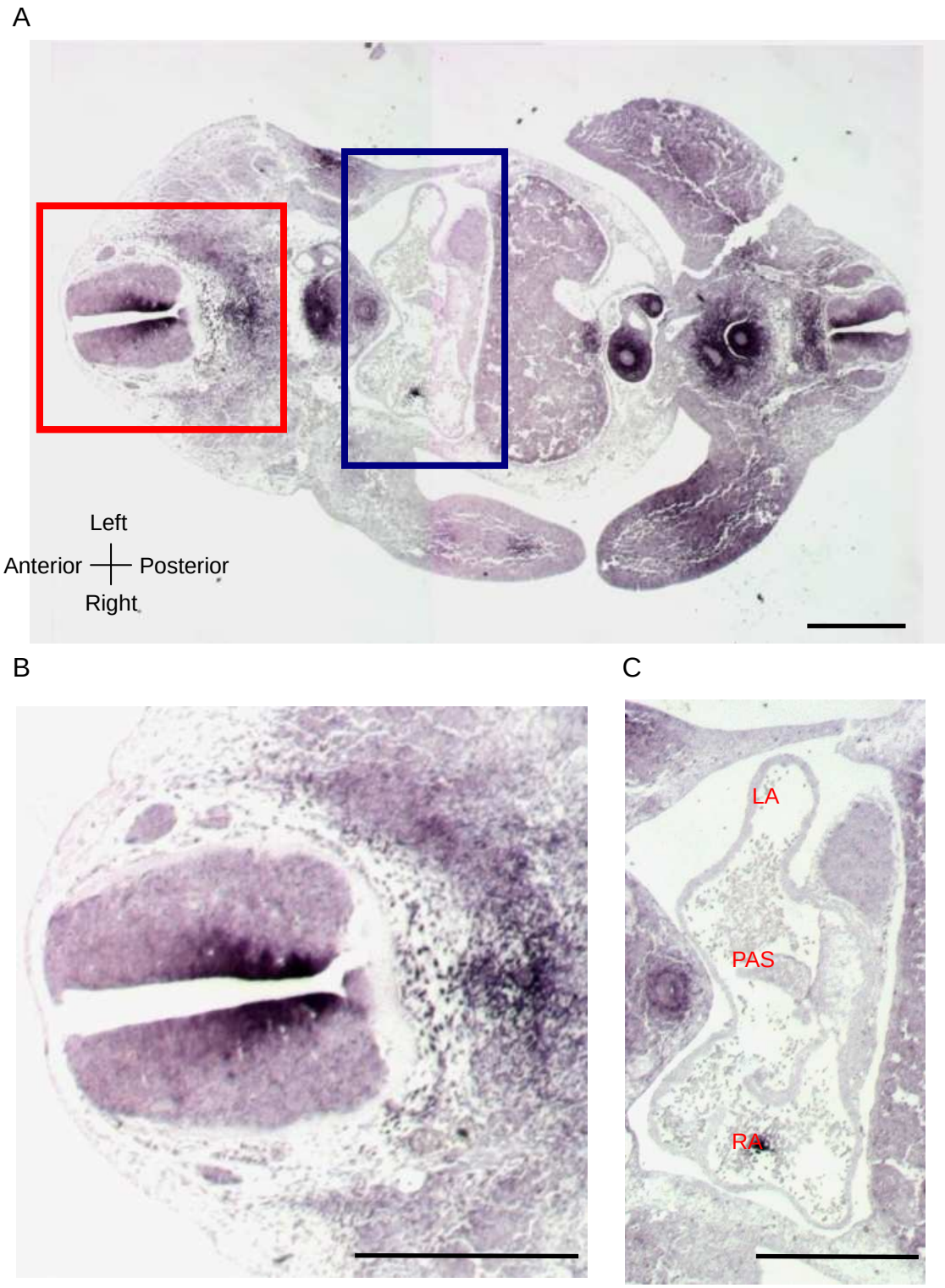

Figure 3.17 *Ptch1* mRNA detected in E11.5 mouse embryo section
Ptch1 transcripts were analyzed in the transverse section of E11.5 mouse embryo using *in situ* hybridization (n=4). (A). *Ptch1* signals were observed around the floor plate and the notochord where the Shh expressed (B). No signals were observed in the heart region (C). Bar: 500μm

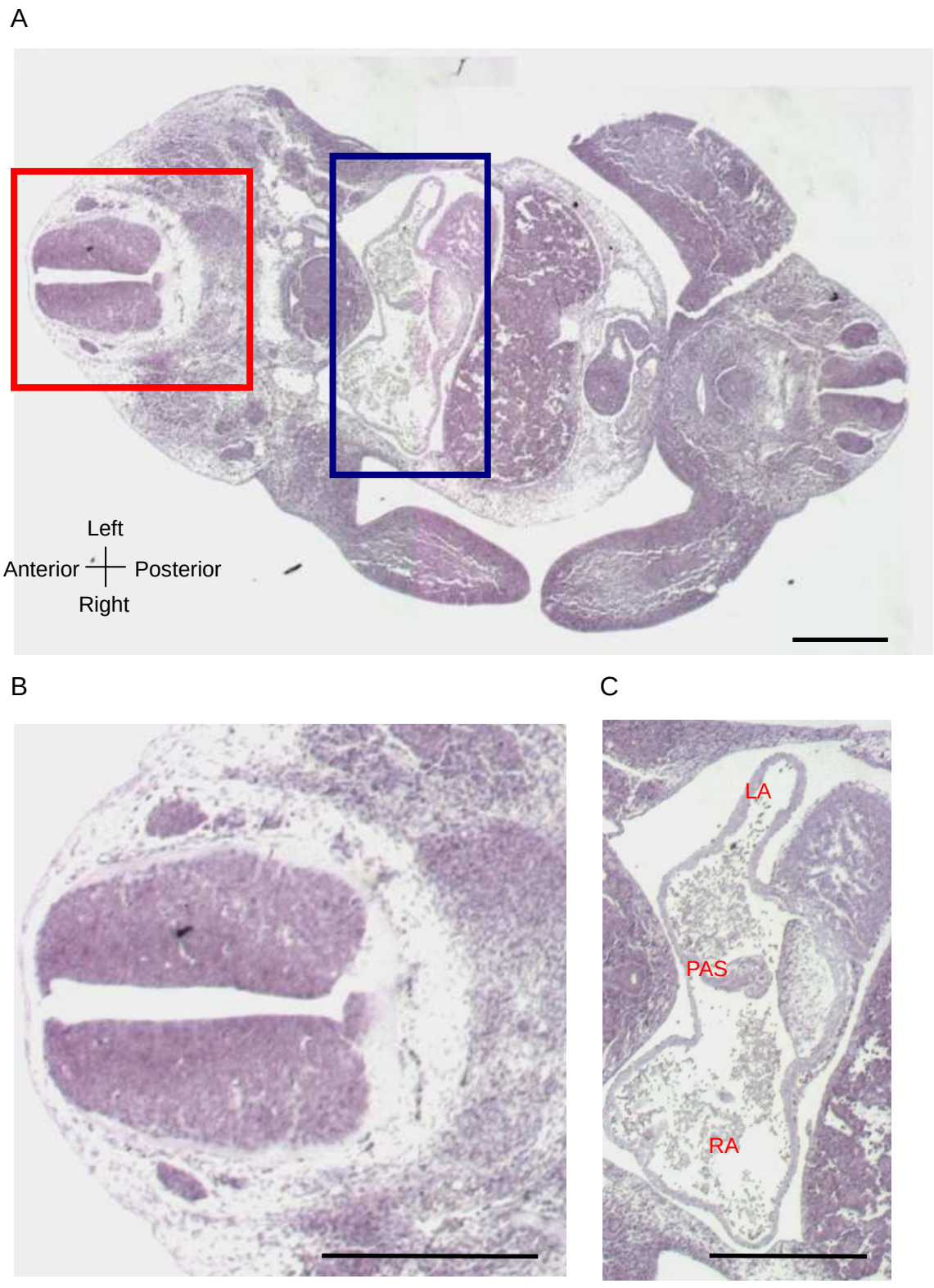

Figure 3.18 *Evc* mRNA detected in the E11.5 mouse embryo section

Evc transcripts were analyzed in the transverse section of E11.5 mouse embryo (A) (n=4). No *Evc* signals were observable around the floor plate, notochord (B), or in the heart region (representative section, C). Bar: 500μm

Since the *Evc* transcript was not detected in E11.5 embryos, the serial transverse sections of the E9.5 embryo were used following the same protocol performed in the E11.5 embryos. Nevertheless, no *Evc* positive cells were observed in these embryos (Figure 3.19). These results suggested that *Evc* mRNA transcripts were either too low to be detected or were not expressed at these developmental stages.

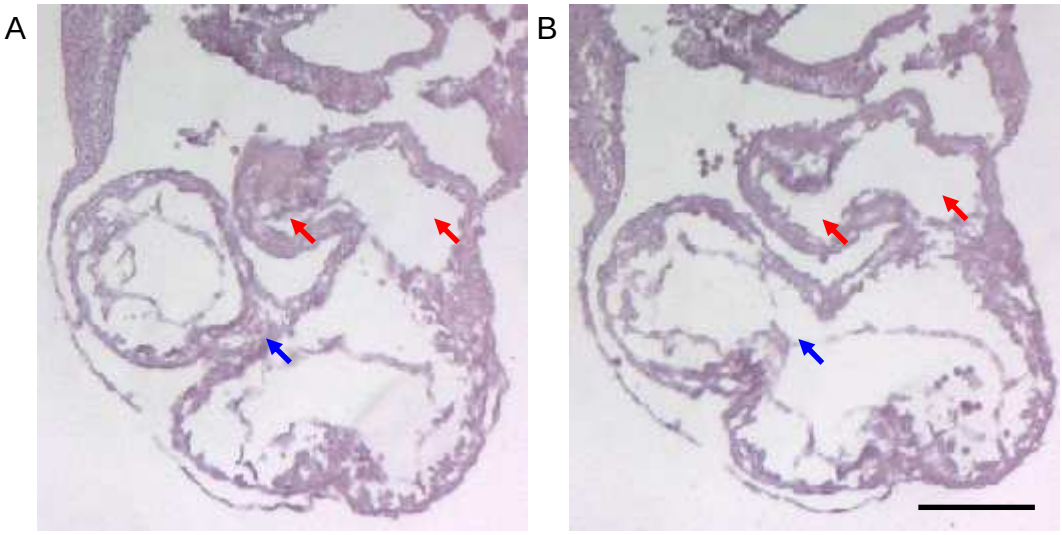

Figure 3.19 Undetected *Evc* transcript in the heart region in E9.5 embryos

Sister sections from the wild-type mouse embryo at E9.5 hybridized with *Evc* antisense probe (n=4). *Evc* mRNA signals were not observed in the heart region. Red arrows indicate the left and right components of the common atrial chamber. Blue arrows indicate the bulbo-ventricular canal. Bar: 100μm

Evc expression was observed at the dorsal side of the atrium wall (E11.5) and the atrial septum (E12.5) during heart development using X-Gal staining. However, the *Evc* transcript was not observable at the heart region of E11.5 and E9.5 embryos. This data indicated that *Evc* expression is low or absent at these development stages.

3.4 Discussion

3.4.1 No heart developmental defects were observed in *Evc*$^{-/-}$ mice

To verify whether the absence of Evc affects heart development, histological analysis was performed in *Evc*$^{-/-}$ mice and compared with that in heterozygous and wild-type littermates. Variations in cardiac morphology were observed in *Evc* deficient mice. However, no significant difference was observed between *Evc*$^{-/-}$, *Evc*$^{+/-}$ and the wild-type control (section 3.2). The atrial septal defect, a common heart defect in EvC patients, was not observed in any of the *Evc*$^{-/-}$ mice.

The uncommon features of the heart position and the heart apex were observed in 12 out of 25 mice and no significant difference was observed between genotypes. These might be artifacts caused during sample preparation. To increase penetration of the fixation solution, the thorax portion of the mouse was extracted after dissecting out the embryos from the uterus. Tissue deformation might have occurred during this procedure. Injecting the fixation solution using thin needles might be an alternative to increase penetration. However, based on the embryo size and softness, even thin needles might damage the tissues. Variations in the degree of the ventricular septum muscle and trabeclae were observed in wild-type, *Evc*$^{+/-}$ and *Evc*$^{-/-}$ mice. No significant difference was observed between genotypes. The heart features were scored based on the figures in the book, “The Atlas of Mouse Development” (Kaufmann, Revised Edition, 1995). Based on the variation among different mouse strains, the unusual features defined in this study might be common phenotypes in the mouse with

C57Bl/6J-129Sv genetic background.

The atrioventricular valves in some samples in this study dilated and formed a bubble shape structure. This abnormality of the atrioventricular valves was observed at a higher occurrence rate in homozygous samples (7 of 14) compared to the wild type (1 of 6) or the heterozygous (1 of 5) littermate. However, this difference is not statistically significant between wild-type/heterozygous and homozygous samples (Fisher's exact test, p=0.2). During heart valve development, the endothelial cells lying at the site of the future valves delaminate and protrude into the extracellular matrix where they proliferate and differentiate into mesenchymal cells. The extracellular matrix and mesenchymal cells undergo differentiation, apoptosis and remodeling to form mature valves (de Lange *et al.*, 2004). Several studies have reported signaling pathways and proteins to be involved in heart valve development including VEGF, NFATc1, Notch, Wnt/β-Catenin, BMP/TGF-β, ErbB, and NF1/Ras (de Lange et al., 2004; Erickson et al., 1997; Gitler et al., 2003; Kim et al., 2001; Lakkis and Epstein, 1998; Miquerol et al., 1999; Ranger et al., 1998; Timmerman et al., 2004). The bubble shaped leaflet of the atrioventricular valves might result from abnormal apoptosis, delayed developmental processes, or other unknown mechanisms. Further study is necessary to determine the functions of Evc protein in valve development.

About 60% of EvC patients demonstrate an atrial septal defect. However, no defect of the atrial septum was observed in *Evc*$^{-/-}$ mice in this study. The absence of the atrium septum defect might be due to differences between mice and humans. Biben and colleagues found that *Nkx2-5* deficient mice

showed a much milder phenotype in atrial development compared to human patients with the same gene deficiency. They found that a similar gene, *Nkx2-6*, expressed at an earlier stage of atrial development, compensated for the deficiency in *Nkx2-5* in mice (Biben *et al.*, 2000). Smith-Lemli-Opitz syndrome (SLOS) is an autosomal recessive disease with extremely variable phenotypes in human patients. The typical SLOS phenotypes are craniofacial malformation, mental retardation, poor growth, and structural anomalies of heart, lungs, brain, limbs, and gastrointestinal tracts. SLOS results from defects of the DHCR7 protein, which converts 7-dehydrocholesterol (7-DHC) to cholesterol at the last step of cholesterol synthesis. As cholesterol is essential for synthesis of a mature hedgehog ligand, perturbed hedgehog signaling might underlie some phenotypes observed in patients with SLOS (Cooper *et al*., 2003). In *Dhcr7*$^{-/-}$ mice, craniofacial malformation and growth retardation were observed, however, no significant abnormalities were observed in the heart, kidney, spleen, liver, and skeletal structure (Wassif *et al*., 2001). This suggests that the low level of cholesterol is sufficient for development or there might be unknown mechanism(s), which compensate in the mouse heart. Thus, *Evc* in the mouse mutant is not unique in failing to display a phenotype observed in patients.

Development of the atrial septum begins at E10.5 and is complete at E13.5 (Webb *et al.*, 1998). During atrial septum development, the primary atrial septum expands from the dorsal side of the atrium wall toward the atrioventricular cushion. Meanwhile, the extracardiac tissue penetrates into the atrium and the superior portion of this structure follows the primary

atrial septum with a mesenchymal cap on its leading edge (Mommersteeg *et al.*, 2006). The left-right connection of the atrium closes when the extra-cardiac tissue, the primary atrial septum, and the superior endocardiac cushion all fuse. Fusion of the atrioventricular endocardial cushion separates the left-right atrioventricular connection (Dalgleish, 1976). Shh signaling from the foregut endoderm is essential for developing normal atrioventricular septation. The dorsal mesocardium shows abnormal differentiation and migration into the atria when Shh is deficient and causes the dorsal mesenchymal protrusion defect which results in atrioventricular septation defects (Goddeeris *et al.*, 2008).

Previous studies have demonstrated that mouse phenotypes are often more apparent with an inbred background than with a mixed background. *Evc*$^{-/-}$ mice with C57Bl/6J-129Sv genetic background were backcrossed with the inbred strain C57Bl/6J for nine generations. After analyzing three litters, no atrial septal defects were observed in *Evc*$^{-/-}$ mice with an inbred C57Bl/6J genetic background. This data suggested that Evc protein is not essential for mouse heart development.

3.4.2 Expression of *Evc* in heart development

Approximately 60% of EvC patients have cardiovascular malformations, indicating EVC plays a role in heart development. β-galactosidase staining positive cells were observed at the dorsal side of the atrial wall and atrial septum at the E11.5 and E12.5 stage of *Evc*$^{-/-}$ embryos (section 3.3.1). However, expression was observed in only a small number of cells at these embryonic stages and the cell types were not defined. The significance of

this study is unclear. Further studies are necessary to define the cell type expressing Evc protein at these developmental stages and the functions of Evc in these cells.

Although β-galactosidase staining in *Evc*$^{-/-}$ is an easy method to analyze the expression of Evc protein, this may reflect gene expression at an earlier stage of development. *Evc* mRNA was not detected in the heart in E11.5 embryos by *in situ* hybridization (Figure 3.18). The data indicated that *Evc* expression in the mouse heart is minimal and hard to detect by *in situ* hybridization at the earlier time point (E9.5) studied.

Lipscomb Sund and colleagues detected *Evc* transcripts at the tip of the primary atrial septum with *in situ* hybridization in wild-type E13.5 mouse embryos. *Evc* transcripts were also observed in the AV cushion, the connective tissue of the outflow tract, and the ribs (Lipscomb Sund *et al.*, 2009). The Lipscomb Sund study used immunofluorescence staining and in situ hybridization to determine *Evc* expression in the heart region. The Immunofluorescence staining images indicated positive signals in the developing atrial septum. However, other signals with equivalent intensity besides those indicated are scattered throughout the same field and not mentioned in the text. The region they state to have positive signal regions in the in situ hybridization panels are the regions with higher cell density. The expression of *Evc* mRNA in the heart region is still under debate.

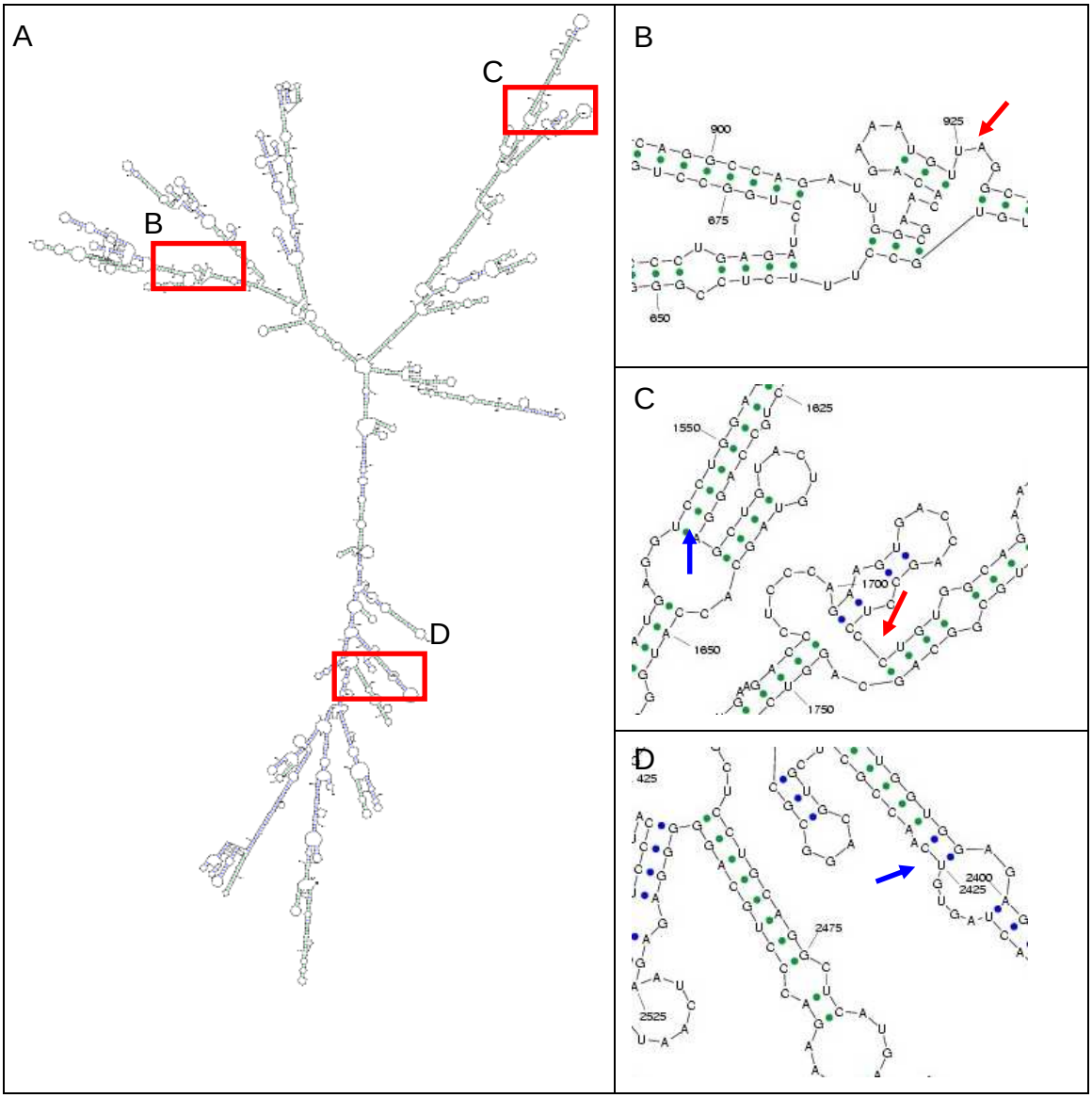

Figure 3.20 Minimum free energy image generated from the *Evc* mRNA sequence (NM_021292) 1-2730 (due to the limitation of prediction program) with Sfold

2730bp (1-2730) of *Evc* mRNA sequence was subjected to predict the minimum free energy structure with Sfold (A). Three red squares indicate both ends of *Evc* probes used in this study and in the Lipscomb Sund study, and the right column shows higher magnificent images. The red arrows in B and C indicate the 926 and 1717 position of the predicted mRNA of the *Evc* probe detected in this study. The blue arrows in C and D indicate the 1633 and 2426 position of the predicted mRNA.

The probes used for in situ hybridization in these two studies are different

and could affect sensitivity of this assay. The *Evc* probe in this thesis was designed against the *Evc* c.926 - c.1717 (length 792 base) based on previous tooth bud studies (Dr. M. Nakatomi, personal communication). In contrast, Lipscomb Sund *et al.* used the probe against *Evc* c.1633 - c.2426 (length 794 base). When predicting by Sfold (http://sfold.wadsworth.org, (Ding and Lawrence, 2003; Ding et al., 2005)), the *Evc* mRNA was Y shaped. The c.926 - c.1717 was located at the compact V head while c.1633 - c.2426 was located at the loose tail (Figure 3.20). The folding might affect hybridization efficiency in tissues.

3.4.3 Study of *Vangl2* and *Evc* double knockout mice

Out of 1,500 *Evc* breeding mice, one of the $Evc^{+/-}$ mice showed a curved tail phenotype, similar to the $Vangl2^{+/-}$ mouse. As the interaction of Wnt and Hh is important in development, it is worth tracing if *Vangl2* expression is able to compensate for the heart phenotype in $Evc^{-/-}$ mice even if the recurrent rate is low (~1/1500). Since only $Evc^{-/-}$ mice have shown phenotypes and *Vangl2* inherits a semi-dominant manner, only $Evc^{-/-};Vangl2^{+/-}$ and $Evc^{-/-};Vangl2^{-/-}$ mice are valuable for analysis. Two double heterozygous female mice were obtained in six litters of $Evc^{+/-}$ and $Vangl2^{+/-}$ cross. In theory, 3/16 of the offspring would be either $Evc^{-/-};Vangl2^{+/-}$ or $Evc^{-/-};Vangl2^{-/-}$. However, among the nine embryos analyzed, none were $Evc^{-/-};Vangl2^{-/-}$ and one $Evc^{-/-};Vangl2^{+/-}$ embryo were obtained (missing in processing) (Table 3.6). The project was eventually abandoned due to time constraints, without reaching a conclusion. The possibility that $Evc^{-/-};Vangl2^{-/-}$ mice are lethal at early embryonic stage cannot be excluded.

3.4 Conclusion

Research has detected EVC mRNA in the developing heart by RT-PCR in human and 60% of EvC patients have demonstrated heart developmental defects (Ruiz-Perez *et al.*, 2000). No significant difference in the occurrence of heart variation indicates that *Evc* might not be involved in the heart development in mice or that other protein or mechanisms in the mouse heart may compensate for the absence of Evc protein In addition, the protein expression study through *LacZ* reporter analysis showed no differences between the heterozygous and $Evc^{-/-}$ mouse. An *in situ* hybridization study of wild-type embryos did not detect *Evc* transcripts in the heart region. Although disappointing and unexpected, these results show that the $Evc^{-/-}$ mouse is not a suitable model to study atrial septal defects observed in human patients. Therefore, the focus of this program has shifted from cardiac development to cell based studies.

Chapter 4 Cellular location of Evc and Evc2 proteins

4.1 Introduction

4.1.1 Depletion of Ihh signaling in the absence of Evc protein

Shortening of the long bones and ribs are major features of EvC syndrome. Although several signaling pathways are involved in skeletal development, Indian hedgehog (IHH) is one of the master regulators (Kronenberg, 2003). Furthermore, *Evc*$^{-/-}$ mice share several phenotypes with mice impaired in Ihh signaling, such as epiphyseal shortening caused by chondrocyte hypertrophy near to the articular region, defective perchondrium to perosteum induction and mineralization of synchondroses, indicating the possibility that Evc plays a role in Ihh signaling. The expression of *Ihh* is normal, but expression of *Ihh* downstream genes *Ptch1* and *Gli1* was markedly decreased in *Evc* deficient mice (Ruiz-Perez *et al.*, 2007). Furthermore, the localization of SMO to primary cilia and GLI3 processing is defective in intraflagellar transport mutants (Huangfu and Anderson, 2005; May et al., 2005). Although cilia are present in *Evc*$^{-/-}$ chondrocyte, western blotting demonstrated that although GLI3 processing appears normal, a significant defect downstream of SMO was observed (Ruiz-Perez *et al.*, 2007). Taken together, these data suggest that Evc is an intracellular component of the hedgehog signal transduction-pathway, required for normal transcriptional activation of Ihh target genes.

4.1.2 Hedgehog signaling and cilia

Hedgehog signaling is one of the most vital key regulators involved in embryo development. The molecules are important in establishing the basis of the body plan and the anterior-posterior body segmentation during stages of development. Previous studies demonstrated that Evc protein was located at the region around the basal body of cilia (Ruiz-Perez *et al.*, 2007) which play an essential role in the Hh pathway. In 2007, Caspary and colleagues described a lethal mouse mutant, *hennin* (*hnn*). The hnn cilia mutant showed short cilia with a specific defect in the structure of the ciliary axoneme and defects in sonic hedgehog signaling. At E8.0, the microtubule doublets were incomplete in the cilia of embryonic nodes of an hnn mouse (Caspary *et al.*, 2007). A T-to-G transversion in the splice acceptor site of exon 2 of *Arl13b* gene, encoded for ADP-ribosylation factor-like 13B protein. This indicated that the mutation of cilia proteins could cause ciliary structural defects.

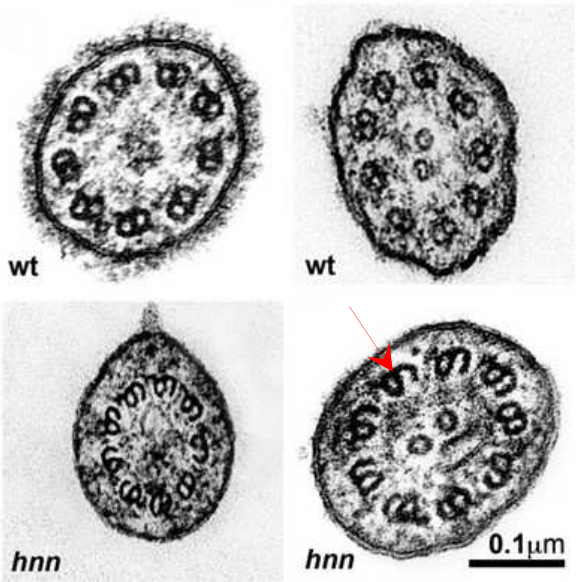

Figure 4.1 Ciliary structure analysis in *hnn* mutant mouse (adapted from Caspary *et al.*, 2007**)**
The doublets of microtubule in cilia from *hnn* mutant embryos were incomplete (red arrow) when comparing with the wild-type siblings.

4.1.3 Choice of cells

Since *Evc* mRNA exists in both bone and kidney, cells isolated from these organs are good materials for investigating the function of Evc protein and its relationship with cilia and the Hh signaling pathway (Ruiz-Perez *et al.*, 2007). Herein, we used primary chondrocytes and osteoblasts and a mouse inner medullary collecting duct (mIMCD-3) cell line for our investigations. Primary chondrocytes and osteoblasts were isolated from the tibial epiphyses and calvaria (section 2.8), respectively, of E18.5 mice. Evc is most highly expressed at these sites, and is most likely to have cellular function. All cells were cultured long enough to obtain sufficient cells for the experiments (usually 5-7 days) without further passage. Results from this study are compared with results from previous studies of the Hh signaling pathway of mouse embryonic fibroblasts (MEF), generated from wild type and $Evc^{-/-}$ proteins.

4.1.4 Deciliation

Previous studies demonstrated that Evc located around the basal body of cilia by immunofluorescence staining (Ruiz-Perez *et al.*, 2007). Since proteins located at different cilia sites might play distinct roles (Li *et al.*, 2010; Zhao *et al.*, 2010; Zhou *et al.*, 2010), precise localization of Evc protein might provide clues to its function. Deciliation, which breaks at the transition zone, is one approach to understand whether proteins are located distal to the transition zone. Several techniques were used for deciliation, one reported by Fliegauf (Fliegauf *et al.*, 2006) uses Ca^{2+} to induce the contractio(Zhao et al., 2010)n of centrin, which then severs the

cilium at the distal end of the transition zone (Figure 4.2). The reactions eventually release the cilium, above the transition zone, into the supernatant. The detached cilia are collected by high-speed centrifugation. Thus, the location of Evc protein can be determined by Immunofluorescence staining on cilia and deciliated cells.

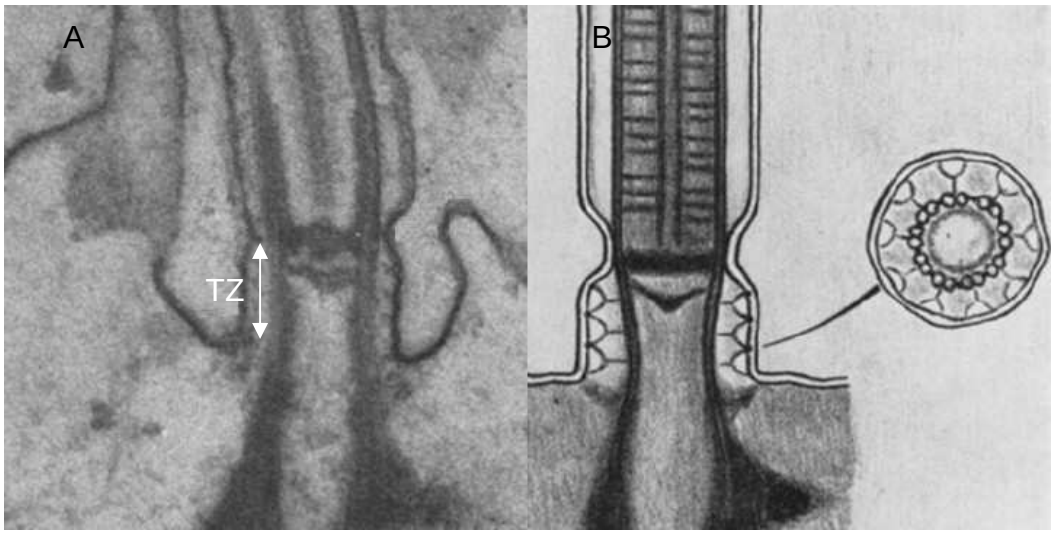

Figure 4.2 Transition zone in Elliptio cilium (adapted from Gilula & Satir, 1972).
Longitudinal view of the transition zone (marked as TZ) in Elliptio cilium (A). Schematic view of the “champagne glass” structures within the transition zone (B).

4.1.5 Aims

Evc$^{-/-}$ mice share several phenotypes with mice impaired in Ihh signaling, for example, epiphyseal shortening caused by chondrocyte hypertrophy near to the articular region, defective perchondrium to perosteum induction, and mineralization of synchondroses. Moreover, diminished Ihh signaling was observed in MEFs generated from *Evc*$^{-/-}$ mice (Ruiz-Perez *et al.*, 2007). In mIMCD-3 cells, Evc protein was located at the region around the basal body of cilia, structures that mediate Hh signaling (Ruiz-Perez *et al.*, 2007).

However, the functions of Evc in Hh signaling are still unknown. To investigate the function of Evc in Ihh signaling pathway, and cilia formation in the absence of Evc proteins, this chapter focuses on refining the subcellular localization of EVC protein by deciliation and immuno-TEM. We analyze the ciliary structure of chondrocytes from *Evc*$^{-/-}$ mice using TEM, investigate the localization of Evc protein in *Evc*$^{-/-}$ cells with Immunofluorescence staining, and examine the inconsistence of nuclear localization between human fibroblasts and MEFs, the detail of which will be described in section 4.2.6, by subcellular fractionation assay.

4.2 Results

4.2.1 Evc localizes to the region of the cilia transition zone

Fliegauf (Fliegauf *et al.*, 2006) reported the deciliation protocol optimized for human respiratory epithelial cells. However, when following this protocol, most of the mIMCD-3 cells became detached from the growth surface. This may have been that the solutions used by Fliegauf were too harsh for these cells. Consequently, the concentration of deciliation solution and treatment time was modified (section 2.9). In the modified method, mIMCD-3 cells were treated with the 30mM Ca^{2+} containing a buffer to induce centrin contraction, a component of contractible proteins within the transition zone. The contraction severed the cilium at the distal end of the transition zone (Figure 4.2). The reactions eventually released the cilium above transition zone into the supernatant, and the broken cilia were collected by high-speed centrifugation. Immnfluorescent stain (section 2.10) of cilia and the deciliated cells then clearly identified the location of Evc protein.

To locate cilia more precisely, acetylated tubulin and γ tubulin were used as cilium and basal body markers respectively. Since cilia are long linear structures, and basal bodies have short tubular structures, the two could also be distinguished by shape under fluorescent microscopy. In mIMCD-3 cells (Figure 4.3, A-C), the cilium protruded out from the membrane. Evc protein (Figure 4.3, A) was localized near the basal body as previously described (Ruiz-Perez *et al.*, 2007). Cilia were successfully removed from the cell surface after deciliation (Figure 4.3, D-I), the basal body (Figure 4.3, E, arrows), and a small portion of cilium (Figure 4.3, E, arrowhead), remained on the cell. Evc protein was detected on the cell portion, whereas no EVC protein was detected in the sheared off cilia (Figure 4.3, G-I). The data indicated that EVC protein was mainly located between the basal body and transition zone of the cilia.

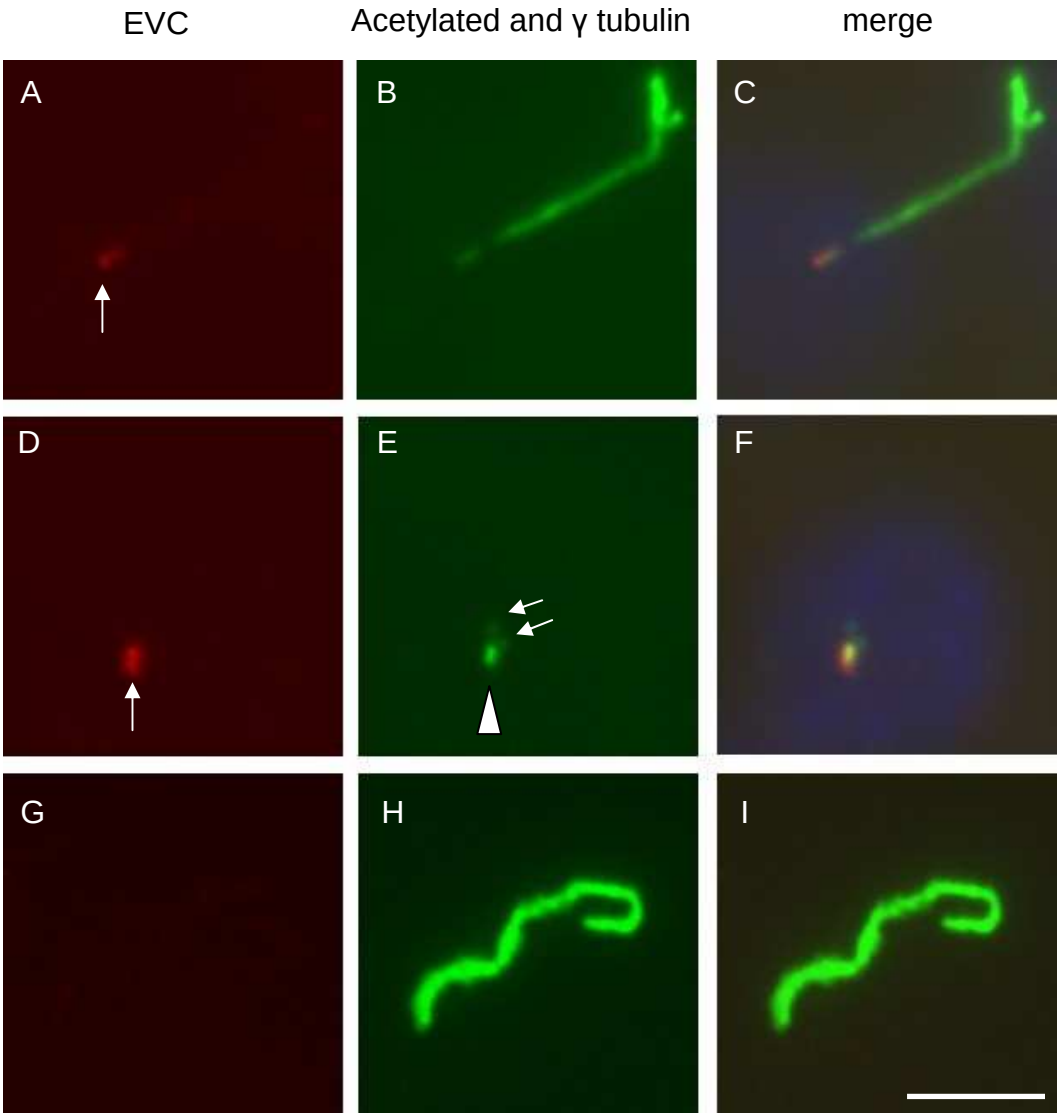

Figure 4.3 Representative figures of deciliation treatments of mIMCD-3 cells

mIMCD-3 cells both with and without deciliation treatment were detected with Evc antibodies (red panel), acetylated tubulin (marker of axoneme, green panel), and γ-tubulin (marker of centrioles/basal body, green panel) (n=3). The faint blue signal indicates a nucleus marked by DAPI (blue, C and F). The upper row (A, B, C) represents cells without deciliation treatment. The EVC protein (A, white arrow) was localized to the base of cilium. The middle row represents the cell after deciliation treatment. EVC protein was detectable in the cells after deciliation treatment (D, white arrow). The γ-tubulin composed daughter centriole and the basal body (E, white arrows) and a small part of axoneme (E, white arrowhead) appeared in the treated cell. The lower row represents the sheared-off cilium. No Evc protein was observed on the sheared-off cilia (G). The absence of DAPI stain (I) indicated that the cilium signal did not come from the cell debris. Bar: 5μm

Following deciliation, only acetyl-tubulin was observed at sheared-off cilia. It is doubtful that the linear structure shown at Figures 4.3, H was true cilium. Therefore, verification of the sheared off cilia by another cilia-specific protein became necessary. Sufu is a component in the hedgehog pathway, and is expressed at the tip of cilia when the hedgehog pathway is activated (Haycraft *et al.*, 2005). Treatment of mouse mIMCD-3 cells with purmorphamine for 72 hours activated the hedgehog pathway. Prior to deciliation, Sufu was observed at the cilium tip prior to deciliation, and after treating with purmorphamine (Figure 4.4, D, arrow), but not following treatment with DMSO alone (Figure 4.4, A).

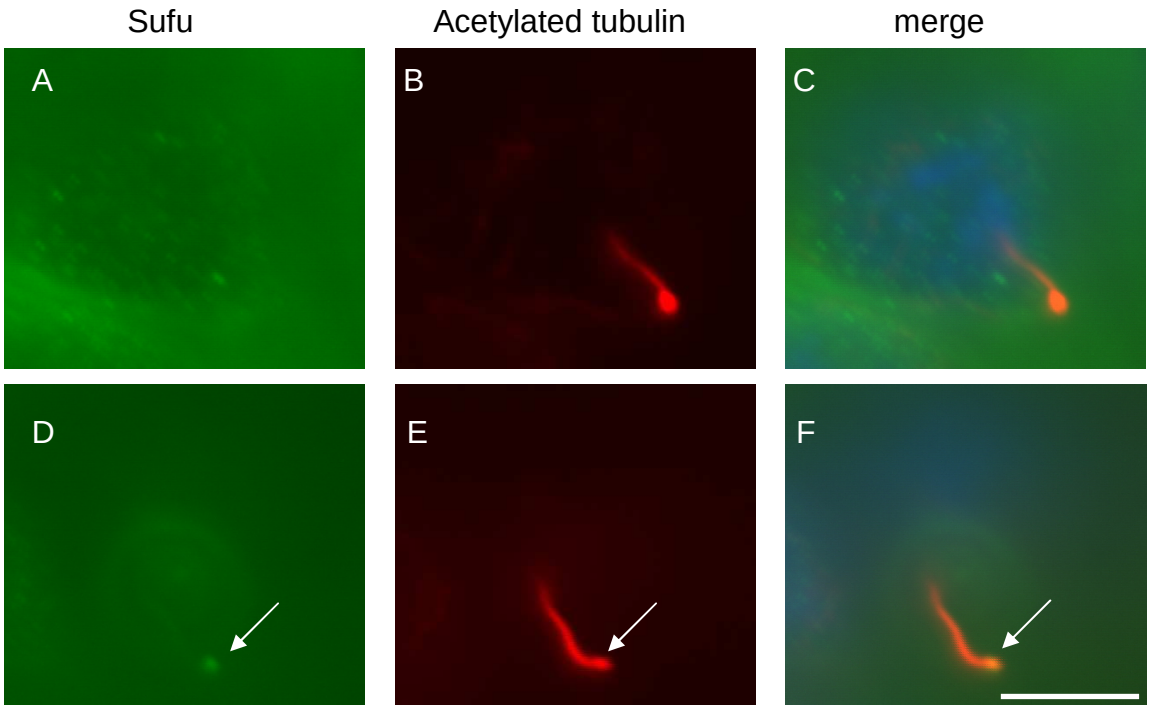

Figure 4.4 Representative figures of localization of Sufu in purmorphamine treated mIMCD-3 cells

MIMCD-3 cells treated with DMSO (upper row) or purmorphamine (lower row) were detected with antibodies against both Sufu (green panel), and acetylated tubulin (red panel) (n=3). Use of DAPI countered stained nuclei. Sufu was not found at the tip of cilia following treatment with DMSO (A). Sufu protein accumulated at the tip of cilium after treating with purmorphamine for 72 hrs (lower row). Bar: 5μm

mIMCD-3 cells were treated with purmorphamine for 72 hours, deciliated, and triple immunofluorecent stained for Evc, acetylated tubulin and Sufu. Figure 4.5.A through D shows the cell without deciliation treatment, and both EVC (Figure 4.5, A, arrow) and Sufu (Figure 4.5, C, arrow) could be observed. After deciliation (Figure 4.5, E through H), Evc (Figure 4.5, E) and small portion of acetylated tubulin (Figure 4.5, F, arrow) was observed, demonstrating successful deciliation. Figure 4.5, I through L, demonstrated immunofluoresecent stain on the putative sheared-off cilia (Figure 4.5, J). However, a Sufu signal was not detected in the linear structure (Figure 4.5, K). The undetectable Sufu signal might results from disruption of cilia structure during deciliation procedure.

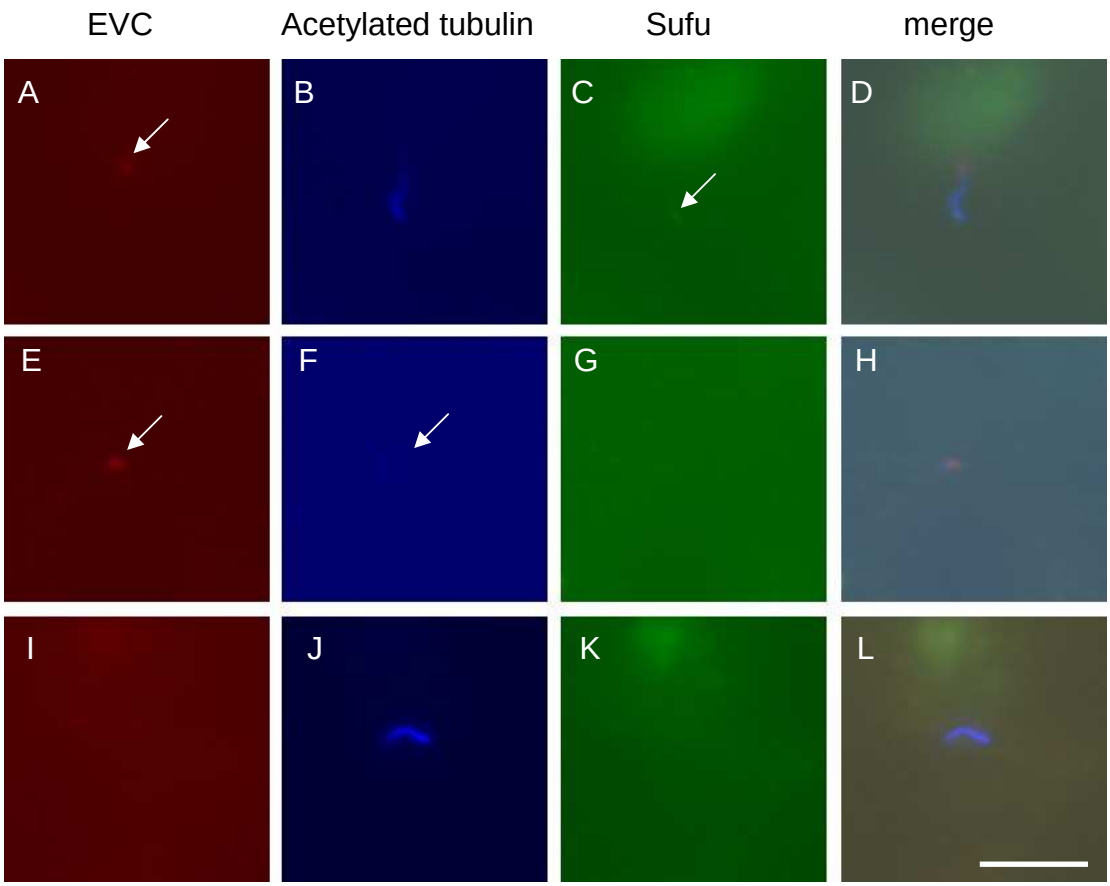

Figure 4.5 Representative figures of deciliation of purmorphamine treated mIMCD-3 cells

Purmorphamine treated mIMCD-3 cells stained with antibodies detected Evc (red panel), acetylated tubulin (blue panel, as a marker for cilium), and Sufu (green panel) (n=3). Without deciliation treatment, Evc was localized to the base of cilium (A, white arrow) and Sufu was localized to the tip of cilium (C, white arrow). After deciliation treatment, Evc (E, white arrow) and a small portion of cilium (F, white arrow) remained localized to cells. No Sufu signals were observed in deciliated cells (G). No Evc proteins were observed on the sheared-off cilium, (I). However, there were no Sufu signals on collected sheared cilia (K). Bar: 5μm

4.2.2 Failure to detect Evc protein by immuno-TEM

To further refine the location of Evc protein, mIMCD-3 cells were examined using immuno-TEM (section 2.11). The immuno-TEM method is reported to determine the subcellular localization of other cilia and basal body proteins successfully (Paoletti *et al.*, 1996). Initially, we used the same staining

method as for Immunofluorescence staining. Figure 4.6 shows that cilia morphology is not good following this protocol. It is likely that this is due to the detergents, triton X-100, and between 20, which were used in the staining steps. The structure of the basal bodies was unseen using this protocol.

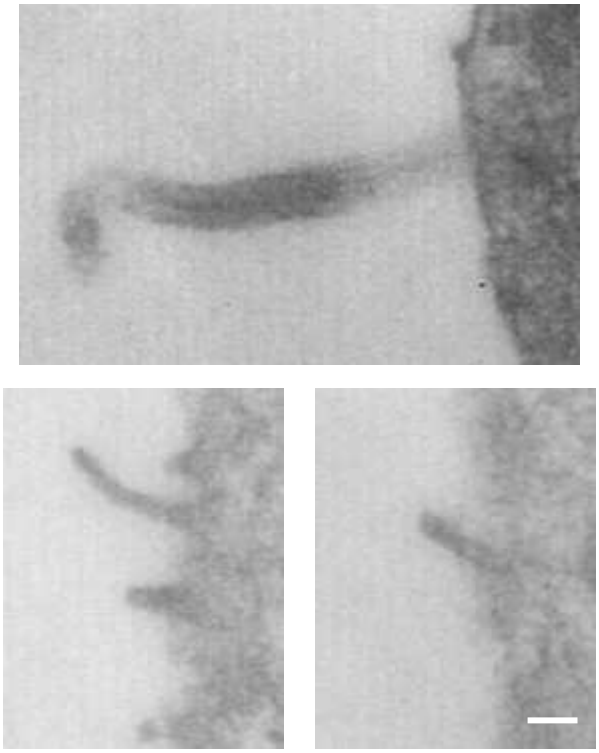

Figure 4.6 Ciliary structure observed after detergent treatment in pre- and post-staining samples. The cilium-like structure was destroyed during immunofluorecent staining (n=3). This may have been due to sensitivity to the detergent, which was applied in order to penetrate the cell membrane and allow the entrance of the primary antibody. Bar: 500nm

To preserve morphology, immuno-TEM followed a modified protocol without using detergent. The cilium morphology appeared unmistakably and basal bodies were found following the detergent-free protocol. Clustered gold particles were located to the base of cilium (Figure 4.7, A, red arrow). However, gold particles also grouped in clusters with no apparent relation to any organelle (Figure 4.7, B, red arrow) or even outside the cell (Figure 4.7, C, red arrow). Single gold particles were randomly scattered both inside and outside the cell (Figure 4.7, D, red

arrows). Some basal bodies did not have associated gold particles (Figure 4.7, E). Based on these observations, gold particle staining in this immuno-TEM protocol was non-specific, and this experiment failed to provide the precise localization of Evc protein.

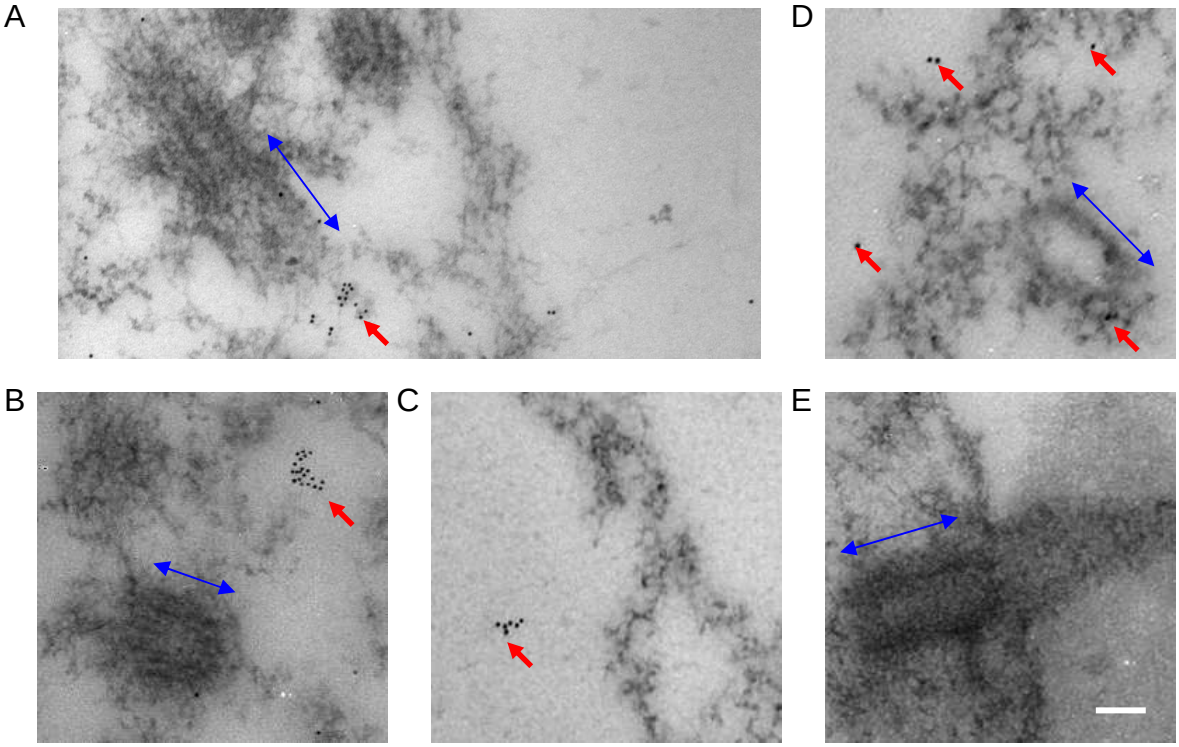

Figure 4.7 Transmission electron micrographics of cilium stain for Evc

Cells treated without detergent underwent the immuno-TEM experiment (n=3). Blue lines indicate the centriole structure (basal body in A and E, basal body or daughter centriole in B and D). Clustered gold particles occurred around the basal body (A, red arrow). However, the gold particles clustering occurred in the absence of any organelle (B, red arrow), or outside the cell (C, red arrow). Some gold particles were randomly scattered (D, red arrows). Some cilia were without any gold particles nearby (E). Bar: 100nm

4.2.3 Normal ciliary structure in *Evc*$^{-/-}$ mouse chondrocytes

Mutation of genes encoding ciliary proteins might lead to the defects of ciliogenesis. To test whether the ciliary structure was affected in the

absence of Evc protein, chondrocytes isolated from E18.5 embryos of wild type and *Evc*$^{-/-}$ mice were used as subjects for ciliary inner structure observation. Initially, sample preparation followed Newcastle University's electron microscopy unit, standard protocol.

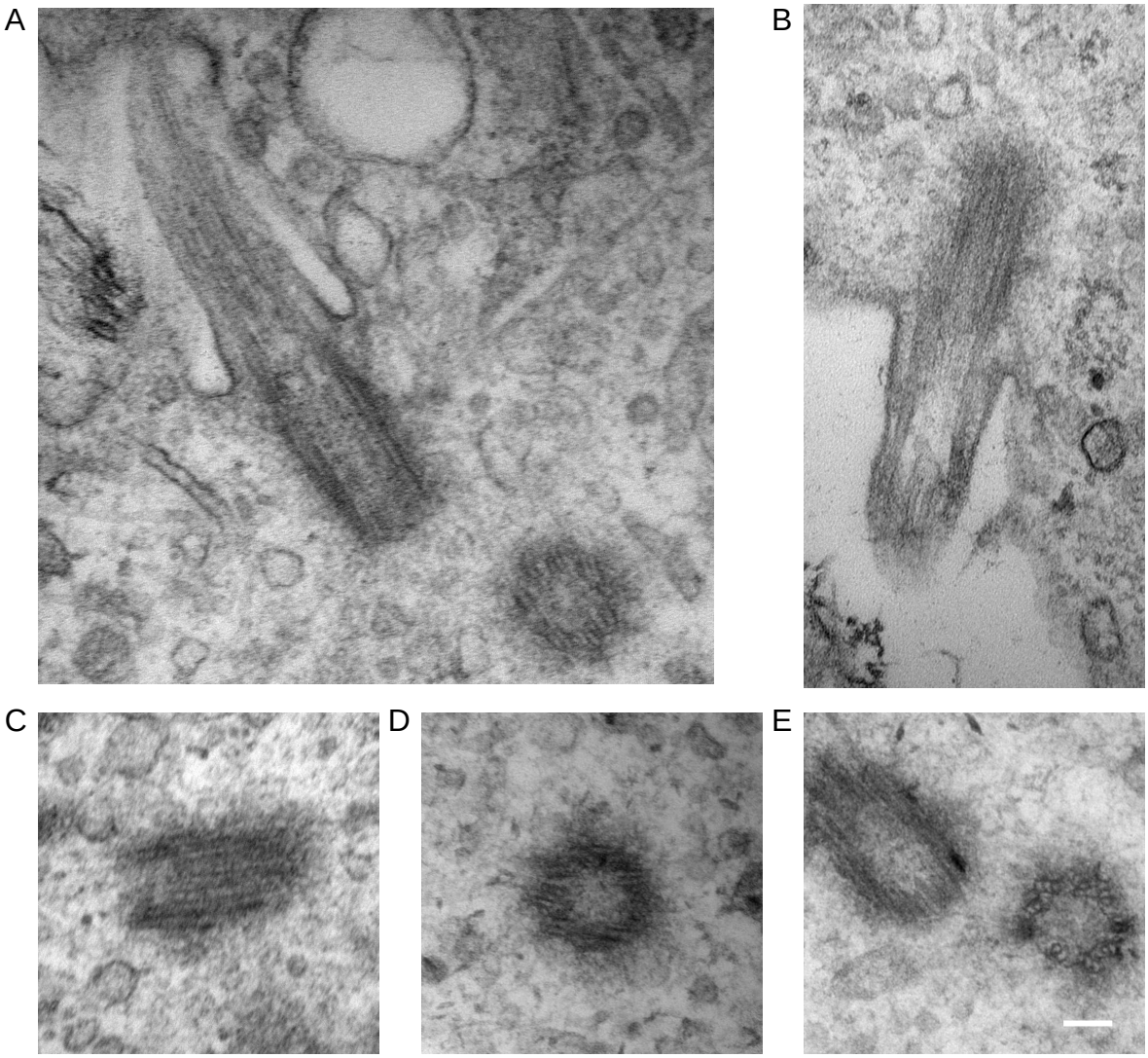

Figure 4.8 Representative figures of ciliary structures observed in sections generated with perpendicular cutting plane
With a vertical cutting plane, cilia were usually found in sagittal sections (Frames A and B) (n=3). Basal bodies and/or daughter centrioles were also observed (C, D, and E). Bar: 100nm

In this protocol, the cutting plane is perpendicular to the culture membrane (Figure 4.9, purple dotted lines). During analysis of 20 grids with sections

generated from *Evc*$^{-/-}$ chondrocytes, we found some cilia related structures. These generated sagittal sections of cilia or basal body/daughter centriole (Figure 4.8). To obtain transverse sections of cilia, we changed the cutting plane from the perpendicular, to parallel to the membrane (Figure 4.9, red dotted lines).

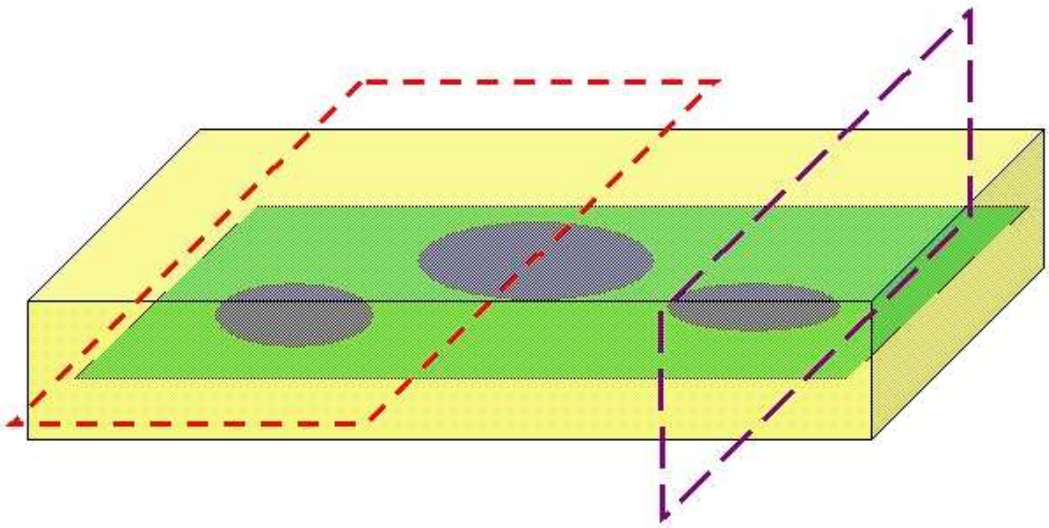

Figure 4.9 Schematic view of the cutting strategy.
Light yellow box indicates the embedding material, cells (light blue) cultured on membrane (light green). The purple dotted lines indicate the initial cutting strategy, perpendicular to the membrane, while the red dotted lines indicates the modified cutting strategy which parallel to the membrane.

Twenty grids with sections from wild type chondrocytes and 20 grids with sections from *Evc*$^{-/-}$ chondrocytes were analyzed. To obtain clear information on the structure of cilia in the absence of Evc, only cilia that could be traced in at least six sequential sections were analyzed. Most of the cilia observed were limited to the basal body/daughter centriole or were less than five transverse sections. In total, three cilia from wild type and two cilia from *Evc*$^{-/-}$ met the criteria.

The longitudinal section of cilia (Figure 4.10, A) showed the two main portions of cilium, the basal body region and the ciliary region. The red lines represent the approximate positions of each transverse section (Figure 4.10, B, and C). In figure 4.10 B, the upper two rows of sections demonstrate that both wild type and *Evc*$^{-/-}$ mouse chondrocytes may contain disorganized doublets wild type (red arrowheads). In the third row, sections crossed the cilia, and showed nine doublets of microtubules. The champagne glass structure (green arrowheads) connecting the doublet to the ciliary membrane was a specific structure in the cilia transition zone. In figure 4.10, each frame in row C shows nine triplets of microtubules and a spiked structure connecting the basal body and plasma membrane (blue arrow). All observed cilia show complete triplet microtubule structures in the proximal region and doublets in the ciliary region (Figure 4.10, B). There were no structural differences between cilia from wild type and *Evc*$^{-/-}$ chondrocytes. Comparison of *Evc*$^{-/-}$ chondrocytes with the wild type cilia found no structural defects in the former. Kiprilov previously reported the circle of disorganized doublets in the distal regions of cilia in wild type cells (Kiprilov *et al.*, 2008).

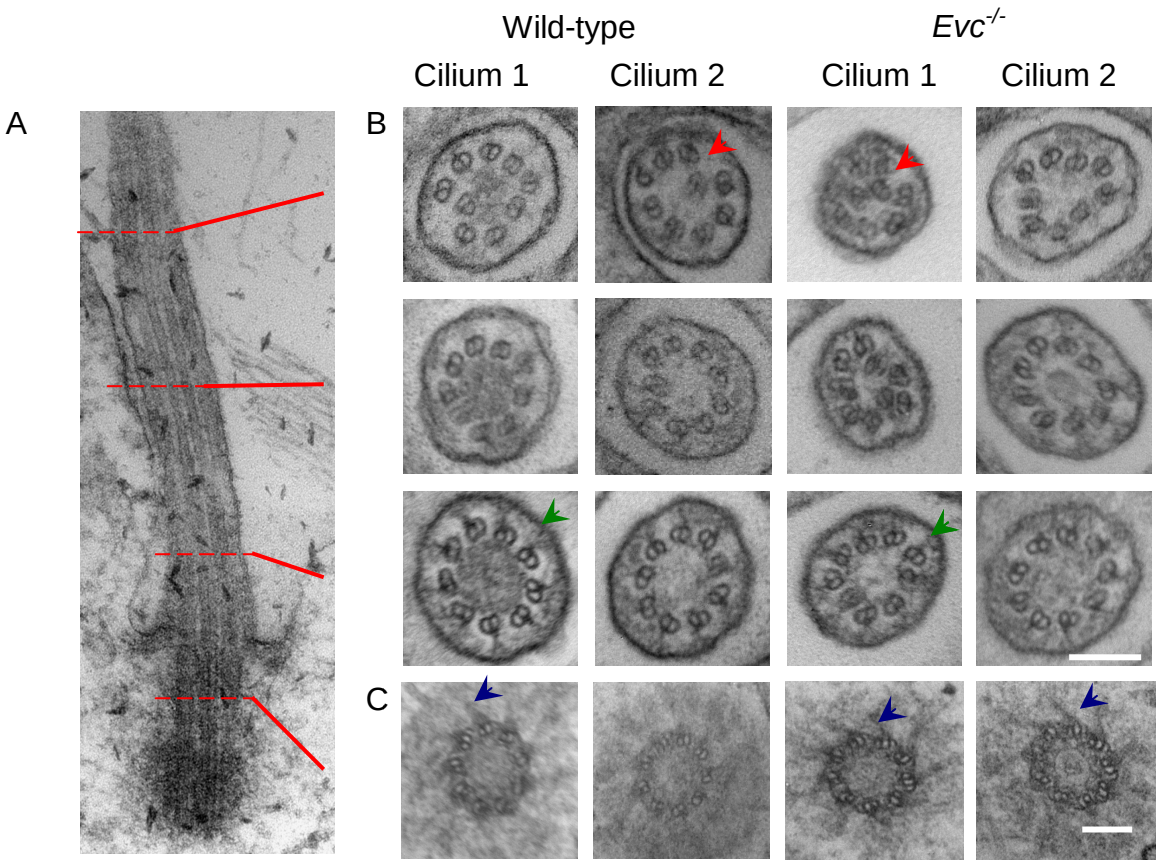

Figure 4.10 Representative figures of longitudinal and transverse sections of chondrocyte cilia.

The longitudinal section (frame A) and red lines indicated the approximate position of the transverse sections seen in frames B and C (n=3). Frame B shows transverse sections of cilia from wild type and *Evc*$^{-/-}$ cells. In both genotypes, disorganized doublets were found in the distal region (red arrowheads) and the champagne glass structures were found in the proximal region (green arrowheads). Nine triplets' microtubules and spiked structures (C, blue arrowheads) were visible in transverse sections of the basal body. Bar: 100nm.

4.2.4 Mis-localization of Evc2 in the absence of Evc protein

A Yeast-two-hybrid study demonstrated that Evc2 is one of the Evc interaction proteins, and that both Evc and Evc2 are present at the base of primary cilia (Dr. S. Tompson, personal communication). To verify the localization of Evc2 protein in the absence of Evc protein, Immunofluorescence staining for Evc2 was performed on MEFs,

chondrocytes and osteoblasts were generated from *Evc*$^{-/-}$ mice and compared to wild type cells. Evc2 was present at the base of cilia in three types of cells generated from wild type mice (Figures 4.11, 4.12 and 4.13). However, no Evc2 signals were detected at the base of cilia in *Evc* deficient cells (Figures 4.11, 4.12 and 4.13).

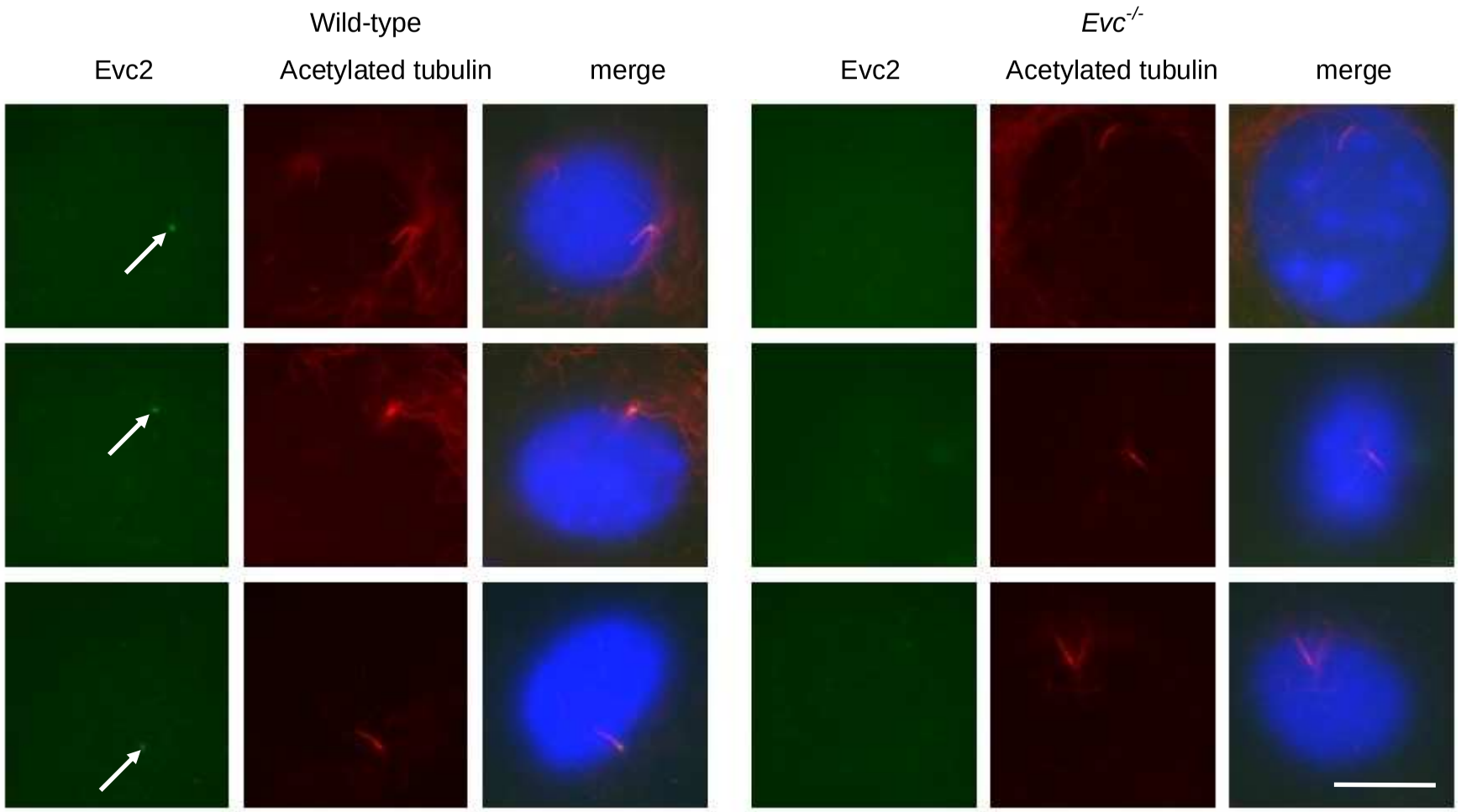

Figure 4.11 Representative figures of disruption of Evc2 localization in MEFs from *Evc*$^{-/-}$ mouse

Three MEFs are shown from *Evc*$^{+/+}$ and *Evc*$^{-/-}$ littermates (n=3). The image on the left in each case is anti-Evc2 (green, white arrows), the middle panel shows the position of the cilium detected by acetylated tubulin antibodies (red) and the merged image shows the nucleus (DAPI stained, blue). In cells from *Evc*$^{+/+}$ mice there is a clear signal at one end of each cilium, this is not seen in the cells derived from *Evc*$^{-/-}$ mice. Bar: 5μm

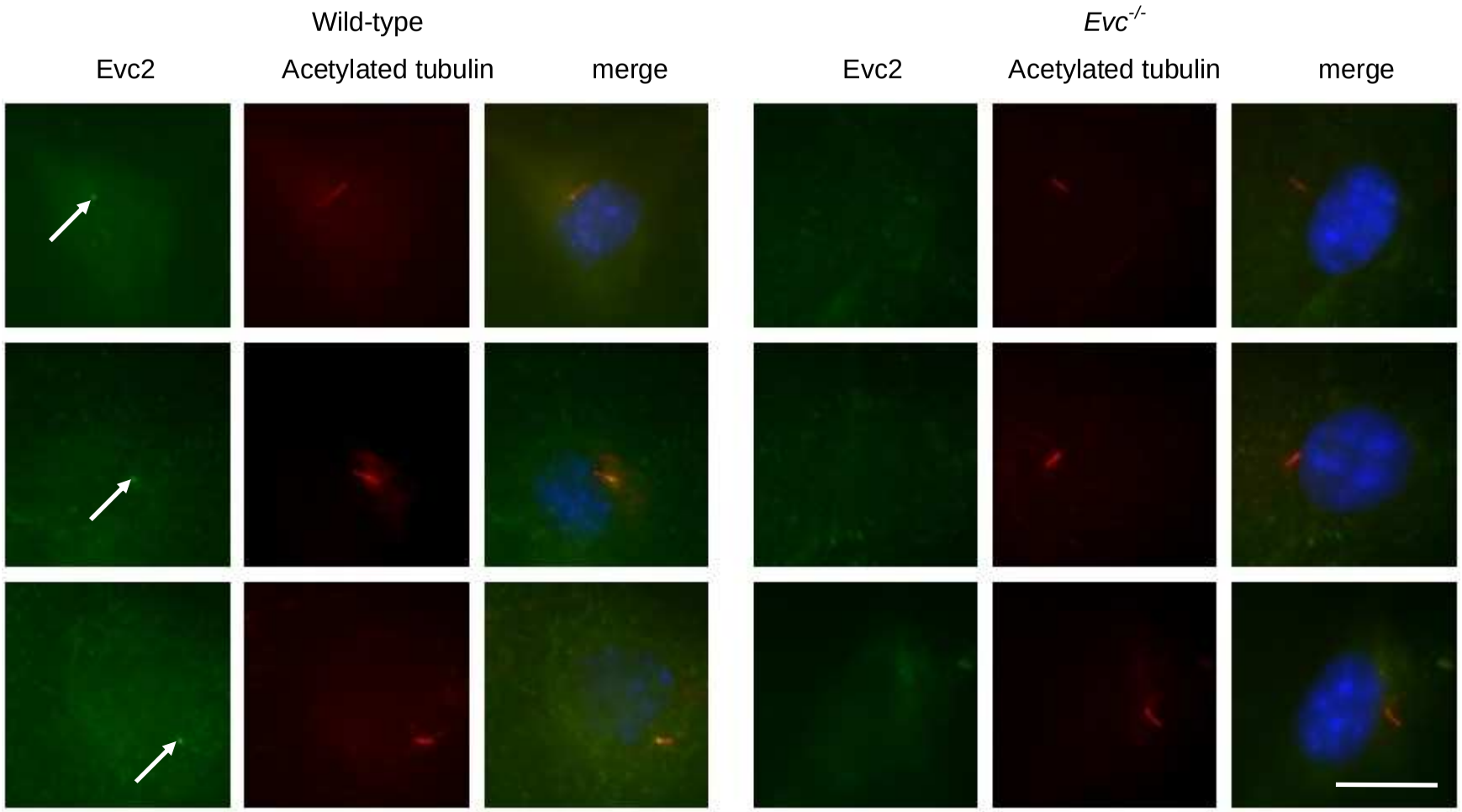

Figure 4.12 Representative figures of disruption of Evc2 localization in chondrocytes from *Evc*$^{-/-}$ mouse

Three chondrocytes are shown from *Evc*$^{+/+}$ and *Evc*$^{-/-}$ littermates (n=3). The image on the left in each case is anti-Evc2 (green, white arrows), the middle panel shows the position of the cilium detected by acetylated tubulin antibodies (red) and the merged image shows the nucleus (DAPI stained, blue). In cells from *Evc*$^{+/+}$ mice there is a clear signal at one end of each cilium, this is not seen in the cells derived from *Evc*$^{-/-}$ mice. Bar: 5µm

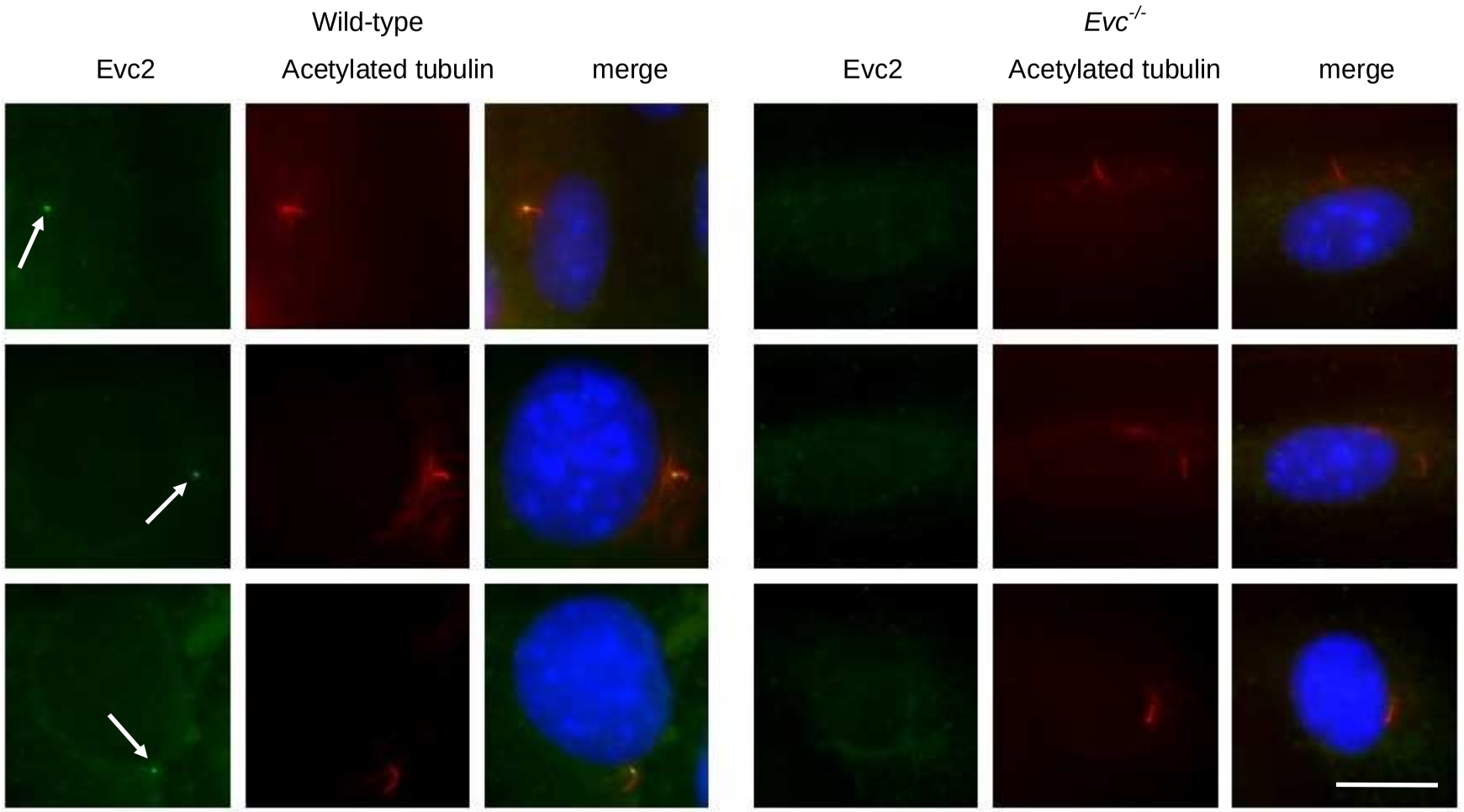

Figure 4.13 Representative figures of disruption of Evc2 localization in osteoblasts from *Evc*$^{-/-}$ mouse

Three osteoblasts are shown from *Evc*$^{+/+}$ and *Evc*$^{-/-}$ littermates (n=3). The image on the left in each case is anti-Evc2 (green, white arrows), the middle panel shows the position of the cilium detected by acetylated tubulin antibodies (red) and the merged image shows the nucleus (DAPI stained, blue). In cells from *Evc*$^{+/+}$ mice there is a clear signal at one end of each cilium, this is not seen in the cells derived from *Evc*$^{-/-}$ mice. Bar: 5μm

4.2.5 Evc2 protein in *Evc*$^{-/-}$ cells

There are two possible reasons for the absence of Evc2 at the basal body in *Evc*$^{-/-}$ cells.

1. Evc2 is absent in these cells.
2. Correct localization of Evc2 is Evc dependent.

To distinguish these two possibilities, total protein was extracted from both wild type and *Evc*$^{-/-}$ MEFs and analyzed by western blot. The specificity of the Evc2 antibody was verified by incubating with specific blocking peptide. Similar intensities of the loading control, actin, showed in both wild type and *Evc*$^{-/-}$ cells. Evc2 signals were observed in both wild type and *Evc*$^{-/-}$ cells, whilst no Evc2 signals were detected after incubating with blocking peptide (Figure 4.14). The data indicated the transcription and translation of Evc2 proteins were unaffected in the absence of Evc protein.

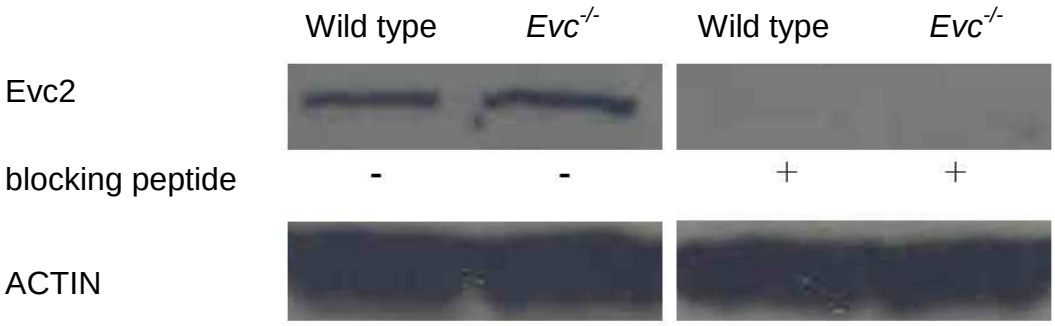

Figure 4.14 Western Blot analysis of Evc2 protein in *Evc*$^{-/-}$ MEF
Western blotting analysis of total protein extracted from MEF and Evc2 protein (~160kDa) were present in both wild type and *Evc*$^{-/-}$ MEF (n=4). No Evc2 proteins were detected when antibodies were pre-incubated with a specific blocking peptide. Actin (~55kDa), used as a loading control, demonstrated that the loading volumes were approximately equivalent.

This supports the second hypothesis, that Evc2 ciliary localization is Evc dependent.

4.2.6 Subcellular fractionation localization of Evc and Evc2

In human fibroblasts, as in MEF, EVC protein is present at the base of cilium. Anti-human-EVC antibody, designed against human EVC-protein amino acid 235 – 952, was purified by antigen affinity purification. Antigen blocking analysis successfully demonstrated specificity. When human fibroblasts were transfected with GFP tagged EVC, immunofluorecent antibody staining showed the co-localization of GFP and EVC. An EVC protein signal arose from nuclei where no Evc signal was present in mouse cells (Dr. H Blair, personal communication) (Figure 4.15). Similar differences in mouse and human proteins were reported for other proteins, such as Werner helicase (Suzuki *et al.*, 2001). This discrepancy of the nuclear localization of EVC protein in human and mouse cells led to the question whether Evc protein is located in mouse nuclei even though it was undetected by immunofluorecent staining. To test the possibility, MEF underwent a subcellular fractionation experiment (section 2.12) and the fractions analyzed by western blotting (section 2.13).

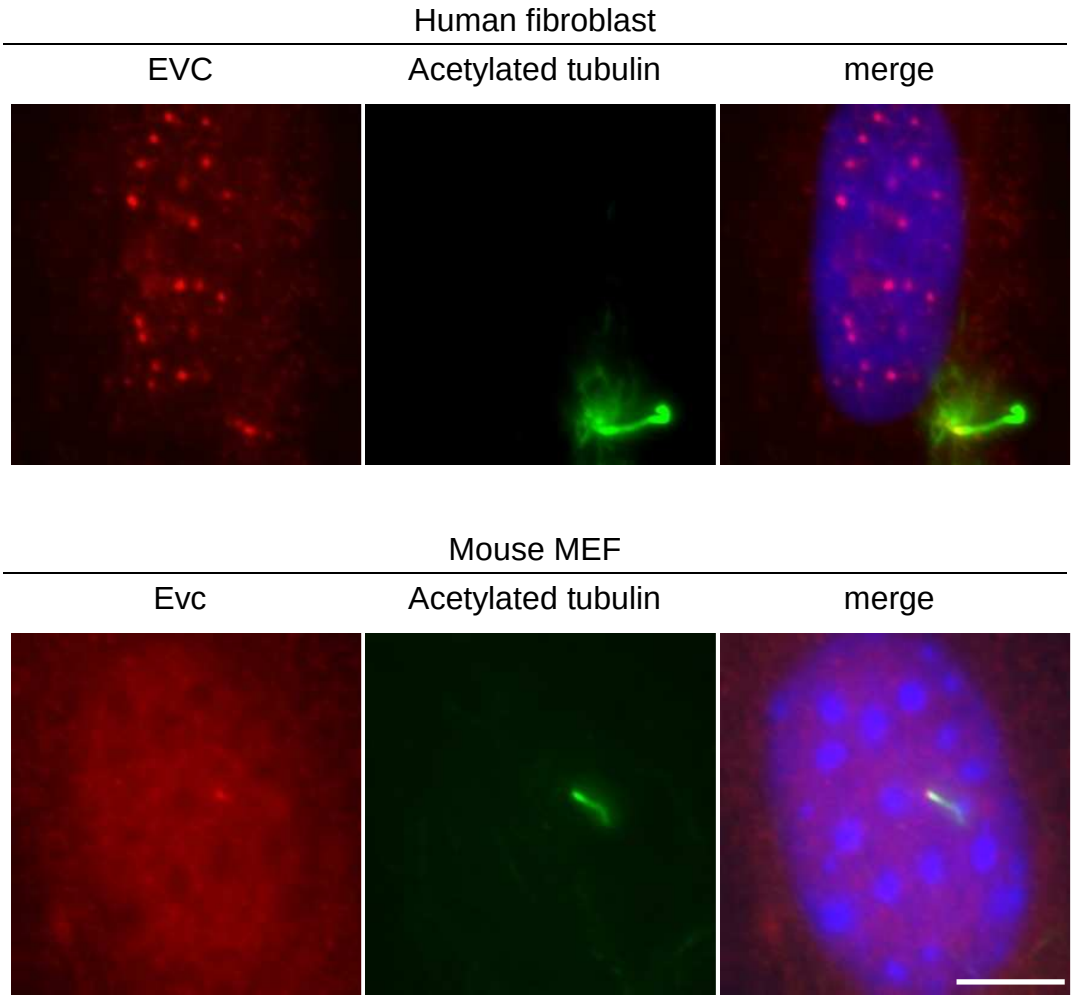

Figure 4.15 Representative figures of immunofluorecent staining detecting EVC in human fibroblasts and MEFs

Human fibroblasts stained for human EVC protein antibody (Dr. H Blair, personal communication). The EVC protein (red) were located at the base of cilia (green, acetylated tubulin) and detected within in the nuclei (blue in merge, DAPI). In MEFs, Evc protein (red) was detected at the base of cilia (green, acetylated tubulin). No specific signals of Evc occurred in MEF nuclei. Bar: 5μm

Seven cytoplasmic fractions were obtained from the supernatant by gentle sequential lysis of MEF plasma membrane generated from wild type and *Evc*$^{-/-}$ mice. The remaining pellet was treated with lysis buffer, and the supernatant harvested as the nuclear fraction. Evc and Evc2 protein expression was analyzed by western blotting, whilst α-tubulin and c-Jun were used as cytoplasmic and nuclear markers respectively (Murakami et

al., 1991; Obungu et al., 2003; Oni, 2002). In both wild type and *Evc*$^{-/-}$ MEF, fraction 7 produced no α-tubulin signals, indicating the complete lysis of plasma membrane. No cytoplasmic protein carried into the nuclear fraction (Figure 4.16).

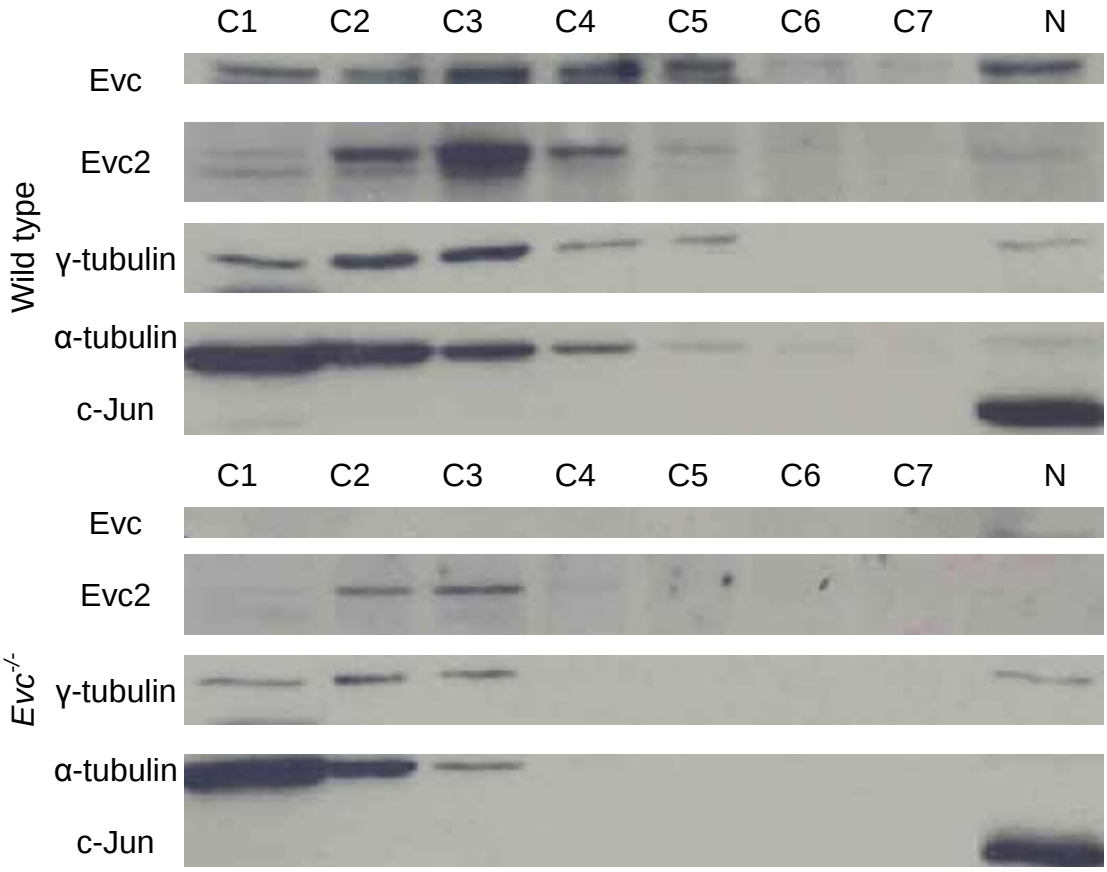

Figure 4.16 Representative figures of western blotting analyses of subcellular fractionations from both genotypes of MEFs (I)
Seven cytoplasmic fractions and one nuclear fraction were detected with Evc (~130kDa), Evc2 (~160kDa) and γ-tubulin (~55kDa) (n=5). α-tubulin (~55kDa) and c-Jun (~48kDa) were used as fraction markers. Evc signals appeared in almost all fractions from wild type MEF and was not found in *Evc*$^{-/-}$ MEF. Evc2 appeared in several fractions though the strongest signal appeared in the C3 fraction.

As reported previously, the centrile protein, γ-tubulin, was observed in the cytoplasmic (Figure 4-16, C1~C5) and nuclear (Figure 4-16, N) fractions. In wild type, both Evc and Evc2 proteins were present in cytoplasmic and

nuclear fractions. The nuclear fraction of *Evc*$^{-/-}$ mouse MEF contained no Evc protein. Data in Figure 4.17 established that Evc2 expression is unchanged in *Evc*$^{-/-}$ mouse MEF. Since it is difficult to accurately analyze chemoluciferase intensity in different western blot membranes, the selected fractions were prepared on the same membrane used for western blotting.

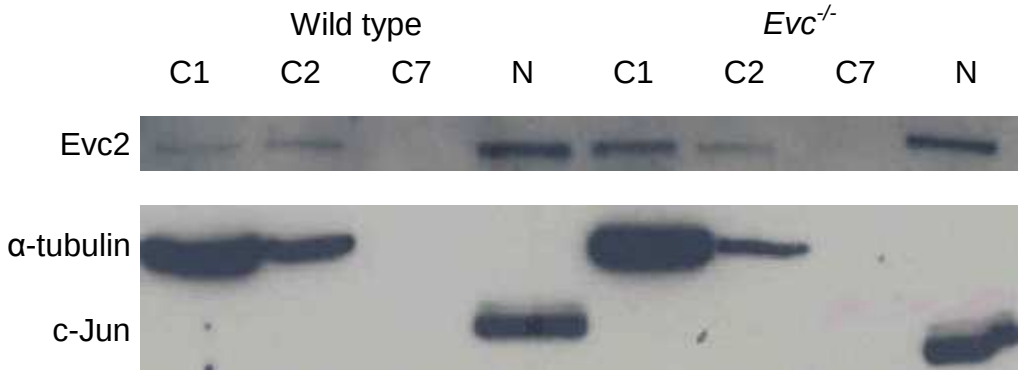

Figure 4.17 Representative figure of western blotting analysis of subcellular fractionations from both genotypes of MEFs (II)
C1, C2, C7, and N fractions from both genotypes of MEFs contained Evc2 antibody (Y-20) (n=5). Evc2 signals appeared in all fractions, except for C7. α-tubulin (~55kDa) and c-Jun (~48kDa) were also detected as cytoplasmic and nuclear fraction markers respectively.

4.2.7 Distribution pattern of SNX5 and SNX6

A yeast two-hybrid study by our group demonstrated the interaction of Evc with Snx5 and Snx6 (Dr. S. Tompson, personal communication). Sorting nexins are a large group of proteins containing a phospholipid-binding (PX) domain. Some members of the sorting nexin family are involved in intracellular trafficking (Wassmer *et al.*, 2007). To investigate whether the localization of Snx5 and Snx6 alter in the absence of Evc, the distribution of Snx5 and Snx6 were analyzed by western blot in the same fractions as

analyzed figure 4.16 and presented in figure 4.18. Snx5 and Snx6 were present in cytoplasmic and nuclear fractions. Although the nuclear expression of Snx5 has not been reported, Snx6 has been observed in the nucleus in another study (Ishibashi *et al.*, 2001). Therefore, the faint signals seen for Snx5 and Snx6 in nuclear fractions might not be contamination from cytoplasmic fractions. Snx5 and Snx6 showed the same distribution pattern in both wild type and *Evc*$^{-/-}$ MEFs. This data indicated that localization Snx5 and Snx6 was not altered in absence of Evc protein.

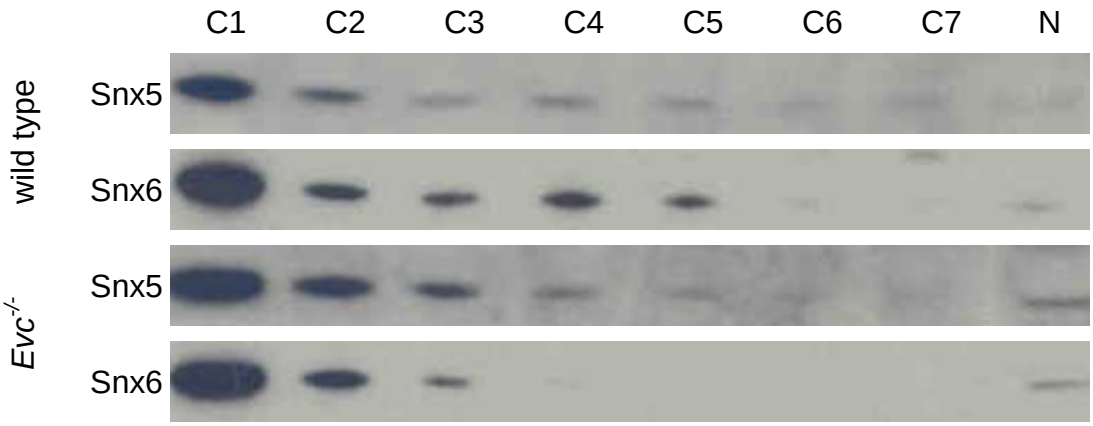

Figure 4.18 Representative figures of western analyses of Snx5 and Snx6 in fractions

Subcellular fractionations from both genotypes of MEFs were detected with Snx5 (~51kDa) and Snx6 (~50kDa) antibodies to analyze the distribution pattern of these two proteins (n=5). The distribution patterns of Snx5 and Snx6 were similar when compared to wild type and *Evc*$^{-/-}$ MEF. This pattern mirrored that for α-tubulin, which showed the strongest signal in C1 and decreased in intensity gradually through the remaining fractions.

4.3 Discussion

4.3.1 Evc localizes between the basal body and the transition zone of cilia and in the nucleus of human MEF

Previous reports from our group highlighted the hedgehog signaling defect in *Evc*$^{-/-}$ mice, and localized Evc proteins to the basal region of cilia (Ruiz-Perez *et al.*, 2007). However, immunofluorescence staining is a relatively low-resolution method. The precise localization of Evc protein might provide a clue to the function of Evc. Herein, we used the deciliation method, which breaks cilia at the distal end of the transition zone, leaving the transition zone and basal body connected with the cell. Immunofluorescence staining demonstrated that Evc was only located at the cell site, and not in the sheared off cilia (Figure 4.3 & 4.4). These data indicated that Evc protein was mainly located between the basal body and transition zone of the cilia. Immuno-TEM was also used to investigate the localization of Evc protein in mIMCD-3 cells. However, the cells are fragile and the cilia structure was destroyed by treatment with triton X-100 or Tween-20. No signal was detected using a gentle permeabilizing protocol. In a detergent free experiment, signals were seen; however, they might result from non-specific binding. It is possible to improve the staining method in several ways, such as using cryosections, or modifying the embedding materials. However, Evc protein was specifically located to the region between the basal body and the transition zone by deciliation experiments, and many proteins with diverse functions are in this region, around the basal body of primary cilia.

Although not detected in mouse cells, EVC is present in the nucleus of human MEF as demonstrated by immunofluorescence staining. Subcellular fractionation followed by western blot analysis confirmed the expression of Evc in the nuclei of mouse MEF. The apparent discrepancy may result from sensitivity differences between the two methods. Western blot with detection by an ECL kit is known to be a sensitive method for proteomic studies (1-10 ng, according to ECL commercial catalog) whilst conventional immunofluorescence staining used in this study is less sensitive, detecting 10-100 ng protein (Bulinski and Borisy, 1980). Examination of the signal by microscope makes immunofluorescence staining useful for obtaining information on the localization of the proteins of interest. Furthermore, immunofluorescence staining sensitivity can be improved 5 to 1000 fold using the tyramide signal amplification (TSA) technique (Loup *et al.*, 1998).

4.3.2 Inner structure of cilium from *Evc*$^{-/-}$ chondrocyte

Since there are no functional domains observed in Evc protein, it is difficult to predict the function of Evc. In this study, the presence of primary cilia in chondrocytes and MEFs from *Evc*$^{-/-}$ mice indicates that Evc might not be required for the formation of cilia. Deciliation followed by immunofluorescence staining localized Evc protein between the basal body and the transition zone of cilia. Further research into Evc function is necessary. Since the dysfunction of ciliary proteins might cause a failure of ciliogenesis or a defect of the substructure of cilia (Blacque *et al.*, 2004; Ferrante *et al.*, 2006), the presence of primary cilia were first analyzed. The presence of primary cilia in chondrocytes and MEF cells from *Evc*$^{-/-}$ mice demonstrated the non-essential nature of Evc protein in the formation of

cilia. Furthermore, other research data indicated that defects of ciliary proteins might affect cilia morphology. Caspary and colleagues described a lethal mouse mutant, *hennin* (*hnn*) with short cilia and a specific defect in the structure of the ciliary axoneme in 2007 (Caspary *et al.*, 2007).

We analyzed ciliary structure in the absence of Evc protein. We used transmission electron microscopy (TEM) to examine cilia from wild type, and *Evc*$^{-/-}$ chondrocyte. TEM is a sensitive technique where cellular and subcellular structures are viewed in detail. Since cilia are small and fragile structures and generally reduced in number and length during TEM preparations (Heller and Gordon, 1986), only cilia which could be observed for 6 serial sections were used for further analysis, in order to eliminate artifacts caused by mishandling. Moreover, correct orientation is necessary to view specific structure within cilia. The TEM method is a time consuming and expensive technique (Ferris *et al.*, 2002), and only 5 reliable cilia, meeting our criteria, were observed. All observed cilia showed nine well-organized doublets of microtubules at the proximal end (Figure 4.10). At the distal end of cilia, disorganized microtubules were present both in chondrocytes from wild type and *Evc*$^{-/-}$ mice. Such disorganized structures have been previously reported by Kiprilov and colleagues in normal human embryonic stem cells (Kiprilov et al., 2008). There were no obvious defects of the inner structure of *Evc*$^{-/-}$ chondrocytes cilia. Analysis of more cilia might be a first priority to understanding the effect of *Evc* deficiency in cilia structure. Moreover, the length and shape of cilia from *Evc*$^{-/-}$ mice were not precisely analyzed in this study. The involvement of Evc protein in ciliogenesis is still not established.

Mutant ciliary proteins altered the generation/length and shape of cilia. Kif3a, components of the Kinesin motor complex, and Tg737, a component of intraflagellar transport, are responsible for the loss/shortening of cilia when disrupted (Lin et al., 2003; Pazour et al., 2000). Mutant tetratricopeptide repeat-containing hedgehog modulator-1 (THM1) could cause a bulb-like structure at the distal tips of cilia (Tran *et al.*, 2008). In this study, we examined only the cilia inner structure and the possibility that Evc protein might function in ciliogenesis still exists.

4.3.3 Precise localization of Evc2 protein is Evc protein dependent

The interactions of Evc and Evc2 proteins were clarified by results from yeast-two hybrid studies (Tompson S. *et al.*, paper in preparation). The interacting proteins usually affect the stability (Thelin *et al.*, 2007), protein activity (Gravel *et al.*, 1977), correct localization, or transportation (Ishibashi *et al.*, 2001). To understand the interactions between two proteins, Evc2 proteins were analyzed in wild type and *Evc*$^{-/-}$ mouse MEFs by western blotting and Immunofluorescence staining. Evc2 proteins were expressed at the base of the cilium in wild type MEF, but no Evc2 protein signal was seen for *Evc*$^{-/-}$ MEF (Figure 4.11, 4.12 & 4.13). Mouse *Evc*$^{-/-}$ chondrocytes and osteoblasts confirmed these observations. Furthermore, the quantity of Evc2 proteins did not affect in the total lysate of *Evc*$^{-/-}$ MEFs during western blotting analysis (Figure 4.14). The data indicated that instead of affecting the stability of Evc2 proteins, the precise localization of Evc2 protein might be Evc protein dependent.

Subcellular fractionation was used to analyze the subcellular localization of

Evc2 protein in wild type and *Evc*$^{-/-}$ cells. In some experiments, the Evc2 protein is low and difficult to be detected in both wild-type and *Evc*$^{-/-}$ cells (figure 4.16) which might be caused by the cell condition in culture. In general, subcellular studies show that Evc2 was present in the cytosol and nuclear fractions both in wild type and in *Evc*$^{-/-}$ mouse MEF. The data suggested that the Evc2 protein is present in cytosol even in the absence of Evc proteins. Since immunofluorescence staining can only detect proteins with more than 100 copies present, the absence of an Evc2 signal from *Evc*$^{-/-}$ cells indicated that the Evc2 is dispersed in the cytosol. The determination of Evc2, in the absence of Evc protein, should depend on high sensitivity methods, such as immuno-TEM or sucrose gradient.

4.3.4 The general distribution of Snx5 and Snx6 was unaffected by the absence of Evc

Other then Evc2, Snx5, and Snx6 interaction was also suggested by yeast two-hybrid analysis (Dr. S. Tompson, personal communication). The results from section 4.2.4 demonstrate that the precise localization of Evc2 is Evc dependent. It is interesting to consider whether Evc would affect the localization of other interacting proteins, such as Snx5 and Snx6. We used a general test for the localization of Snx5 and Snx6 on subcellular fractionation (Figure 4.18). Merino-Trigo reported the transportation of Snx5 in cytosol (Merino-Trigo *et al.*, 2004) whilst Ishibashi *et al*. demonstrated that Snx6 was localized in both the cytosol and in the nucleus (Ishibashi *et al.*, 2001). Snx6 was present in the cytosol and nucleus of wild type and *Evc*$^{-/-}$ cell fractions. We observed Snx5 to be present in cytosol and nuclear fractions in wild type and *Evc*$^{-/-}$ cells. The

general localization of neither Snx5 nor Snx6 altered in the absence of Evc protein. Only cytosol and nuclear fractions were of interest in the subcellular fractionation. Disturbed localization of these two proteins in small organelles cannot be excluded, as Snx5 was translocated from endosome to cell membrane in the EGF stimulation. Further studies, such as the trace of GFP or tag fused Snx5 or Snx6 protein, are necessary to address the effects of Evc on Snx5 and Snx6.

4.4 Conclusion

Evc and Evc2 are unique proteins, which do not share known functional domains with any other proteins. We identified Evc protein localization as the cilia basal body-transition zone. Although the functions of Evc and Evc2 are unclear, the immunofluorescence staining study demonstrated that the correct localization of Evc2 protein is Evc dependent. Furthermore, Evc and Evc2 were present in nuclei, in addition to their presence at the base of cilia.

Chapter 5 Discussion

5.1 Summary of achievement for this thesis

A review of the aims of this thesis proposed in Chapter 1, and relisted below, reveals that progress has been made on all aims.

STATEMENT OF AIMS

- To analyze heart development in *Evc*$^{-/-}$ mice (chapter 3)
- To characterize *Evc* expression in the heart development of mice (chapter 3)
- To determine the precise localization of Evc protein in cells (chapter 4)
- To verify the ciliary structure of *Evc*$^{-/-}$ cells (chapter 4)
- To verify subcellular distribution of potential Evc interacting proteins in *Evc*$^{-/-}$ cells (chapter 4)

Histological analysis of the heart in the absence of Evc was performed. In the chapter 3 in this thesis, no significant difference in the occurrence rate of the variations observed between *Evc*$^{-/-}$ and wild type embryos was demonstrated (Table 3.3). Cells positive for *LacZ*, a reporter gene of Evc expression in *Evc*$^{+/-}$ and *Evc*$^{-/-}$ mice, were observed on the dorsal side of the atrium wall in E11.5 as well as the atrial septum in E12.5 embryos (section 3.3.1). However, the *in situ* hybridization did not reveal gene expression (section 3.3.2). This implied that levels of expression were low, the method was not sensitive enough to detect expression in a small number of cells, or that *LacZ* reflected earlier gene expression. These data also indicated that Evc is not essential for heart

development or that other proteins or mechanisms can compensate for Evc in mice.

Evc localization was limited to an area between the basal body and the transition zone (section 4.2.1). No significant defects of the ciliary structure were observed in *Evc*$^{-/-}$ chondrocytes.

This study has conclusively shown that correct localization of Evc2 is Evc dependent (section 4.2.4 & 4.2.5). The presence of Evc in the nucleus of MEFs was also confirmed.

5.2 Strengths of the work

Evc and Evc2 proteins are unique proteins, which do not share known functional domains with any other proteins. At the beginning of this project, knowledge of EvC syndrome was limited to its definition - an autosomal recessive disease caused by mutations in either the *EVC* or *EVC2* gene. *Evc*$^{-/-}$ mice revealed a similar phenotype to human EvC syndrome in skeletal development. Ihh signaling was diminished in these mice. A thorough study of heart structure was undertaken, but no malformations were observed in *Evc*$^{-/-}$ mice. Although complete ablation of Shh signaling leads to defects in heart development in mice, it appears that the developing mouse heart is able to compensate for signaling modulation in the *Evc* mutant.

Correct localization of the Evc protein should prove useful for understanding protein function. Due to time constraints and technical difficulties, it was not possible to improve the immuno-TEM enough to obtain the precise localization of the EVC protein. The results were inconclusive due to the relatively low

resolution of immunoflurorescence staining in deciliation studies. Clearly, further optimization of immuno-TEM is required to address the precise localization of the Evc protein.

The interaction of Evc and Evc2 was first detected by using yeast two-hybrid screen in our group. This interaction was then confirmed by co-immunoprecipitation (Dr. S. Tompson, personal communication).In this study, the immunofluorescence staining, which demonstrated the mis-localization of Evc2 proteins in *Evc* deficient MEFs, confirmed the hypothesis. Furthermore, an important outcome of this thesis was that Evc2 protein localization is dependent on the Evc protein.

5.3 Limitations of the work

Due to time constraints and technical difficulties, immuno-TEM did not determine the precise localization of the Evc protein in cilia. It was disappointing that localizing the Evc to the region between the basal body and the transition zone by immunofluorescence staining after deciliation did not provide enough information on the function of the Evc protein. As mouse EVC antibody worked successfully in immunofluorescence staining, one possible reason for the failure of immuno-TEM could be the masking of epitopes during sample preparation. Clearly, further optimization of immuno-TEM procedures is necessary to be successful.

5.4 Prospective future work to address the functions of Evc

5.4.1 Optimization of methods used in this study

Localization in the same subcellular compartment is necessary for interacting proteins to co-operate towards a common biological function. Therefore, native subcellular localization of a protein is important for the understanding of its function (Nair and Rost, 2003). Precise localization of Evc and Evc2 proteins at the base of cilia may shed light on their functions. It is disappointing that the immuno-TEM did not provide a result. Further attempts to optimize immuno-TEM are worth pursuing. Further studies can focus on permeabilization by gentle methods and blocking with rabbit or sheep serum. Alternation of concentration and incubation times of primary and secondary antibodies may provide another method for stain improvement.

5.4.2 *Evc2*$^{-/-}$ mice and cells

Recently, our group has generated an *Evc2* knockout mice, which provides a great resource for investigating the pathomechanism of EvC syndrome. Histological analysis of heart development in *Evc2* knockout embryos is necessary. The expression of Evc2 during heart development should be further analyzed. Moreover, analysis of heart development in *Evc* and *Evc2* double knockout may provide a clue to the functions of these two proteins.

In this study, the mis-localization of Evc2 was observed in *Evc*$^{-/-}$ MEFs. This indicated that the correct localization of Evc2 is Evc protein dependent. Further research of interest would be the use of *Evc2*$^{-/-}$ cells to determine whether Evc localization is Evc2 dependent.. Immunofluorescence staining could be performed to address this.

5.4.3 Protein profile in *Evc*$^{-/-}$ cilia

No morphological changes were observed in the structure of the cilia in *Evc*$^{-/-}$ MEFs compared to wild-type cells. However, the possibility that some proteins are lost by absence of Evc is not excluded. Herein, it is vital to analyze the protein contents of *Evc*$^{-/-}$ cilia. The cilia can be collected by the deciliation method presented in this thesis. Proteomic studies follow cilia collection. . Two-dimensional gel electrophoresis is a reliable technique used to identify different proteins between wild type and *Evc*$^{-/-}$ cells. Different regions can be isolated from electrophoresis gels and then analyzed by mass spectrometry.

References

Alvarez-Medina R., Cayuso J., Okubo T., Takada S., Marti E. (2008) Wnt canonical pathway restricts graded Shh/Gli patterning activity through the regulation of Gli3 expression. Development 135:237-47.

Bajolle F., Zaffran S., Kelly R.G., Hadchouel J., Bonnet D., Brown N.A., Buckingham M.E. (2006) Rotation of the myocardial wall of the outflow tract is implicated in the normal positioning of the great arteries. Circulation Research 98:421-8.

Baujat G., Le Merrer M. (2007) Ellis-van Creveld syndrome. Orphanet Journal of Rare Diseases 2:27.

Becker J., Brabletz T., Kirchner T., Conrad C., Bröcker E., Reisfeld R. (1995) Negative transcriptional regulation in anergic T cells. Proceedings of the National Academy of Sciences of the United States of America 92:2375-2378.

Bellaiche Y., The I., Perrimon N. (1998) Tout-velu is a Drosophila homologue of the putative tumour suppressor EXT-1 and is needed for Hh diffusion.[see comment]. Nature 394:85-8.

Biben C., Weber R., Kesteven S., Stanley E., McDonald L., Elliott D.A., Barnett L., Koentgen F., Robb L., Feneley M., Harvey R.P. (2000) Cardiac septal and valvular dysmorphogenesis in mice heterozygous for mutations in the homeobox gene Nkx2-5.[see comment]. Circulation Research 87:888-95.

Biggerstaff R.H., Mazaheri M. (1968) Oral manifestations of the Ellis-van Creveld syndrome. Journal of the American Dental Association 77:1090-5.

Bijlsma M.F., Spek C.A., Zivkovic D., van de Water S., Rezaee F., Peppelenbosch M.P. (2006) Repression of smoothened by patched-dependent (pro-)vitamin D3 secretion. Plos Biology 4:e232.

Bitgood M.J., Shen L., McMahon A.P. (1996) Sertoli cell signaling by Desert hedgehog regulates the male germline. Current Biology 6:298-304.

Blacque O.E., Reardon M.J., Li C., McCarthy J., Mahjoub M.R., Ansley S.J., Badano J.L., Mah A.K., Beales P.L., Davidson W.S., Johnsen R.C., Audeh M., Plasterk R.H., Baillie D.L., Katsanis N., Quarmby L.M., Wicks S.R., Leroux M.R. (2004) Loss of C. elegans BBS-7 and BBS-8 protein function results in cilia defects and compromised intraflagellar transport. Genes & Development 18:1630-42.

Blumer M.J., Longato S., Fritsch H. (2008) Structure, formation and role of cartilage canals in the developing bone. Annals of Anatomy 190:305-15.

Borycki A., Brown A.M., Emerson C.P., Jr. (2000) Shh and Wnt signaling pathways

converge to control Gli gene activation in avian somites. Development 127:2075-87.

Boutros M., Mihaly J., Bouwmeester T., Mlodzik M. (2000) Signaling specificity by Frizzled receptors in Drosophila. Science 288:1825-8.

Bulinski J., Borisy G. (1980) Immunofluorescence Localization of HeLa Cell Microtubule-associated Proteins on Microtubules In Vitro and In Vivo. The Journal of Cell Biology 87:792-801.

Burke R., Nellen D., Bellotto M., Hafen E., Senti K.A., Dickson B.J., Basler K. (1999) Dispatched, a novel sterol-sensing domain protein dedicated to the release of cholesterol-modified hedgehog from signaling cells. Cell 99:803-15.

Cadigan K.M., Nusse R. (1997) Wnt signaling: a common theme in animal development. Genes & Development 11:3286-305.

Caetano-Lopes J., Canhao H., Fonseca J.E. (2007) Osteoblasts and bone formation. Acta Reumatologica Portuguesa 32:103-10.

Cahuana A.P., C., Gonzáles W., Geán E. (2004) Oral manifestations in Ellis-van Creveld syndrome: report of five cases. Pediatric Dentistry 26:277-282.

Caspary T., Larkins C.E., Anderson K.V. (2007) The graded response to Sonic Hedgehog depends on cilia architecture. Developmental Cell 12:767-78.

Cayuso J., Marti E. (2005) Morphogens in motion: growth control of the neural tube. Journal of Neurobiology 64:376-87.

Chamoun Z., Mann R.K., Nellen D., von Kessler D.P., Bellotto M., Beachy P.A., Basler K. (2001) Skinny hedgehog, an acyltransferase required for palmitoylation and activity of the hedgehog signal. Science 293:2080-4.

Chang D.T., Lopez A., von Kessler D.P., Chiang C., Simandl B.K., Zhao R., Seldin M.F., Fallon J.F., Beachy P.A. (1994) Products, genetic linkage and limb patterning activity of a murine hedgehog gene. Development 120:3339-53.

Chen J.K., Taipale J., Cooper M.K., Beachy P.A. (2002a) Inhibition of Hedgehog signaling by direct binding of cyclopamine to Smoothened. Genes & Development 16:2743-8.

Chen J.K., Taipale J., Young K.E., Maiti T., Beachy P.A. (2002b) Small molecule modulation of Smoothened activity. Proceedings of the National Academy of Sciences of the United States of America 99:14071-6.

Chen M.H., Gao N., Kawakami T., Chuang P.T. (2005) Mice deficient in the fused homolog do not exhibit phenotypes indicative of perturbed hedgehog signaling during embryonic development. Molecular & Cellular Biology 25:7042-53.

Chen Y., Struhl G. (1996) Dual roles for patched in sequestering and transducing Hedgehog. Cell 87:553-63.

Chiang C., Litingtung Y., Lee E., Young K.E., Corden J.L., Westphal H., Beachy P.A.

(1996) Cyclopia and defective axial patterning in mice lacking Sonic hedgehog gene function. Nature 383:407-13.

Christoffels V.M., Habets P.E., Franco D., Campione M., de Jong F., Lamers W.H., Bao Z.Z., Palmer S., Biben C., Harvey R.P., Moorman A.F. (2000) Chamber formation and morphogenesis in the developing mammalian heart.[erratum appears in Dev Biol 2000 Sep 1;225(1):266]. Developmental Biology 223:266-78.

Cole D.G., Diener D.R., Himelblau A.L., Beech P.L., Fuster J.C., Rosenbaum J.L. (1998) Chlamydomonas kinesin-II-dependent intraflagellar transport (IFT): IFT particles contain proteins required for ciliary assembly in Caenorhabditis elegans sensory neurons. Journal of Cell Biology 141:993-1008.

Cooper A.F., Yu K.P., Brueckner M., Brailey L.L., Johnson L., McGrath J.M., Bale A.E. (2005) Cardiac and CNS defects in a mouse with targeted disruption of suppressor of fused. Development 132:4407-17.

Cooper M.K., Wassif C.A., Krakowiak P.A., Taipale J., Gong R., Kelley R.I., Porter F.D., Beachy P.A. (2003) A defective response to Hedgehog signaling in disorders of cholesterol biosynthesis. Nature Genetics 33:508-13.

Corbit K.C., Aanstad P., Singla V., Norman A.R., Stainier D.Y., Reiter J.F. (2005) Vertebrate Smoothened functions at the primary cilium. Nature 437:1018-21.

da Silva E.O., Janovitz D., de Albuquerque S.C. (1980) Ellis-van Creveld syndrome: report of 15 cases in an inbred kindred. Journal of Medical Genetics 17:349-56.

Dale T.C., Weber-Hall S.J., Smith K., Huguet E.L., Jayatilake H., Gusterson B.A., Shuttleworth G., O'Hare M., Harris A.L. (1996) Compartment switching of WNT-2 expression in human breast tumors. Cancer Research 56:4320-3.

Dalgleish A.E. (1976) The development of the septum primum relative to atrial septation in the mouse heart. Journal of Morphology 149:369-82.

de Lange F.J., Moorman A.F., Anderson R.H., Manner J., Soufan A.T., de Gier-de Vries C., Schneider M.D., Webb S., van den Hoff M.J., Christoffels V.M. (2004) Lineage and morphogenetic analysis of the cardiac valves. Circulation Research 95:645-54.

Dickinson M.E., McMahon A.P. (1992) The role of Wnt genes in vertebrate development. Current Opinion in Genetics & Development 2:562-6.

Dickinson M.E., Krumlauf R., McMahon A.P. (1994) Evidence for a mitogenic effect of Wnt-1 in the developing mammalian central nervous system. Development 120:1453-71.

Digilio M.C., Marino B., Ammirati A., Borzaga U., Giannotti A., Dallapiccola B. (1999) Cardiac malformations in patients with oral-facial-skeletal syndromes:

clinical similarities with heterotaxia. American Journal of Medical Genetics 84:350-6.

Ding Y., Lawrence C.E. (2003) A statistical sampling algorithm for RNA secondary structure prediction. Nucleic Acids Res. 31.

Ding Y., Chan C.Y., Lawrence C.E. (2005) RNA secondary structure prediction by centroids in a Boltzmann weighted ensemble. RNA 11.

Drake C.J., Wessels A., Trusk T., Little C.D. (2006) Elevated vascular endothelial cell growth factor affects mesocardial morphogenesis and inhibits normal heart bending. Developmental Dynamics 235:10-8.

Dwyer J.R., Sever N., Carlson M., Nelson S.F., Beachy P.A., Parhami F. (2007) Oxysterols are novel activators of the hedgehog signaling pathway in pluripotent mesenchymal cells. Journal of Biological Chemistry 282:8959-68.

Dyer M.A., Farrington S.M., Mohn D., Munday J.R., Baron M.H. (2001) Indian hedgehog activates hematopoiesis and vasculogenesis and can respecify prospective neurectodermal cell fate in the mouse embryo. Development 128:1717-30.

Echelard Y., Epstein D.J., St-Jacques B., Shen L., Mohler J., McMahon J.A., McMahon A.P. (1993) Sonic hedgehog, a member of a family of putative signaling molecules, is implicated in the regulation of CNS polarity. Cell 75:1417-30.

Eisenberg L.M., Markwald R.R. (1995) Molecular regulation of atrioventricular valvuloseptal morphogenesis. Circulation Research 77:1-6.

Ellis R.W.B., Van Creveld S. (1940) A syndrome characterized by ectodermal dysplasia, polydactyly, chondro-dysplasia and congenital morbus cordis. Archives of Disease in Childhood 15:65-84.

Erickson S.L., O'Shea K.S., Ghaboosi N., Loverro L., Frantz G., Bauer M., Lu L.H., Moore M.W. (1997) ErbB3 is required for normal cerebellar and cardiac development: a comparison with ErbB2-and heregulin-deficient mice. Development 124:4999-5011.

Ferrante M.I., Zullo A., Barra A., Bimonte S., Messaddeq N., Studer M., Dolle P., Franco B. (2006) Oral-facial-digital type I protein is required for primary cilia formation and left-right axis specification. Nature Genetics 38:112-7.

Ferris M., Stoffel C., Maurer T., Rowlen K. (2002) Quantitative intercomparison of transmission electron microscopy, flow cytometry, and epifluorescence microscopy for nanometric particle analysis. Analytical Biochemistry 304:249-256.

Fisher R. (1922) On the interpretation of $\chi 2$ from contingency tables, and the calculation of P. Journal of the Royal Statistical Society 85:87-94.

Fliegauf M., Horvath J., von Schnakenburg C., Olbrich H., Muller D., Thumfart J., Schermer B., Pazour G.J., Neumann H.P., Zentgraf H., Benzing T., Omran H. (2006) Nephrocystin specifically localizes to the transition zone of renal and respiratory cilia and photoreceptor connecting cilia. Journal of the American Society of Nephrology 17:2424-33.

Galdzicka M., Patnala S., Hirshman M.G., Cai J.F., Nitowsky H., Egeland J.A., Ginns E.I. (2002) A new gene, EVC2, is mutated in Ellis-van Creveld syndrome. Molecular Genetics & Metabolism 77:291-5.

Gavin B.J., McMahon J.A., McMahon A.P. (1990) Expression of multiple novel Wnt-1/int-1-related genes during fetal and adult mouse development. Genes & Development 4:2319-32.

Gitler A.D., Zhu Y., Ismat F.A., Lu M.M., Yamauchi Y., Parada L.F., Epstein J.A. (2003) Nf1 has an essential role in endothelial cells.[see comment]. Nature Genetics 33:75-9.

Goddeeris M.M., Schwartz R., Klingensmith J., Meyers E.N. (2007) Independent requirements for Hedgehog signaling by both the anterior heart field and neural crest cells for outflow tract development. Development 134:1593-604.

Goddeeris M.M., Rho S., Petiet A., Davenport C.L., Johnson G.A., Meyers E.N., Klingensmith J. (2008) Intracardiac septation requires hedgehog-dependent cellular contributions from outside the heart. Development 135:1887-95.

Goodrich L.V., Milenkovic L., Higgins K.M., Scott M.P. (1997) Altered neural cell fates and medulloblastoma in mouse patched mutants. Science 277:1109-13.

Gravel R., Lam K., Scully K., Hsia Y. (1977) Genetic complementation of propionyl-CoA carboxylase deficiency in cultured human fibroblasts. American Journal of Human Genetics 29.

Habas R., Kato Y., He X. (2001) Wnt/Frizzled activation of Rho regulates vertebrate gastrulation and requires a novel Formin homology protein Daam1. Cell 107:843-54.

Hall B.K., Miyake T. (2000) All for one and one for all: condensations and the initiation of skeletal development. Bioessays 22:138-47.

Han C., Belenkaya T.Y., Wang B., Lin X. (2004a) Drosophila glypicans control the cell-to-cell movement of Hedgehog by a dynamin-independent process. Development 131:601-11.

Han C., Belenkaya T.Y., Khodoun M., Tauchi M., Lin X., Lin X. (2004b) Distinct and collaborative roles of Drosophila EXT family proteins in morphogen signalling and gradient formation.[see comment]. Development 131:1563-75.

Hart M.J., de los Santos R., Albert I.N., Rubinfeld B., Polakis P. (1998) Downregulation of beta-catenin by human Axin and its association with the

APC tumor suppressor, beta-catenin and GSK3 beta. Current Biology 8:573-81.

Hartmann C. (2006) A Wnt canon orchestrating osteoblastogenesis. Trends in Cell Biology 16:151-8.

Haycraft C.J., Banizs B., Aydin-Son Y., Zhang Q., Michaud E.J., Yoder B.K. (2005) Gli2 and Gli3 localize to cilia and require the intraflagellar transport protein polaris for processing and function. PLoS Genetics 1:e53.

Heller R., Gordon R. (1986) Chronic effects of nitrogen dioxide on cilia in hamster bronchioles. Experimental Lung Research 10:137-152.

Hildebrandt F., Otto E., Rensing C., Nothwang H.G., Vollmer M., Adolphs J., Hanusch H., Brandis M. (1997) A novel gene encoding an SH3 domain protein is mutated in nephronophthisis type 1. Nature Genetics 17:149-53.

Hoffmann A.D., Peterson M.A., Friedland-Little J.M., Anderson S.A., Moskowitz I.P. (2009) sonic hedgehog is required in pulmonary endoderm for atrial septation. Development 136:1761-1770.

Hong D.H., Yue G., Adamian M., Li T. (2001) Retinitis pigmentosa GTPase regulator (RPGRr)-interacting protein is stably associated with the photoreceptor ciliary axoneme and anchors RPGR to the connecting cilium. Journal of Biological Chemistry 276:12091-9.

Hong D.H., Pawlyk B., Sokolov M., Strissel K.J., Yang J., Tulloch B., Wright A.F., Arshavsky V.Y., Li T. (2003) RPGR isoforms in photoreceptor connecting cilia and the transitional zone of motile cilia. Investigative Ophthalmology & Visual Science 44:2413-21.

Hooper J.E. (2003) Smoothened translates Hedgehog levels into distinct responses. Development 130:3951-63.

Howard T.D., Guttmacher A.E., McKinnon W., Sharma M., McKusick V.A., Jabs E.W. (1997) Autosomal dominant postaxial polydactyly, nail dystrophy, and dental abnormalities map to chromosome 4p16, in the region containing the Ellis-van Creveld syndrome locus. American Journal of Human Genetics 61:1405-12.

Hsu W., Zeng L., Costantini F. (1999) Identification of a domain of Axin that binds to the serine/threonine protein phosphatase 2A and a self-binding domain. Journal of Biological Chemistry 274:3439-45.

Huangfu D., Anderson K.V. (2005) Cilia and Hedgehog responsiveness in the mouse. Proceedings of the National Academy of Sciences of the United States of America 102:11325-30.

Huangfu D., Liu A., Rakeman A.S., Murcia N.S., Niswander L., Anderson K.V. (2003) Hedgehog signalling in the mouse requires intraflagellar transport

proteins. Nature 426:83-7.
Hui C.C., Slusarski D., Platt K.A., Holmgren R., Joyner A.L. (1994) Expression of three mouse homologs of the Drosophila segment polarity gene cubitus interruptus, Gli, Gli-2, and Gli-3, in ectoderm- and mesoderm-derived tissues suggests multiple roles during postimplantation development. Developmental Biology 162:402-13.
Hynes M., Stone D.M., Dowd M., Pitts-Meek S., Goddard A., Gurney A., Rosenthal A. (1997) Control of cell pattern in the neural tube by the zinc finger transcription factor and oncogene Gli-1. Neuron 19:15-26.
Iozzo R.V., Eichstetter I., Danielson K.G. (1995) Aberrant expression of the growth factor Wnt-5A in human malignancy. Cancer Research 55:3495-9.
Ishibashi Y., Maita H., Yano M., Koike N., Tamai K., Ariga H., Iguchi-Ariga S.M. (2001) Pim-1 translocates sorting nexin 6/TRAF4-associated factor 2 from cytoplasm to nucleus. FEBS Letters 506:33-8.
Iwatsuki K., Liu H.X., Gronder A., Singer M.A., Lane T.F., Grosschedl R., Mistretta C.M., Margolskee R.F. (2007) Wnt signaling interacts with Shh to regulate taste papilla development. Proceedings of the National Academy of Sciences of the United States of America 104:2253-8.
Jeong J., Mao J., Tenzen T., Kottmann A.H., McMahon A.P. (2004) Hedgehog signaling in the neural crest cells regulates the patterning and growth of facial primordia. Genes & Development 18:937-51.
Jessell T.M. (2000) Neuronal specification in the spinal cord: inductive signals and transcriptional codes. Nature Reviews Genetics 1:20-9.
Jia J., Tong C., Jiang J. (2003) Smoothened transduces Hedgehog signal by physically interacting with Costal2/Fused complex through its C-terminal tail. Genes & Development 17:2709-20.
Jia J., Tong C., Wang B., Luo L., Jiang J. (2004) Hedgehog signalling activity of Smoothened requires phosphorylation by protein kinase A and casein kinase I. Nature 432:1045-50.
Katsanis N., Ansley S.J., Badano J.L., Eichers E.R., Lewis R.A., Hoskins B.E., Scambler P.J., Davidson W.S., Beales P.L., Lupski J.R. (2001) Triallelic inheritance in Bardet-Biedl syndrome, a Mendelian recessive disorder.[see comment]. Science 293:2256-9.
Katsouras C.S., Thomadakis C., Michalis L.K. (2003) Cardiac Ellis-van Creveld syndrome. International Journal of Cardiology 87:315-6.
Kibar Z., Vogan K.J., Groulx N., Justice M.J., Underhill D.A., Gros P. (2001) Ltap, a mammalian homolog of Drosophila Strabismus/Van Gogh, is altered in the mouse neural tube mutant Loop-tail. Nature Genetics 28:251-5.

Kim R.Y., Robertson E.J., Solloway M.J. (2001) Bmp6 and Bmp7 are required for cushion formation and septation in the developing mouse heart. Developmental Biology 235:449-66.

Kiprilov E.N., Awan A., Desprat R., Velho M., Clement C.A., Byskov A.G., Andersen C.Y., Satir P., Bouhassira E.E., Christensen S.T., Hirsch R.E. (2008) Human embryonic stem cells in culture possess primary cilia with hedgehog signaling machinery. Journal of Cell Biology 180:897-904.

Kirby M.L., Gale T.F., Stewart D.E. (1983) Neural crest cells contribute to normal aorticopulmonary septation. Science 220:1059-61.

Kishida S., Yamamoto H., Ikeda S., Kishida M., Sakamoto I., Koyama S., Kikuchi A. (1998) Axin, a negative regulator of the wnt signaling pathway, directly interacts with adenomatous polyposis coli and regulates the stabilization of beta-catenin. Journal of Biological Chemistry 273:10823-6.

Kozminski K.G., Johnson K.A., Forscher P., Rosenbaum J.L. (1993) A motility in the eukaryotic flagellum unrelated to flagellar beating. Proceedings of the National Academy of Sciences of the United States of America 90:5519-23.

Kronenberg H.M. (2003) Developmental regulation of the growth plate. Nature 423:332-6.

Kruithof B.P., Van Den Hoff M.J., Tesink-Taekema S., Moorman A.F. (2003) Recruitment of intra- and extracardiac cells into the myocardial lineage during mouse development. Anatomical Record. Part A, Discoveries in Molecular, Cellular, & Evolutionary Biology 271:303-14.

Lakkis M.M., Epstein J.A. (1998) Neurofibromin modulation of ras activity is required for normal endocardial-mesenchymal transformation in the developing heart. Development 125:4359-67.

Lee J.J., Ekker S.C., von Kessler D.P., Porter J.A., Sun B.I., Beachy P.A. (1994) Autoproteolysis in hedgehog protein biogenesis.[see comment]. Science 266:1528-37.

Lefers M.A., Wang Q.T., Holmgren R.A. (2001) Genetic dissection of the Drosophila Cubitus interruptus signaling complex. Developmental Biology 236:411-20.

Lei Q., Jeong Y., Misra K., Li S., Zelman A.K., Epstein D.J., Matise M.P. (2006) Wnt signaling inhibitors regulate the transcriptional response to morphogenetic Shh-Gli signaling in the neural tube. Developmental Cell 11:325-37.

Levay-Young B.K., Navre M. (1992) Growth and developmental regulation of wnt-2 (irp) gene in mesenchymal cells of fetal lung. American Journal of Physiology 262:L672-83.

Li X., Kuromi H., Briggs L., Green D., Rocha J., Sweeney S., Bullock S. (2010) Bicaudal-D binds clathrin heavy chain to promote its transport and augments

synaptic vesicle recycling. EMBO J 29:992-1006.

Lin F., Hiesberger T., Cordes K., Sinclair A.M., Goldstein L.S., Somlo S., Igarashi P. (2003) Kidney-specific inactivation of the KIF3A subunit of kinesin-II inhibits renal ciliogenesis and produces polycystic kidney disease.[see comment]. Proceedings of the National Academy of Sciences of the United States of America 100:5286-91.

Lipscomb Sund K., Roelker S., Ramachandran V., Durbin L., Benson D.W. (2009) Analysis of Ellis van Creveld Syndrome Gene Products; Implications for Cardiovascular Development and Disease. Hum. Mol. Genet.:ddp098. DOI: 10.1093/hmg/ddp098.

Liu A., Wang B., Niswander L.A. (2005) Mouse intraflagellar transport proteins regulate both the activator and repressor functions of Gli transcription factors. Development 132:3103-11.

Loup F., Weinmann O., Yonekawa Y., Aguzzi A., Wieser H., Fritschy J. (1998) A Highly Sensitive Immunofluorescence Procedure for Analyzing the Subcellular Distribution of GABA A Receptor Subunits in the Human Brain. The Journal of Histochemistry & Cytochemistry 46:1129-1139.

Lum L., Zhang C., Oh S., Mann R.K., von Kessler D.P., Taipale J., Weis-Garcia F., Gong R., Wang B., Beachy P.A. (2003) Hedgehog signal transduction via Smoothened association with a cytoplasmic complex scaffolded by the atypical kinesin, Costal-2. Molecular Cell 12:1261-74.

Manner J. (2004) On rotation, torsion, lateralization, and handedness of the embryonic heart loop: new insights from a simulation model for the heart loop of chick embryos. Anatomical Record. Part A, Discoveries in Molecular, Cellular, & Evolutionary Biology 278:481-92.

May S.R., Ashique A.M., Karlen M., Wang B., Shen Y., Zarbalis K., Reiter J., Ericson J., Peterson A.S. (2005) Loss of the retrograde motor for IFT disrupts localization of Smo to cilia and prevents the expression of both activator and repressor functions of Gli. Developmental Biology 287:378-89.

McKusick V.A., Egeland J.A., Eldridge R., Krusen D.E. (1964) Dwarfism in the Amish I. the Ellis-Van Creveld Syndrome. Bulletin of the Johns Hopkins Hospital 115:306-36.

McMahon A.P., Bradley A. (1990) The Wnt-1 (int-1) proto-oncogene is required for development of a large region of the mouse brain. Cell 62:1073-85.

Megason S.G., McMahon A.P. (2002) A mitogen gradient of dorsal midline Wnts organizes growth in the CNS. Development 129:2087-98.

Merino-Trigo A., Kerr M., Houghton F., Lindberg A., Mitchell C., Teasdale R., Gleeson P. (2004) Sorting nexin 5 is localized to a subdomain of the early

endosomes and is recruited to the plasma membrane following EGF stimulation. Journal of Cell Science 117:6413-6424.

Miquerol L., Gertsenstein M., Harpal K., Rossant J., Nagy A. (1999) Multiple developmental roles of VEGF suggested by a LacZ-tagged allele. Developmental Biology 212:307-22.

Mollet G., Salomon R., Gribouval O., Silbermann F., Bacq D., Landthaler G., Milford D., Nayir A., Rizzoni G., Antignac C., Saunier S. (2002) The gene mutated in juvenile nephronophthisis type 4 encodes a novel protein that interacts with nephrocystin.[erratum appears in Nat Genet 2002 Nov;32(3):459]. Nature Genetics 32:300-5.

Mommersteeg M.T., Soufan A.T., de Lange F.J., van den Hoff M.J., Anderson R.H., Christoffels V.M., Moorman A.F. (2006) Two distinct pools of mesenchyme contribute to the development of the atrial septum. Circulation Research 99:351-3.

Moon R.T., Bowerman B., Boutros M., Perrimon N. (2002) The promise and perils of Wnt signaling through beta-catenin. Science 296:1644-6.

Motoyama J., Heng H., Crackower M., Takabatake T., Takeshima K., Tsui L., Hui C. (1998) Overlapping and non-overlapping Ptch2 expression with Shh during mouse embryogenesis. Mechanisms of Development 78:81-84.

Murakami Y., Satake M., Yamaguchi-Iwai Y., Sakai M., Muramatsu M., Ito Y. (1991) The nuclear protooncogenes c-jun and c-fos as regulators of DNA replication. Proceedings of the National Academy of Sciences of the United States of America 88:3947-3951.

Muroyama Y., Fujihara M., Ikeya M., Kondoh H., Takada S. (2002) Wnt signaling plays an essential role in neuronal specification of the dorsal spinal cord. Genes & Development 16:548-53.

Nair R., Rost B. (2003) LOC3D: annotate sub-cellular localization for protein structures. Nucleic Acids Research 31:3337-3340.

Nemeth M., Bodine D. (2007) Regulation of hematopoiesis and the hematopoietic stem cell niche by Wnt signaling pathways. Cell Research 17:746-758.

Nonaka S., Tanaka Y., Okada Y., Takeda S., Harada A., Kanai Y., Kido M., Hirokawa N. (1998) Randomization of left-right asymmetry due to loss of nodal cilia generating leftward flow of extraembryonic fluid in mice lacking KIF3B motor protein.[erratum appears in Cell 1999 Oct 1;99(1):117]. Cell 95:829-37.

Noonan K.J., Hunziker E.B., Nessler J., Buckwalter J.A. (1998) Changes in cell, matrix compartment, and fibrillar collagen volumes between growth-plate zones. Journal of Orthopaedic Research 16:500-8.

Nusslein-Volhard C., Wieschaus E. (1980) Mutations affecting segment number and polarity in Drosophila. Nature 287:795-801.

Obungu V., Lee Burns A., Agarwal S., Chandrasekharapa S., Adelstein R., Marx S. (2003) Menin, a tumor suppressor, associates with nonmuscle myosin II-A heavy chain. Oncogene 22:6347-6358.

Ohlmeyer J.T., Kalderon D. (1998) Hedgehog stimulates maturation of Cubitus interruptus into a labile transcriptional activator. Nature 396:749-53.

Olbrich H., Fliegauf M., Hoefele J., Kispert A., Otto E., Volz A., Wolf M.T., Sasmaz G., Trauer U., Reinhardt R., Sudbrak R., Antignac C., Gretz N., Walz G., Schermer B., Benzing T., Hildebrandt F., Omran H. (2003) Mutations in a novel gene, NPHP3, cause adolescent nephronophthisis, tapeto-retinal degeneration and hepatic fibrosis.[see comment]. Nature Genetics 34:455-9.

Oni O. (2002) The expression of the nuclear oncogenes c-myc and c-jun in the groove of Ranvier of the rabbit growth plate. Africa Journal of Medicine and Medical Sciences 31:325-327.

Otto E., Hoefele J., Ruf R., Mueller A.M., Hiller K.S., Wolf M.T., Schuermann M.J., Becker A., Birkenhager R., Sudbrak R., Hennies H.C., Nurnberg P., Hildebrandt F. (2002) A gene mutated in nephronophthisis and retinitis pigmentosa encodes a novel protein, nephroretinin, conserved in evolution. American Journal of Human Genetics 71:1161-7.

Otto E.A., Schermer B., Obara T., O'Toole J.F., Hiller K.S., Mueller A.M., Ruf R.G., Hoefele J., Beekmann F., Landau D., Foreman J.W., Goodship J.A., Strachan T., Kispert A., Wolf M.T., Gagnadoux M.F., Nivet H., Antignac C., Walz G., Drummond I.A., Benzing T., Hildebrandt F. (2003) Mutations in INVS encoding inversin cause nephronophthisis type 2, linking renal cystic disease to the function of primary cilia and left-right axis determination.[see comment]. Nature Genetics 34:413-20.

Otto E.A., Loeys B., Khanna H., Hellemans J., Sudbrak R., Fan S., Muerb U., O'Toole J.F., Helou J., Attanasio M., Utsch B., Sayer J.A., Lillo C., Jimeno D., Coucke P., De Paepe A., Reinhardt R., Klages S., Tsuda M., Kawakami I., Kusakabe T., Omran H., Imm A., Tippens M., Raymond P.A., Hill J., Beales P., He S., Kispert A., Margolis B., Williams D.S., Swaroop A., Hildebrandt F. (2005) Nephrocystin-5, a ciliary IQ domain protein, is mutated in Senior-Loken syndrome and interacts with RPGR and calmodulin. Nature Genetics 37:282-8.

Paoletti A., Moudjou M., Paintrand M., Salisbury J.L., Bornens M. (1996) Most of centrin in animal cells is not centrosome-associated and centrosomal centrin is confined to the distal lumen of centrioles. Journal of Cell Science

109:3089-102.

Pazour G.J., Dickert B.L., Vucica Y., Seeley E.S., Rosenbaum J.L., Witman G.B., Cole D.G. (2000) Chlamydomonas IFT88 and its mouse homologue, polycystic kidney disease gene tg737, are required for assembly of cilia and flagella. Journal of Cell Biology 151:709-18.

Pelttari K., Steck E., Richter W. (2008) The use of mesenchymal stem cells for chondrogenesis. Injury 39 Suppl 1:S58-65.

Phillips H.M., Hildreth V., Peat J.D., Murdoch J.N., Kobayashi K., Chaudhry B., Henderson D.J. (2008) Non-cell-autonomous roles for the planar cell polarity gene Vangl2 in development of the coronary circulation. Circulation Research 102:615-23.

Piperno G., Siuda E., Henderson S., Segil M., Vaananen H., Sassaroli M. (1998) Distinct mutants of retrograde intraflagellar transport (IFT) share similar morphological and molecular defects. Journal of Cell Biology 143:1591-601.

Pirazzoli P., Mazzanti L., Mandini M., Cau M., Ravagli L., Cacciari E. (1989) GH-deficiency in Ellis-van-Crefeld Syndrome: response to remplacementtherapy. Growth Abnormalities 56:391-393.

Polymeropoulos M.H., Ide S.E., Wright M., Goodship J., Weissenbach J., Pyeritz R.E., Da Silva E.O., Ortiz De Luna R.I., Francomano C.A. (1996) The gene for the Ellis-van Creveld syndrome is located on chromosome 4p16. Genomics 35:1-5.

Poole C.A., Flint M.H., Beaumont B.W. (1985) Analysis of the morphology and function of primary cilia in connective tissues: a cellular cybernetic probe? Cell Motility 5:175-93.

Poole C.A., Zhang Z.J., Ross J.M. (2001) The differential distribution of acetylated and detyrosinated alpha-tubulin in the microtubular cytoskeleton and primary cilia of hyaline cartilage chondrocytes. Journal of Anatomy 199:393-405.

Porter J.A., Young K.E., Beachy P.A. (1996) Cholesterol modification of hedgehog signaling proteins in animal development.[see comment][erratum appears in Science 1996 Dec 6;274(5293):1597]. Science 274:255-9.

Praetorius H.A., Spring K.R. (2001) Bending the MDCK cell primary cilium increases intracellular calcium. Journal of Membrane Biology 184:71-9.

Praetorius H.A., Spring K.R. (2003) Removal of the MDCK cell primary cilium abolishes flow sensing. Journal of Membrane Biology 191:69-76.

Price M.A., Kalderon D. (2002) Proteolysis of the Hedgehog signaling effector Cubitus interruptus requires phosphorylation by Glycogen Synthase Kinase 3 and Casein Kinase 1. Cell 108:823-35.

Rana A.A., Barbera J.P., Rodriguez T.A., Lynch D., Hirst E., Smith J.C., Beddington

R.S. (2004) Targeted deletion of the novel cytoplasmic dynein mD2LIC disrupts the embryonic organiser, formation of the body axes and specification of ventral cell fates. Development 131:4999-5007.

Ranger A.M., Grusby M.J., Hodge M.R., Gravallese E.M., de la Brousse F.C., Hoey T., Mickanin C., Baldwin H.S., Glimcher L.H. (1998) The transcription factor NF-ATc is essential for cardiac valve formation.[see comment]. Nature 392:186-90.

Reddi A.H., Anderson W.A. (1976) Collagenous bone matrix-induced endochondral ossification hemopoiesis. Journal of Cell Biology 69:557-72.

Rohatgi R., Milenkovic L., Scott M.P. (2007) Patched1 regulates hedgehog signaling at the primary cilium.[see comment]. Science 317:372-6.

Rohatgi R., Milenkovic L., Corcoran R.B., Scott M.P. (2009) Hedgehog signal transduction by Smoothened: pharmacologic evidence for a 2-step activation process. Proceedings of the National Academy of Sciences of the United States of America 106:3196-201.

Rozen S., Skaletsky H. (2000) Primer3 on the WWW for general users and for biologist programmers. Methods in Molecular Biology 132:365-86.

Ruiz-Perez V., Goodship J. (2009) Ellis-van Creveld syndrome and Weyers acrodental dysostosis are caused by cilia-mediated diminished response to hedgehog ligands. American Journal of Medical Genetics 151C:341-351.

Ruiz-Perez V.L., Blair H.J., Rodriguez-Andres M.E., Blanco M.J., Wilson A., Liu Y.N., Miles C., Peters H., Goodship J.A. (2007) Evc is a positive mediator of Ihh-regulated bone growth that localises at the base of chondrocyte cilia. Development 134:2903-12.

Ruiz-Perez V.L., Tompson S.W., Blair H.J., Espinoza-Valdez C., Lapunzina P., Silva E.O., Hamel B., Gibbs J.L., Young I.D., Wright M.J., Goodship J.A. (2003) Mutations in two nonhomologous genes in a head-to-head configuration cause Ellis-van Creveld syndrome. American Journal of Human Genetics 72:728-32.

Ruiz-Perez V.L., Ide S.E., Strom T.M., Lorenz B., Wilson D., Woods K., King L., Francomano C., Freisinger P., Spranger S., Marino B., Dallapiccola B., Wright M., Meitinger T., Polymeropoulos M.H., Goodship J. (2000) Mutations in a new gene in Ellis-van Creveld syndrome and Weyers acrodental dysostosis.[see comment][erratum appears in Nat Genet 2000 May;25(1):125]. Nature Genetics 24:283-6.

Ruiz i Altaba A. (1998) Combinatorial Gli gene function in floor plate and neuronal inductions by Sonic hedgehog. Development 125:2203-12.

Sampath K., Cheng A.M., Frisch A., Wright C.V. (1997) Functional differences among Xenopus nodal-related genes in left-right axis determination.

Development 124:3293-302.
Sarkar L., Cobourne M., Naylor S., Smalley M., Dale T., Sharpe P.T. (2000) Wnt/Shh interactions regulate ectodermal boundary formation during mammalian tooth development. Proceedings of the National Academy of Sciences of the United States of America 97:4520-4.
Satir P. (2005) Tour of organelles through the electron microscope: a reprinting of Keith R. Porter's classic Harvey Lecture with a new introduction.[comment]. Anatomical Record. Part A, Discoveries in Molecular, Cellular, & Evolutionary Biology 287:1184-5.
Sayer J.A., Otto E.A., O'Toole J.F., Nurnberg G., Kennedy M.A., Becker C., Hennies H.C., Helou J., Attanasio M., Fausett B.V., Utsch B., Khanna H., Liu Y., Drummond I., Kawakami I., Kusakabe T., Tsuda M., Ma L., Lee H., Larson R.G., Allen S.J., Wilkinson C.J., Nigg E.A., Shou C., Lillo C., Williams D.S., Hoppe B., Kemper M.J., Neuhaus T., Parisi M.A., Glass I.A., Petry M., Kispert A., Gloy J., Ganner A., Walz G., Zhu X., Goldman D., Nurnberg P., Swaroop A., Leroux M.R., Hildebrandt F. (2006) The centrosomal protein nephrocystin-6 is mutated in Joubert syndrome and activates transcription factor ATF4. Nature Genetics 38:674-81.
Schilling T.F., Concordet J.P., Ingham P.W. (1999) Regulation of left-right asymmetries in the zebrafish by Shh and BMP4. Developmental Biology 210:277-87.
Schneider L., Clement C.A., Teilmann S.C., Pazour G.J., Hoffmann E.K., Satir P., Christensen S.T. (2005) PDGFRalphaalpha signaling is regulated through the primary cilium in fibroblasts. Current Biology 15:1861-6.
Sedmera D., Pexieder T., Hu N., Clark E.B. (1997) Developmental changes in the myocardial architecture of the chick. Anatomical Record 248:421-32.
Seeman E. (2008) Bone quality: the material and structural basis of bone strength. Journal of Bone & Mineral Metabolism 26:1-8.
Shimada T., Fujii H., Lin H. (1989) A 165-base pair sequence between the dihydrofolate reductase gene and the divergently transcribed upstream gene is sufficient for bidirectional transcriptional activity. Journal of Biological Chemistry 264:20171-4.
Snarr B.S., Wirrig E.E., Phelps A.L., Trusk T.C., Wessels A. (2007) A spatiotemporal evaluation of the contribution of the dorsal mesenchymal protrusion to cardiac development. Developmental Dynamics 236:1287-94.
Solomon H.M., Wier P.J., Fish C.J., Hart T.K., Johnson C.M., Posobiec L.M., Gowan C.C., Maleeff B.E., Kerns W.D. (1997) Spontaneous and induced alterations in the cardiac membranous ventricular septum of fetal, weanling, and adult

rats. Teratology 55:185-94.

St-Jacques B., Hammerschmidt M., McMahon A.P. (1999) Indian hedgehog signaling regulates proliferation and differentiation of chondrocytes and is essential for bone formation.[erratum appears in Genes Dev 1999 Oct 1;13(19):2617]. Genes & Development 13:2072-86.

Stamataki D., Ulloa F., Tsoni S.V., Mynett A., Briscoe J. (2005) A gradient of Gli activity mediates graded Sonic Hedgehog signaling in the neural tube. Genes & Development 19:626-41.

Standring S., Ellis H. (2005) Gray's anatomy. 39th ed. Edinburgh ; New York : Churchill Livingstone.

Sugishita Y., Leifer D.W., Agani F., Watanabe M., Fisher S.A. (2004) Hypoxia-responsive signaling regulates the apoptosis-dependent remodeling of the embryonic avian cardiac outflow tract. Developmental Biology 273:285-96.

Susami T., Kuroda T., Yoshimasu H., Suzuki R. (1999) Ellis-van Creveld syndrome: craniofacial morphology and multidisciplinary treatment. The Cleft Palate-Craniofacial Journal 36:345-352.

Sussman D.J., Klingensmith J., Salinas P., Adams P.S., Nusse R., Perrimon N. (1994) Isolation and characterization of a mouse homolog of the Drosophila segment polarity gene dishevelled. Developmental Biology 166:73-86.

Suzuki T., Shiratori M., Furuichi Y., Matsumoto T. (2001) Diverged nuclear localization of Werner helicase in human and mouse cells. Oncogene 20:2551-2558.

Syftestad G.T., Weitzhandler M., Caplan A.I. (1985) Isolation and characterization of osteogenic cells derived from first bone of the embryonic tibia. Developmental Biology 110:275-83.

Takeda H., Takami M., Oguni T., Tsuji T., Yoneda K., Sato H., Ihara N., Itoh T., Kata S.R., Mishina Y., Womack J.E., Moritomo Y., Sugimoto Y., Kunieda T. (2002) Positional cloning of the gene LIMBIN responsible for bovine chondrodysplastic dwarfism. Proceedings of the National Academy of Sciences of the United States of America 99:10549-54.

Tam P.P., Parameswaran M., Kinder S.J., Weinberger R.P. (1997) The allocation of epiblast cells to the embryonic heart and other mesodermal lineages: the role of ingression and tissue movement during gastrulation. Development 124:1631-42.

Taylor G.A., Jordan C.E., Dorst S.K., Dorst J.P. (1984) Polycarpaly and other abnormalities of the wrist in chondroectodermal dysplasia: the Ellis-van Creveld syndrome. Radiology 151:393-6.

Taylor J., Abramova N., Charlton J., Adler P.N. (1998) Van Gogh: a new Drosophila tissue polarity gene. Genetics 150:199-210.

Tenzen T., Allen B.L., Cole F., Kang J.S., Krauss R.S., McMahon A.P. (2006) The cell surface membrane proteins Cdo and Boc are components and targets of the Hedgehog signaling pathway and feedback network in mice. Developmental Cell 10:647-56.

The I., Bellaiche Y., Perrimon N. (1999) Hedgehog movement is regulated through tout velu-dependent synthesis of a heparan sulfate proteoglycan. Molecular Cell 4:633-9.

Thelin W., Chen Y., Gentzsch M., Kreda S., Sallee J., Scarlett C., Borchers C., Jacobson K., Stutts M., Milgram S. (2007) Direct interaction with filamins modulates the stability and plasma membrane expression of CFTR. The Journal of Clinical Investigation 117:364-374.

Timmerman L.A., Grego-Bessa J., Raya A., Bertran E., Perez-Pomares J.M., Diez J., Aranda S., Palomo S., McCormick F., Izpisua-Belmonte J.C., de la Pompa J.L. (2004) Notch promotes epithelial-mesenchymal transition during cardiac development and oncogenic transformation. Genes & Development 18:99-115.

Tompson S.W., Ruiz-Perez V.L., Blair H.J., Barton S., Navarro V., Robson J.L., Wright M.J., Goodship J.A. (2007) Sequencing EVC and EVC2 identifies mutations in two-thirds of Ellis-van Creveld syndrome patients. Human Genetics 120:663-70.

Tran P.V., Haycraft C.J., Besschetnova T.Y., Turbe-Doan A., Stottmann R.W., Herron B.J., Chesebro A.L., Qiu H., Scherz P.J., Shah J.V., Yoder B.K., Beier D.R. (2008) THM1 negatively modulates mouse sonic hedgehog signal transduction and affects retrograde intraflagellar transport in cilia. Nature Genetics 40:403-10.

Tsukui T., Capdevila J., Tamura K., Ruiz-Lozano P., Rodriguez-Esteban C., Yonei-Tamura S., Magallon J., Chandraratna R.A., Chien K., Blumberg B., Evans R.M., Belmonte J.C. (1999) Multiple left-right asymmetry defects in Shh(-/-) mutant mice unveil a convergence of the shh and retinoic acid pathways in the control of Lefty-1. Proceedings of the National Academy of Sciences of the United States of America 96:11376-81.

Van Den Berg D.J., Sharma A.K., Bruno E., Hoffman R. (1998) Role of members of the Wnt gene family in human hematopoiesis. Blood 92:3189-202.

van den Hoff M.J., Moorman A.F., Ruijter J.M., Lamers W.H., Bennington R.W., Markwald R.R., Wessels A. (1999) Myocardialization of the cardiac outflow tract. Developmental Biology 212:477-90.

Varjosalo M., Li S.P., Taipale J. (2006) Divergence of hedgehog signal transduction mechanism between Drosophila and mammals. Developmental Cell 10:177-86.

Vinay C., Reddy R., Uloopi K., Sekhar R. (2009) Clinical manifestations of Ellis-van Creveld syndrome. Journal of India Society of Pedodontics and Preventive Dentistry 27:256-259.

Vortkamp A., Lee K., Lanske B., Segre G.V., Kronenberg H.M., Tabin C.J. (1996) Regulation of rate of cartilage differentiation by Indian hedgehog and PTH-related protein.[see comment]. Science 273:613-22.

Waldo K., Miyagawa-Tomita S., Kumiski D., Kirby M.L. (1998) Cardiac neural crest cells provide new insight into septation of the cardiac outflow tract: aortic sac to ventricular septal closure. Developmental Biology 196:129-44.

Wang G., Wang B., Jiang J. (1999) Protein kinase A antagonizes Hedgehog signaling by regulating both the activator and repressor forms of Cubitus interruptus. Genes & Development 13:2828-37.

Washington Smoak I., Byrd N.A., Abu-Issa R., Goddeeris M.M., Anderson R., Morris J., Yamamura K., Klingensmith J., Meyers E.N. (2005) Sonic hedgehog is required for cardiac outflow tract and neural crest cell development. Developmental Biology 283:357-72.

Wassif C.A., Zhu P., Kratz L., Krakowiak P.A., Battaile K.P., Weight F.F., Grinberg A., Steiner R.D., Nwokoro N.A., Kelley R.I., Stewart R.R., Porter F.D. (2001) Biochemical, phenotypic and neurophysiological characterization of a genetic mouse model of RSH/Smith--Lemili--Opitz syndrome. Human Molecular Genetics 10(6):555-64.

Wassmer T., Attar N., Bujny M.V., Oakley J., Traer C.J., Cullen P.J. (2007) A loss-of-function screen reveals SNX5 and SNX6 as potential components of the mammalian retromer. Journal of Cell Science 120:45-54.

Watanabe Y., Nakamura H. (2000) Control of chick tectum territory along dorsoventral axis by Sonic hedgehog. Development 127:1131-40.

Webb S., Brown N.A., Anderson R.H. (1998) Formation of the atrioventricular septal structures in the normal mouse.[see comment]. Circulation Research 82:645-56.

Wessels A., Markman M.W., Vermeulen J.L., Anderson R.H., Moorman A.F., Lamers W.H. (1996) The development of the atrioventricular junction in the human heart. Circulation Research 78:110-7.

Wessels A., Anderson R.H., Markwald R.R., Webb S., Brown N.A., Viragh S., Moorman A.F., Lamers W.H. (2000) Atrial development in the human heart: an immunohistochemical study with emphasis on the role of mesenchymal

tissues. Anatomical Record 259:288-300.

Wijgerde M., Ooms M., Hoogerbrugge J.W., Grootegoed J.A. (2005) Hedgehog signaling in mouse ovary: Indian hedgehog and desert hedgehog from granulosa cells induce target gene expression in developing theca cells. Endocrinology 146:3558-66.

Willert K., Shibamoto S., Nusse R. (1999) Wnt-induced dephosphorylation of axin releases beta-catenin from the axin complex. Genes & Development 13:1768-73.

Wilson C.W., Chen M.-H., Chuang P.-T. (2009) Smoothened Adopts Multiple Active and Inactive Conformations Capable of Trafficking to the Primary Cilium. PLoS ONE 4:e5182.

Winkelbauer M.E., Schafer J.C., Haycraft C.J., Swoboda P., Yoder B.K. (2005) The C. elegans homologs of nephrocystin-1 and nephrocystin-4 are cilia transition zone proteins involved in chemosensory perception. Journal of Cell Science 118:5575-87.

Wolf M.T., Lee J., Panther F., Otto E.A., Guan K.L., Hildebrandt F. (2005) Expression and phenotype analysis of the nephrocystin-1 and nephrocystin-4 homologs in Caenorhabditis elegans. Journal of the American Society of Nephrology 16:676-87.

Wolff T., Rubin G.M. (1998) Strabismus, a novel gene that regulates tissue polarity and cell fate decisions in Drosophila. Development 125:1149-59.

Yao H.H., Whoriskey W., Capel B. (2002) Desert Hedgehog/Patched 1 signaling specifies fetal Leydig cell fate in testis organogenesis. Genes & Development 16:1433-40.

Yao S., Lum L., Beachy P. (2006) The ihog cell-surface proteins bind Hedgehog and mediate pathway activation.[see comment]. Cell 125:343-57.

Ye X., Song G., Fan M., Shi L., Jabs E.W., Huang S., Guo R., Bian Z. (2006) A novel heterozygous deletion in the EVC2 gene causes Weyers acrofacial dysostosis. Human Genetics 119:199-205.

You L., Takamoto N., Yu C., Tanaka T., Kodama T., Demayo F., Tsai S., Tsai M. (2005) Mouse lacking COUP-TFII as an animal model of Bochdalek-type congenital diaphragmatic hernia. Proceedings of the National Academy of Sciences of the United States of America 102:16351-16356.

Zhang C., Williams E.H., Guo Y., Lum L., Beachy P.A. (2004) Extensive phosphorylation of Smoothened in Hedgehog pathway activation. Proceedings of the National Academy of Sciences of the United States of America 101:17900-7.

Zhang X.M., Ramalho-Santos M., McMahon A.P. (2001) Smoothened mutants reveal

redundant roles for Shh and Ihh signaling including regulation of L/R asymmetry by the mouse node.[republished in Cell. 2001 Jul 27;106(2):781-92; PMID: 11517919]. Cell 105:781-92.

Zhao Y., Tong C., Jiang J. (2007) Hedgehog regulates smoothened activity by inducing a conformational switch. Nature 450:252-8.

Zhao Y., Könen-Waisman S., Taylor G., Martens S., Howard J. (2010) Localisation and mislocalisation of the interferon-inducible immunity-related GTPase, Irgm1 (LRG-47) in mouse cells. PLos One 5:e8648.

Zhou J., Qiao X., Xiao L., Sun W., Wang L., Li H., Wu Y., Ding X., Hu X., Zhou C., Zhang J. (2010) Identification and characterization of the novel protein CCDC106 that interacts with p53 and promotes its degradation. FEBS Letters 584:1085-1090.

Ziemer L.T., Pennica D., Levine A.J. (2001) Identification of a mouse homolog of the human BTEB2 transcription factor as a beta-catenin-independent Wnt-1-responsive gene. Molecular & Cellular Biology 21:562-74.